UNIVERSITY NAPOLI "FEDERICO II"
PhD Program
Molecular Pathology and Physiopathology

School of Molecular Medicine

XXVII Cycle

Ubiquitin-dependent control of Kinase Suppressor of Ras 1 (KSR1) signaling by the RING ligase praja2.

Supervisor
Ch.mo Prof. Antonio Feliciello

CANDIDATE
Dott.ssa Rossella Delle Donne

PhD COORDINATOR

Prof. Vittorio Enrico Avvedimento

Academic Year 2013-2014

TABLE OF CONTENTS

ORIGINAL PUBBLICATIONS

1. Lignitto L, Arcella A, Sepe M, Rinaldi L, **Delle Donne R**, Gallo A, Stefan E, Bachmann VA, Oliva MA, Tiziana Storlazzi C, L'Abbate A, Brunetti A, Gargiulo S, Gramanzini M, Insabato L, Garbi C, Gottesman ME, Feliciello A.(2013) Proteolysis of MOB1 by the ubiquitin ligase praja2 attenuates Hippo signalling and supports glioblastoma growth.*Nature Communication*. 2013, 4:1822. doi: 10.1038/ncomms2791.;

2. Sepe M, Lignitto L, Porpora M, **Delle Donne R**, Rinaldi L, Belgianni G, Colucci G, Cuomo O, Viggiano D, Scorziello A, Garbi C, Annunziato L, Feliciello A. (2014) Proteolytic control of neurite outgrowth inhibitor NOGO-A by the cAMP/PKA pathway. *Proc. Natl. Acad. Sci.*2014, 111(44):15729-15734.

3. **Delle Donne R.,*** Rinaldi L.,* Sepe M., Porpora M., Lignitto L., Gallo A., Garbi C.,Stefan E., Taylor S.S., Russo T. Feliciello A.(2015)Ubiquitin-dependent control of Kinase Suppressor of Ras 1 by praja2. *Manuscript in preparation.*

LIST OF ABBREVIATIONS

KSR1 Kinase Suppressor of Ras 1

MAPK Mitogen-Activated Protein Kinases

MAP3K MAPK kinase kinase

MAP2K MAPK kinase

EGF epidermal growth factor

EGFR EGF receptor

GTP guanosine triphosphate

PKC Protein Kinase C

GPCR G-protein couple receptor

PKA Protein Kinase A

NGF Nerve Growth Factor

cAMP cyclic-AMP

GST Glutathione S-transferase

ABSTRACT

Kinase Suppressor of Ras 1 (KSR1) is an evolutionally conserved protein kinase that plays a fundamental role in mitogenic pathway. In response to Ras activation, KSR1 assembles a tripartite kinase complex that optimally transfers signals generated at cell membrane to downstream ERK signaling. The role of KSR1 in Ras signaling has been largely explored. However, the impact of attenuating signals on KSR1 was still elusive. Here, I contributed to identify a novel mechanism of ERK attenuation based on the ubiquitin-dependent control of KSR1. Stimulation of membrane receptors by growth factor induced a rapid poly-ubiquitination of KSR1, which paralleled the decay of ERK signaling. We identified praja2 as the principal E3 ligase that ubiquitinates KSR1. Interfering with praja2 expression or activity impeded KSR1 ubiquitination and sustained ERK signaling.

Thus, the dynamic interplay between the ubiquitin system and scaffold components of the Ras pathway contributes to shape the profile of ERK signaling, profoundly impacting on fundamental aspects of cell behavior.

INTRODUCTION

1.1. Mitogen-Activated Protein Kinases (MAPK) pathway and their scaffold proteins

Several responses to hormones, or any extracellular stimulus, are transmitted to various intracellular targets through a series of protein networks that regulate and govern many cellular processes. The extracellular ligands interact with receptors on the cell membrane, which in turn activate the intracellular second messengers, thus initiating a cascade of signal transduction towards several target proteins. Among the repertoire of the cascades of signaling molecules there is a family of protein kinase known as mitogen-activated protein (MAP) kinase. All these cascades must contain at least three protein kinases in series that culminate in the activation of a multifunctional MAP kinase (*Lewis TS. 1998*). MAP kinases are the main components of the pathways that control embryogenesis, differentiation, proliferation, and cell death. The mammalian MAP kinases consist of a cytoplasmic protein serine\treonine kinases that include the extracellular signal-regulated kinase (ERK) family, the p 38 family, the c-Jun N-terminal kinase family.

Each MAP kinase is
regulated by a phosphorylation cascade that starts with a MAPK kinase kinase (MAP3K) that phosphorylates and activates a MAPK kinase (MAP2K). MAPK kinase (MAP2K) phosphorylates and activates causing the phosphorylation of several downstream substrates such as transcription factors and other functional proteins. In ERK1\2 pathway these kinases are called Raf, MEK, and ERK (**Figure 1**);

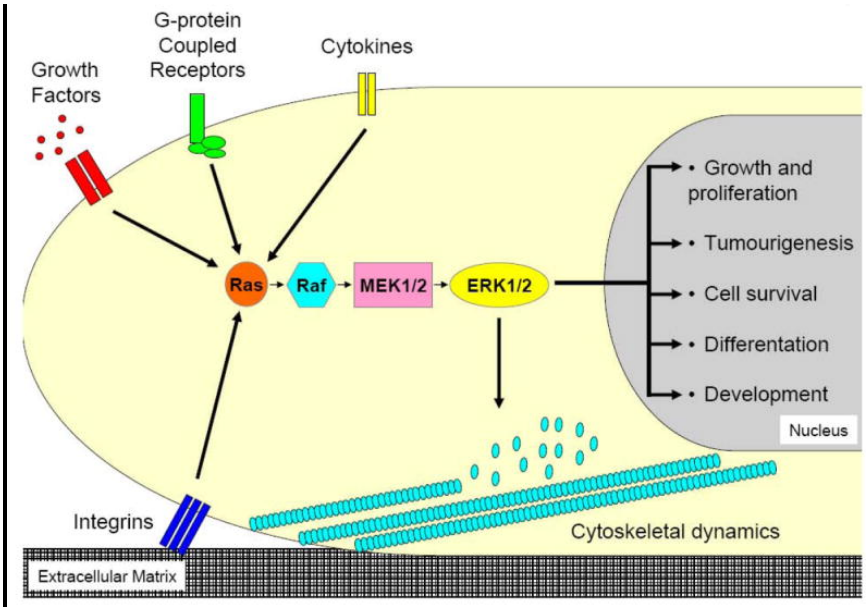

Figure 1.MAPK specificity Diverse extracellular inputs active the Ras/Raf/MEK/ERK cascade and each can give a different cellular outcome

The amplitude and the attenuation of the signal stimulated by MAP kinases are tighty regulated. In particular, the cascade of phosphorylation of the ERK1/2 pathway is amplified at the step of RAF phosphorylation on MEK, because MEK is about 100 times more abundant than the other two kinases (RAF and ERK) (*Huang C-YF. 1996; Ferrell Jr JE. 1996*).

This pathway is activated by protein tyrosine kinase receptors, like EGF receptor (EGFR) or VEGF receptor (VEGFR) (*Pearson G,; 2001*). In response to the ligand stimulus, the receptors dimerize, inducing trans-phosphorylation by intrinsic tyrosine kinases. This event leads to the recruitment ofsome proteins and to the activation of Ras. Ras is a GTPase, which hydrolyses guanosine triphosphate (GTP) to guanosine diphosphate (GDP). Active GTP-Ras , kicks off to the signal. There are three Ras isoforms in mammals, namely H-Ras, K-Ras and N-Ras and it has been shown that mutations in the Ras gene are found in about 30% of human cancers, such as melanoma and biliary cancer (*Vakiani E. et al. 2011*).

Ras activates Raf kinase, recruiting it to the membrane. There are three known isoforms of Raf, called A-Raf, B-Raf and C-Raf (also known as Raf-1), each of them has distinct functions

(*Wellbrock C. 2004*)**.** Each isoform contains three conserved regions, termed CR1, CR2, and CR3, where it is located the kinase domain. In turn, Raf becomes active and catalyses phosphorylation and activation of MEK1 and MEK2, which in turn activate ERK1/2.These are ubiquitous protein kinases of a 44 and 42 kDa, respectively. ERK1 and ERK2 have 85% of identity, especially in the region involved in binding substrates (*Boulton TG,; 1991*).Nevertheless, some studies have shown that functions of the two isoforms are different. Indeed mice ERK2 - \ - are not viable (*Yao Y. et al;. 2003*), while mice ERK1$^{-\backslash -}$ seem to have only a defect in the maturation of CD4+ and CD8+ cells (*Pagès G. et al; 1999*),. Once activated, ERKs dimerize and translocate to the nucleus, where they phosphorylate transcription factors, or remain in the cytosol where they phosphorylate substrates in multiple cellular compartments(*Matthew D. Brown; 2009*) (**Figure 2**)

Since Raf can translocate to the plasma membrane Raf\MEK\ERK pathway may be also activated by some stimuli such as Src and PKC kinases, and by GPCR activation. It is shown that isoproterenol (a drug that acting through a GPCR, increases the intracellular level of cyclic AMP) treatment is able to increase the level of the active form of ERK in human embryonic kidney cells (*Daaka Y,; 1997 Copik AJ1,; 2015*).

Instead, the effects caused by cAMP-dependent protein kinase A (PKA) are disputable , because some evidence indicate that PKA reduces Raf-1 activity (*Wu J et al. 1993; Hafner S. et al. 1994; Kikuchi A. et al. 1996; Mischak H. et al. 1996*). On the other hand, studies in neuronal cells demonstrated that PKA phosphorylates Rap1a, which increases ERK phosphorylation, through activation of B-Raf (*Vossler MR. et al. 1997 - Grewal SS. et al. 2000*).

Temporal modulation of ERK cascade arouses distinct cellular responses(*Murphy LO et al. 2006*). In pheocromocytoma cells (PC12), different responses are observed after different stimuli that activate the same MEK/ERK pathway.PC12 cells proliferate in response to EGF, while nerve growth factor (NGF) induces differentiation *(York RD1 1998)***.** Further investigation has shown that EGF-dependent MAPK signaling is transient, lasting minutes from activation, while NGF-dependent signaling is sustained for hours from stimulation(*Marshall CJ1 1995*).

So, who regulates the signal duration and intensity? And also, which upstream stimulus leads to the activation of every specific downstream signal?

The mechanisms that regulate these phenomena have been unknown for long time. Presently, there are some evidences that

the scaffold proteins may be the answers to these questions. The presence of scaffold proteins as relevant components of MAPK pathway was studied firstly in the yeast *S.Ceervisiae*, where mutations in Ste5, a protein involved in the three-MAPK cascade assembly , destroyed the response to pheromone (*Choi et al.1994; Marcus et al. 1994*). There are evidences that also in mammalian MEK\ERK MAPK pathway the scaffold proteins have an important role for the correct activation, the signal propagation and turn off of the cascade. Moreover, scaffold proteins regulate and compartmentalize the signal diffusion to a specific subcellular location (*Roskoski,2012*). Scaffolds are thought to minimize crosstalk with other signaling cascades (*Dhanasekaran et al. 2007*)and similarly mediate crosstalk of different pathways (*Kolch,2005*) and protect kinases from phosphatases action (*Perlson et al. 2006*).

In the last years, different mammalian scaffold proteins have been isolated and characterized: KSR1 and KSR2, β-arrestin, paxilin MP1, MORG1, Sef and IQGAP1, but are located in different cellular districts, and so, they direct the signal amplification on different cellular compartments. In this context, KSR1/2 binds the kinases in the cytosol, β-arrestin in clathrin vesicles, MP1 active complex in late endosomes and Sef locates the kinase complex in the Golgi apparatus. Thus, different stimuli can activate a complex formation with a different scaffold protein. When the stimulus starts from an activated GPCR and is directed to early endosomes, β-arrestin captures the kinases and compartmentalizes there the signal (**Figure 2**).

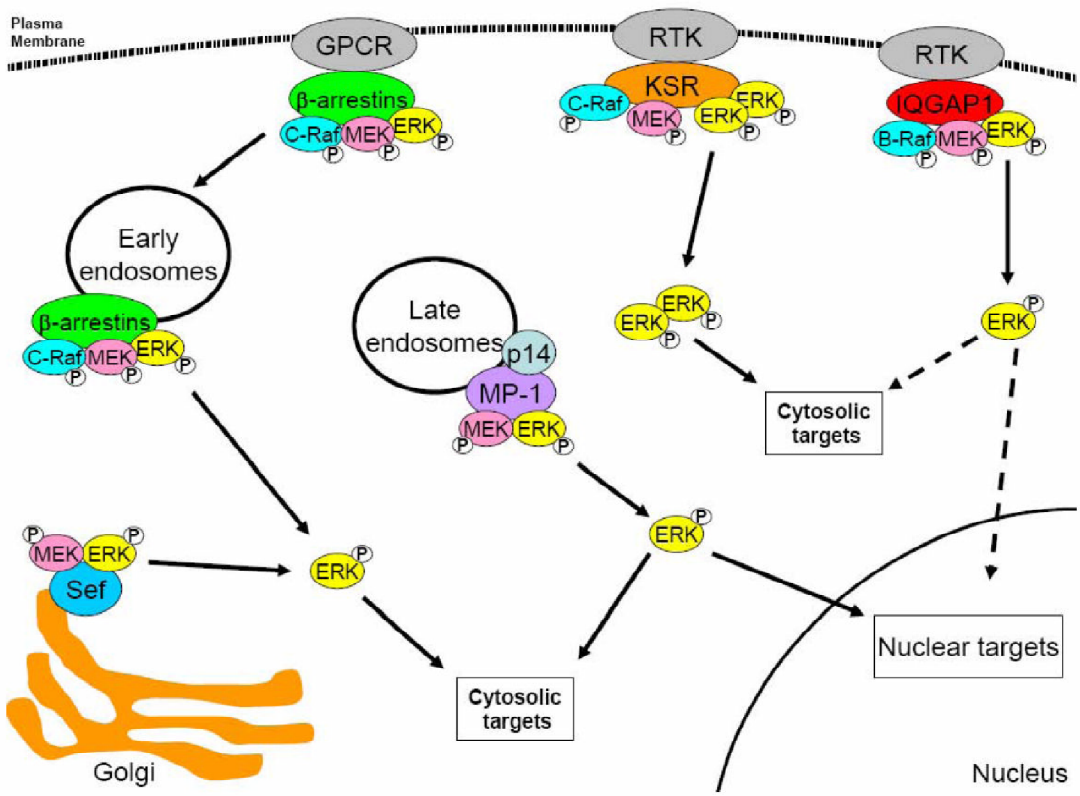

Figure 2. Spatial regulation of MEK/ERK signaling by protein scaffolds. Scaffolds can regulate the subcellular distribution MAPK proteins. **B**oth IQGAP1 and KSR bind to Raf, MEK and ERK and localize the kinases to the plasma membrane, while MP-1localizes the kinase complex to endosomes. After activation, ERK phosphorylates the downstream targets, or translocate to the nucleus and activate nuclear targets. KSR binds ERK dimers and restricts them to cytosolic targets. Like MP-1, β-arrestins localize Raf, MEK and ERK to endosomes. However, once activated, ERK cannot translocate to the nucleus and phosphorylates mostly cytosolic targets by an unknown mechanism. Sef restricts MEK and ERK to the Golgi and, like β-arrestin, prevents translocation of ERK to the nucleus, limiting it to cytosolic substrates. GPCR, G-protein coupled receptor; RTK, receptor tyrosine kinase.

1.2 Kinase Suppressor of Ras1 (KSR1)

The KSR family proteins consist of two members namely KSR1 and KSR2. They are widely conserved from invertebrate to mammals and the similarity of amino acids between them is approximately 60%.The structure of these proteins consists of 5 domains called CA1-CA5.The CA1 domain is located in the N-terminus and it is involved in the formation of a KSR1-MEK-RAF complex; it comprises 40 amino acids which are exclusive to KSR1, but absent from KSR2; CA2 is a proline-rich domain with unknown function; CA3 is a cysteine rich domain, needful for membrane recruitment by phospholipids (*Michaud N.R. 1997*); CA4 is a serine/threonine-rich region containing an FXFP (Phe-Xaa-Phe–Pro) motif that is an ERK docking-site *(Kolch W. 2005)* and CA5 is highly homologous to the kinase domain of RAF proteins (see **Figure 3**) and, for this reason, it is considered a putative kinase domain which lacks the conserved lysine residue, required for phosphorylation*(Kolch W. 2005*) (**Figure 3**). Furthermore a new domain of KSR1 composed by a coiled-coil (CC) and a sterile α(SAM)motifs, thus called CC-SAM, has been recently characterized. This domain targets KSR-1 in response to growth factor at the plasma membrane, and binds directly to various micelles and bicelles in vitro. (*Koveal D. 2012*).

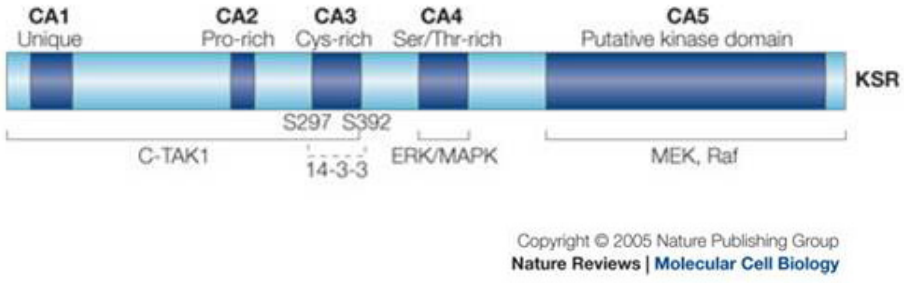

Figure 3. KSR structure.KSR is composed by 5 domains called CA1-CA5. The CA1 domain is responsible of the formation of a KSR1-MEK-RAF complex; CA2 is a proline-rich domain with unknown function; CA3 is a cysteine rich domain, needful for membrane recruitment with phospholipids; CA4 is a serine/threonine-rich region containing an FXFP (Phe-Xaa-Phe–Pro) motif that is an ERK docking-site and CA5 is a putative kinase domain in which the conserved lysine residue.

KSR1 and KRS2 were initially characterized as scaffold proteins involved in different pathways. KSR2 has several functions; it contains a region of 63 amino acids between the portion C3-C4, which is a specific region for binding AMPK and calcineurin. Calcineurin, when activated by intracellular calcium, binds KSR2 and activates ERK signaling *(Costanzo-Garvey DL. 2009 ; Dougherty MK. 2009).* KSR2 gains an important function in energy metabolism regulation, as KSR2 knockout mice show an obese phenotype(Brommage R. 2008).

On the other hand, KSR1 is recruited in the Ras/Raf/MAPK signaling cascade. In un-stimulated cells, C-TAK1 (Cdc25C-associated kinase 1) phosphorylates KSR1 at Ser392. Hence, KSR1 is sequestrated in the cytosol, where it constitutively interacts with MEK and ERK. Upon growth factor stimulation, Ras is activated and triggers dephosphorylation of KSR1 at Ser392 by PP2A (protein phosphatase 2A). After that, KSR1 shifts to the cell membrane, where it forms a complex with Raf, MEK and ERK.KSR1 thus potentially makes easy the phosphorylation of Raf, MEK and ERK, facilitating the MAPK signaling, as well as the phosphorylation of multiple substrates in the cytoplasm and nucleus. Through this way, KSR1 regulates proliferation, cell cycle and apoptosis(*Muller j. 2001; Roy F. 2002; Ory S. 2003*)(**Figure 4**).

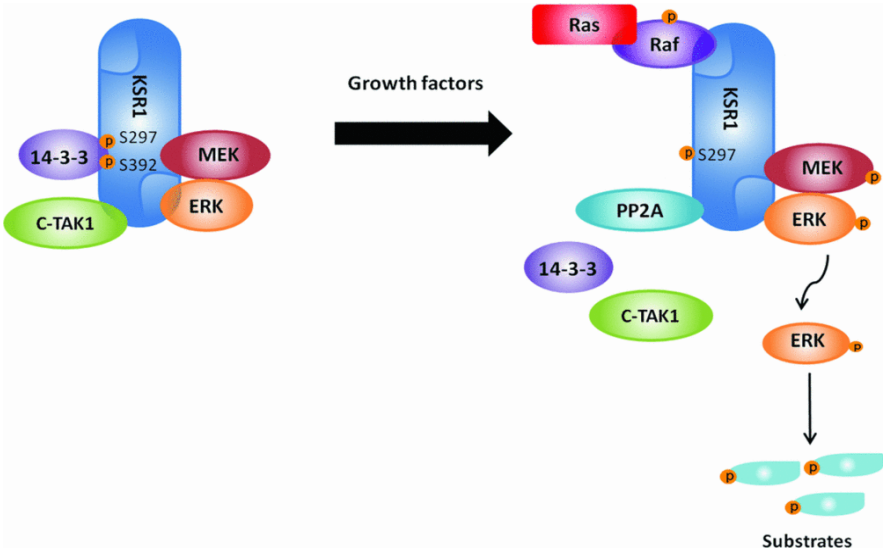

Figure 4. KSR1 regulation in thel Ras/Raf/MAPK pathway. In resting conditions,KSR1 is sequestered in the cytosol through 14-3-3 protein binding, after phosphorylation by C-TAK1 at Ser297 and Ser392. Meantime, KSR1 constitutively interacts with MEK and ERK. Under stimulated conditions, it activates Ras that triggers dephosphorylation of KSR1 at Ser392 by PP2A, leading to the release of 14-3-3 protein from its binding sites.KSR1switches to the cell membrane, where it forms a complex with Raf, MEK and ERK, and promotes phosphorylation of downstream substrates.

However, different groups found conflicting results on the role of KSR in the regulation of MAPK. Denouel-Galy showed that the MEK subpopulation complexed with exogenous KSR1in COS-1 cells or PC12 cells have no kinase activity because KSR1 blocks MEK in an inactive form. This block has a surprising biological effect: KSR1 did not transform NIH3T3 cells, and, furthermore, reduced Ras-induced transformation. Similarly, KSR1 inhibited the proliferation of embryonic neuroretinal cells induced by Ras (*Denouel-Galy, A. 1998*).

Protein scaffolds must be expressed in the cell at certain levels. Indeed, KSR1 may have different effects in the regulation of MAPK signaling according to its intracellular concentration. In fact, KSR1 at low concentrations can increase the Ras downstream signaling, while high levels of KSR1have inhibitory effects on Ras pathway (*Cacace AM. ; 1999*).

KSR1 is also an important regulator of the immune response. Thus, KSR1 plays a role in the protection from the inflammation,

bacterial infections, and in T cells proliferation. KSR1$^{-/-}$ are more susceptible to the manifestation of colitis induced by TNF alpha (*Yan, F. 2004; Yan, F. 2001*) and to infection by Pseudomonas aeruginosa (*Zhang, Y. 2011*). Perhaps, this was a consequence ofKSR1-mediated cytotoxic response of natural killer cells. Furthermore, in these mice the attenuation of the ERK pathway also causes a reduction of T-cell proliferation (*Nguyen, A. 2002*). However, KSR1 has not only the role of scaffold protein. KSR1 has been classified as inactive pseudo-kinase.However,*in vitro* studies have shown that KSR1 owns a real kinase activity and it is capable both of auto-phosphorylation and of MEK phosphorylation(*Goettel, J.A. 2011*). Furthermore, KSR1 phosphorylates other substrates, even if not bound to MEK (*Xing, H.R. 2004*).In addition, KSR1 is able to regulate the temporal duration of the signal. McKay and collaborators demonstrated that KSR1 is subjected to phosphorylation and inhibition by activated ERK. In this circumstances, the scaffold is temporally inactivated and the multikinase complex is disassembled(*McKay, M. et al. 2009*) (**Figure 5**).

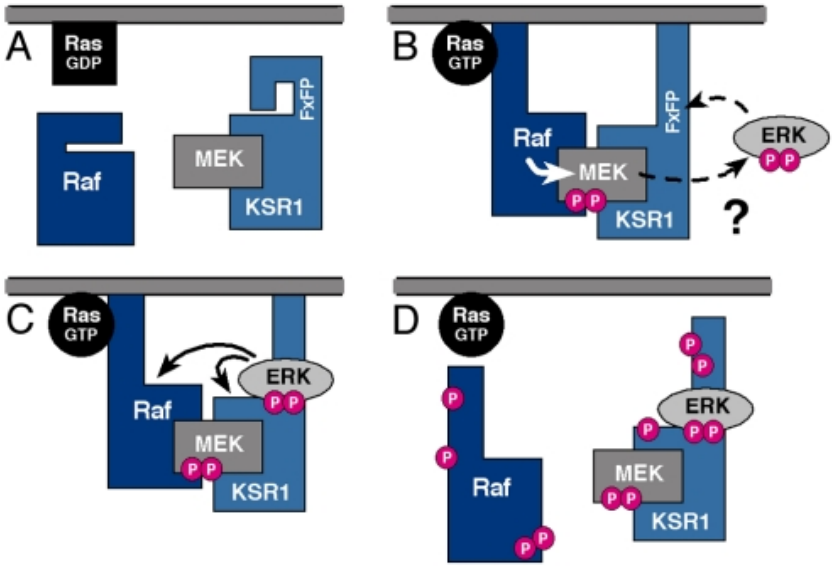

Figure 5.KSR1 regulates the intensity and duration of ERK cascade. In resting cells, KSR1 binds MEK and keeps it away from Raf (***A***). In stimulated cells, KSR1 facilitates the Raf/MEK interaction and first increases the signal transmission (***B***) and then attenuates the signal. Active ERK, in fact, can phosphorylate KSR1 facilitating the disruption of the KSR1 scaffold complex (***C***and***D***).

1.3 The ubiquitin proteasome system

The amount of protein within the cell is usually kept constant or varied according to the needs of the latter. Dysregulation in the amount of specific proteins can lead to the development of diseases or disorders, including cancer. The balance between the synthesis and degradation of proteins is regulated by the ubiquitin-proteasome system. Ubiquitination is crucial for several physiological processes, including cell survival, differentiation, innate and adaptive immunity.

The cellular functions of ubiquitination include proteolytic and non-proteolytic roles such as proteasomal degradation of proteins, receptor internalization and down regulation, intracellular trafficking, inflammatory signaling and assembly or disassembly of multi-protein complexes *(Grabbe C. et all 2011)*. Thus, a wrong regulation of ubiquitination might have pathological consequences, as degenerative disorders and cancer.

Ubiquitination is largely mediated by ubiquitin ligases, which mark their substrates for, with a series of ubiquitin molecules *(Hershko et al. 1998).* The conjugation of ubiquitin molecules to substrates requires coordinated action of the ubiquitin activating enzyme (E1), the ubiquitin conjugating enzyme E2 and the E3 ligase. The E3 ligase enzyme associates with the substrate and thereby determines the specificity in degradation or inactivation of various substrates *(Ciechanover, 1998)* (**Figure 6**).As already mentioned, ubiquitination does not always lead to protein degradation. Indeed in recent years have been identified more than 100 de-ubiquitination enzymes (DUB) that remove ubiquitin from substrates, making them available again (*Amerik A.Y. et al. 2004 ;Huang OW et al. 2013*)(**Figure 6**).

The RING finger ubiquitin E3 ligases contain a characteristic cysteine-rich zinc binding domain defined by a pattern of conserved cysteine and histidine residues. These ligases efficiently catalyze poly-ubiquitination of given substrates *(Joazeiro et al. 2000)*. Characteristic of RING finger ubiquitin E3 ligases is the ability to mediate degradation of their substrates, by promoting their own ubiquitin-dependent degradation *(Lorick et al. 1999)*.

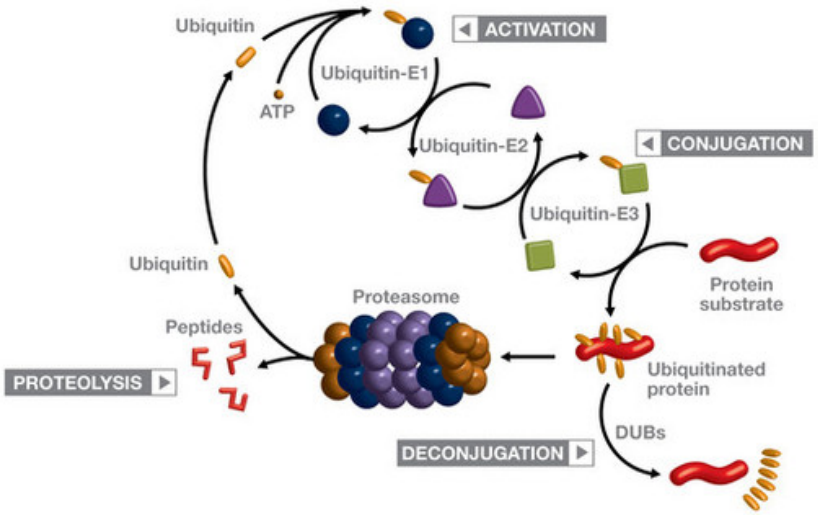

Figure 6. Schematic representation of ubiquitin system. The conjugation of ubiquitin molecules to substrates requires coordinated action of three enzymes: the ubiquitin activating enzyme (E1), the ubiquitin conjugating enzyme E2 and the E3 ligase, that associates the ubiquitin molecules to the substrates. Once ubiquitinated, the proteins can be degraded by the proteasome or de-ubiquitinated by a specific DUBs enzyme.

1.4 RING ligase Praja2

Praja2 belongs to the Ring H2 finger E3 ubiquitin ligase subfamily. It contains, in fact, at COOH-terminal end (aa 629-678) a characteristic sequence domain known as the RING-H2-finger motif *(Freemont, 1993).* The RING-H2-finger motif is similar to the RING-finger motif, and Cys4 in the RING-finger motif is replaced by His *(Freemont, 1993)*.

Praja E3 ligase family is composed by two members, namely praja1 and praja2, that share high sequence homology.
praja2 gene is localized on the long arm of human chromosome 5 (5q21) and its transcript encodes for a protein of 708 amino-acidic with an estimate weight of 78 KDa *(Nakayama et al. 1995).*But SDS-polyacrylamide electrophoresis gel show that the molecular mass of praja2 is estimated to be about 140 kDa . This discrepancy between the expected and observed molecular masses might be explained by anomaly of protein migration rates on SDS-polyacrylamide gel *(Ohara and Teraoka, 1987).*Instead,praja1 gene

mapped on human chromosome X. Northern blot analysis identify a 2.7 Kbp ribonucleotide transcript, coding for a protein of 643 amino-acids, with an estimate weight of 71 kDa *(Ping et al. 2002)*.

Praja1 and praja2 show high sequence homology, more or less of 52.3% of identity and their COOH terminal domains contain a RING H2 Finger domain highly conserved. It is demonstrated that in mice, praja1 has an important role in neuronal plasticity that is the basis for learning and memory *(Ping et al. 2002),* in fact praja1 expression shows learning-specific induction in the basolateral complex of the amygdala during formation of fear memory*(Stork et al. 2001).*Structural data and sequence analysis identified in praja2 COOH terminal domain (aa 583-600) a particular motif, highly conserved among all the praja family members, encoding an α-amphipathic helix. This domain is characteristic of AKAPs family proteins, and is known to be fundamental for PKA anchoring (**Figure 7**)

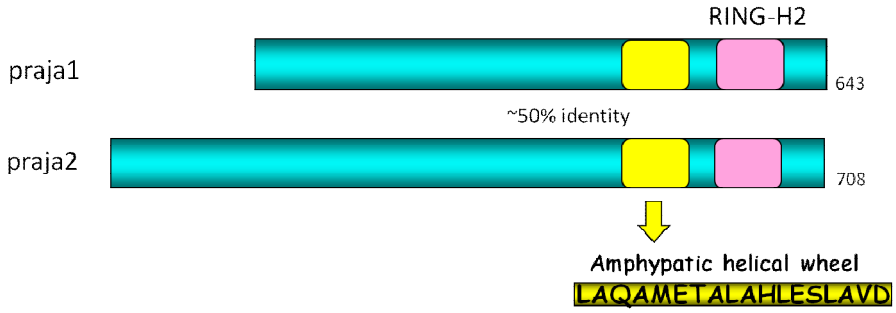

Figure 7. Schematic representation of praja proteins. Praja1 and praja2 are composed respectively by 643 and 708 amminoacids. Both proteins are characterized by a RING-H2 motif (in rose) and a putative amphypatic helical wheel (in yellow) at COOH-terminal.

Following axotomy, axonal degeneration and neuronal cell death correlate with strong down-regulation of praja2 expression levels in rat *(Nakayama et al. 1995)*. Thus, regulating synaptic communication and plasticity, praja family proteins play a crucial role in neuronal activity and development *(Nakayama et al. 1995)*. praja2 plays an important role in several molecular mechanisms that mostly involve the cAMP-dependent signal transduction pathway. First of all, praja2 controls the stability of mammalian regulatory subunits of Protein Kinase A settling the strength and duration of PKA signal output in response to cAMP, so it is required for efficient nuclear cAMP signaling and PKA-

mediated long-term memory *(Lignitto et al. 2011).* Moreoverpraja2 is involved in cAMP-induced neurite outgrowth, promoting proteasomal degradation of NOGO-A, a major inhibitor of neurite outgrowth in mammalian brain *(Sepe et al. 2014)* (**Figure 8)**

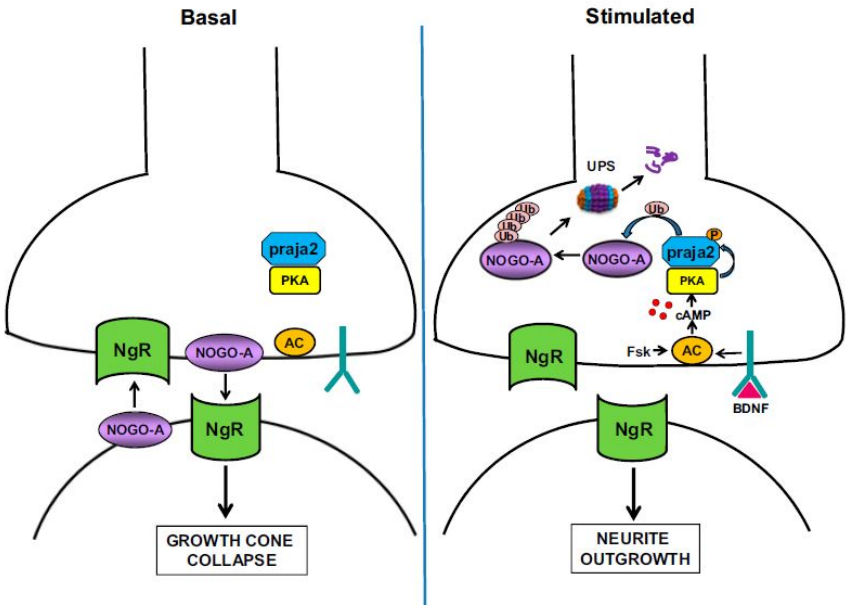

Copyright Sepe et al. 2014, Pnas

Figure 8. Model of praja2–NOGO-A pathway. Under basal conditions, NOGO-A inhibits neurite outgrowth. Activation of adenylate cyclase (AC) by BDNF or by Forskolin (Fsk) increases cAMP levels and dissociates PKAholoenzyme. Active PKA catalytic subunit phosphorylates praja2, which in turn ubiquitinates and degrades NOGO-A through the UPS. The drop in NOGO-A levels promotes neurite outgrowth*(Sepe et al. 2014).*

In addition, praja2 has a role in a tumor growth, indeed it ubiquitinates and degrades MOB1, a core component of NDR/LATS kinase and a positive regulator of the tumor-suppressor Hippo cascade. This degradation attenuates the Hippo cascade, controls the organ size and sustains glioblastoma growth in vivo *(Lignitto et al. 2013)*(**Figure 9**).

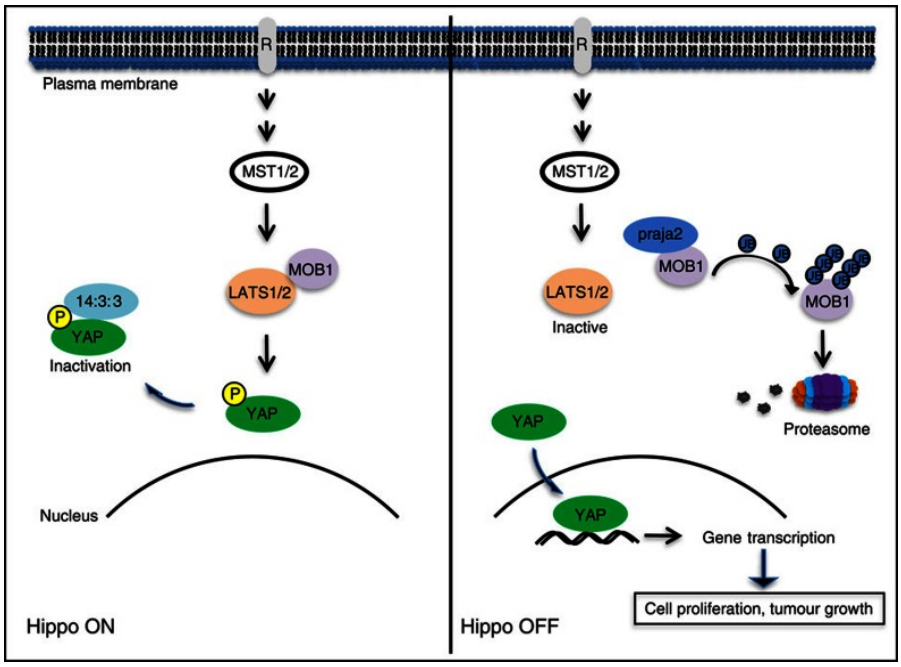

Figure 9.Schematic representation of the role of praja2 in the Hippo pathway. Praja2 ubiquitinates MOB1 and degrades it thorugh the proteasome system. MOB1 degradation attenuates LATS1/2 kinase activity, preventing phosphorylation and inactivation of YAP. Un-phosphorylated YAP accumulates in the nucleus and drives gene transcription, promoting cell proliferation and tumor growth.

On the other hand,praja2 is markedly over-expressed in differentiated thyroid cancer, and its levels inversely correlate with the malignant phenotype of the tumor *(Cantara et al. 2012)*. Finally, praja2 also seems to be involved in the regulation of insulin secretion. Indeed, in response to glucose stimulation, praja2 ubiquitinates and degrades p35, activating calcium signaling and promoting insulin secretion (*Sakamaki J. et al. 2014)*

Many RING proteins have functions unknown or unrelated to the ubiquitination in evident manner. Interestingly, several RING finger genes have been found mutated in human diseases *(Mattson et al. 2001; Kitada et al. 1998).* For instance, the parkin gene was found mutated in autosomal recessive familial juvenile Parkinsonism *(Kitada et al. 1998).*

AIM OF THE STUDY

Kinase Suppressor of Ras 1 (KSR1) is an evolutionally conserved protein kinase that plays a fundamental role for correct activation, propagation and attenuation of the mitogenic pathway (*Roskoski et al. 2012*). In response to Ras activation, KSR1 assembles a kinase complex that optimally transfers signals generated at cell membrane to downstream ERK signaling.

Ubiquitination is a post-translational mechanism that controls the activity/stability of a wide array of cellular target proteins. By modulating protein stability, the ubiquitin pathway controls key physiological processes, such as survival, differentiation and cell proliferation (*Grabbe C. et all 2011)*.

Our laboratory is involved in the regulation of the ubiquitin pathway by the E3 ubiquitin-ligase praja2. Recently, we identifiedpraja2 as a component of the complex assembled by KSR1. During the PhD program, my principal aim was to understand if KSR1 and praja2 formed a complex in living cells and how the complex regulates MAPK signaling. More specifically, I focused my attention on the following issues:

- Verify the existence of KSR1-praja2 complex in living cells.
- Test if praja2 ubiquitinates KSR1*in vitro* and *in vivo*.
- Define the functional relevance of praja2 in KSR1-dependent mitogenic pathway.

RESULTS

2.1 praja2 and KSR1 form a stable complex

To gain insights into praja2 action, I tested if praja2 interacts with protein/adaptors involved in mitogenic signaling. To this end, I performed co-immunoprecipitation assays using antibodies directed against distinct components of the ERK pathway. This analysis allowed the identification of Kinase Suppressor of Ras 1 (KSR1) as a relevant interactor of praja2. A proteomic screening previously identified praja2 as component of a macromolecular complex that includes KSR1(*Dougherty M.K. et al. 2009*).
First, I investigated whether endogenous praja2 and KSR1 interact in cells. Lysates from HEK293 cells were immunoprecipitated with anti-praja2 or with non-immune IgG. Precipitates were immunoblotted with anti-KSR1 and anti-praja2 polyclonal antibody. As shown, an endogenous praja2-KSR1 complex could be detected (**Figure 10**).

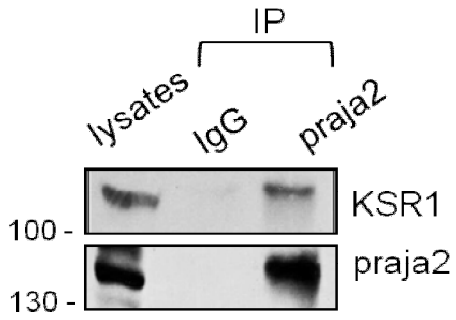

Figure 10. praja2 binds KSR1. Lysates (2mg) from HEK293 cells were immunoprecipitated with anti-praja2or non-immune IgG. Precipitates were immunoblotted with anti-KSR1or anti-praja2 polyclonal antibody.

2.2 praja2 directly interacts with KSR1

As shown before, praja2 interacts with KSR1 protein. To demonstrate whether this binding is direct, I performed a pull down assay using recombinant proteins. Thus, a fusion protein carrying the full-length praja2, appended to the C-terminus of glutathione S-transferase polypeptide (GST), pulled down *in vitro* translated ^{35}S-labeled KSR1 (**Figure 11)**

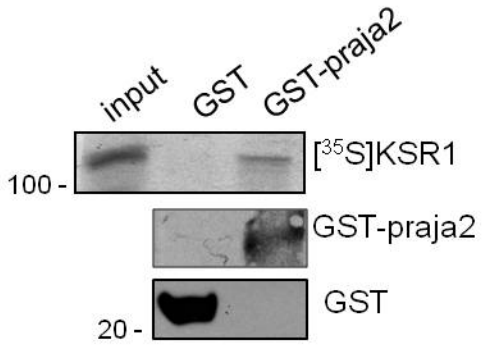

Figure 11. praja2 directly interacts with KSR1 *in vitro*. *In vitro* translated, ^{35}S-labeled KSR1 was subjected to pull-down assays with purified GST or GST-praja2 fusions.

2.3 praja2-KSR1 binding is regulated by serum

Next, I assessed whether praja2-KSR1 interaction is regulated by serum. Lysates from growing or serum-deprived HEK293 cells were immunoprecipitated with anti-praja2 or non-immune IgG. Precipitates were immunoblotted with anti-KSR1 or anti-praja2 polyclonal antibody. As shown in **Figure 12,** the praja2-KSR1 interaction is regulated by serum. Indeed, praja2-KSR1 complex was more evident when cells have been grown in the presence of serum.

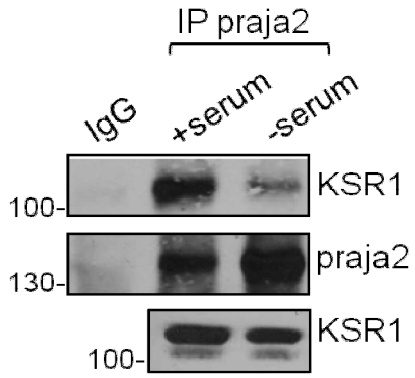

Figure 12.praja2-KSR1 binding is regulated by serum. Lysates (2mg) from growing or serum-deprived (18h)HEK293 cells were immunoprecipitated with anti-praja2or non-immune IgG. Precipitates were immunoblotted with anti-KSR1or anti-praja2 polyclonal antibody.

2.4 Endogenous KSR1 and praja2 co-localize in Human Embryonic Kidney 293 cells.

Next, to demonstrate that KSR1 and praja2 are located within the same cell compartment, I analyzed the localization of both proteins in Human Embryonic Kidney 293 cells (HEK293). To this end, I performed double immunofluorescence using anti-KSR1 and anti-praja2 antibodies. As suspected, the results indicate that both proteins have a partial co-localization within the cytoplasm and at the perinuclear region, as confirmed by the Pearson's statistic analysis (**Figure 13**).

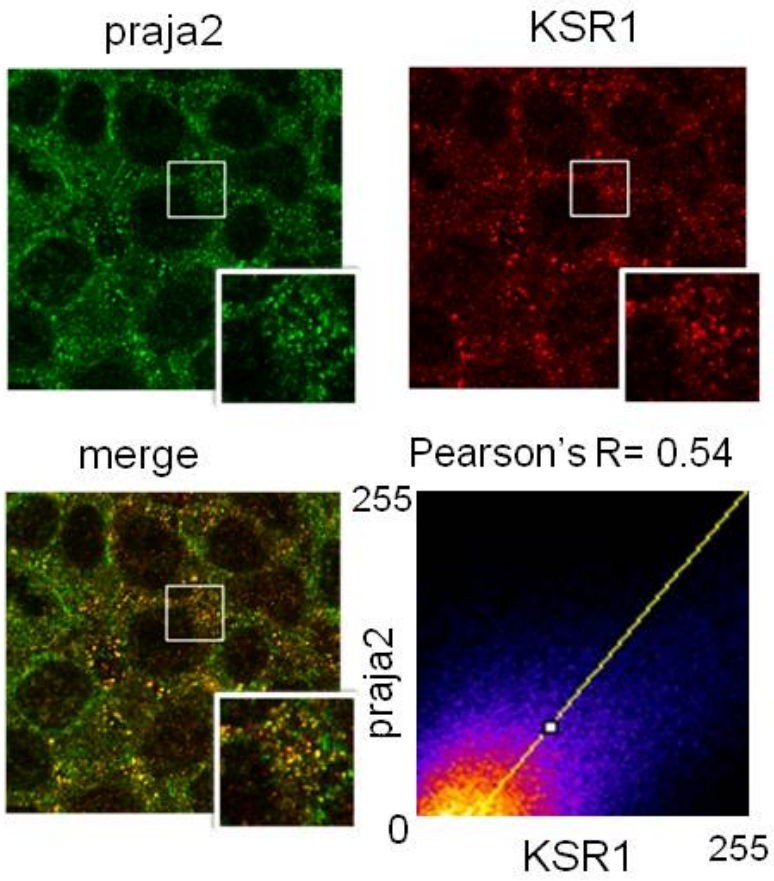

Figure 13. praja2 and KSR1 co-localize in Human Embryonic Kidney (HEK) 293 cells.HEK293 cells were subjected to double immunostaining with anti-ksr1 and anti-praja2 antibodies. Images were collected and analyzed by confocal microscopy. Magnification of selected areas is shown (insets). Co-localization Pearson's coefficient praja2-KSR1~0.54. Scale bar: 10 μm.

2.5 Mapping the praja2 binding domain on KSR1.

The data above demonstrate thatKSR1 and praja2 form a stable complex in lysates and partly co-localize within the same sub-cellular compartment. To determine whether praja2 ligase activity is required for KSR1 binding, HEK293 cells were transiently transfected with flag-tagged praja2 or with a flag-tagged praja2RING mutant. The mutant protein carries cysteine to alanine substitutions within the RING domain (cys634 and cys671) (praja2rm) that interferes with the transfer of the ubiquitin moiety from E2 to the substrate. Lysates were immunoprecipitated with anti-flag antibody. Results show that praja2 ligase activity was not necessary for KSR1 binding, since praja2rm binds KSR1 as wild type protein. To identify the domain of praja2 that mediates the binding to KSR1, I generated a series of deletion mutants lacking distinct segments of praja2. Flag-tagged praja2 mutants were co-expressed with KSR1 in HEK293 cells. Lysates were immunoprecipitated with anti-KSR1 antibody, and immunoblotted with anti-flag antibody.

The results show that the mutant lacking aminoacids from 402 to 708 was not able to bind KSR1, suggesting that residues 402 to 531 of praja2 are most likely required for optimal binding to KSR1 (**Figure 14**).

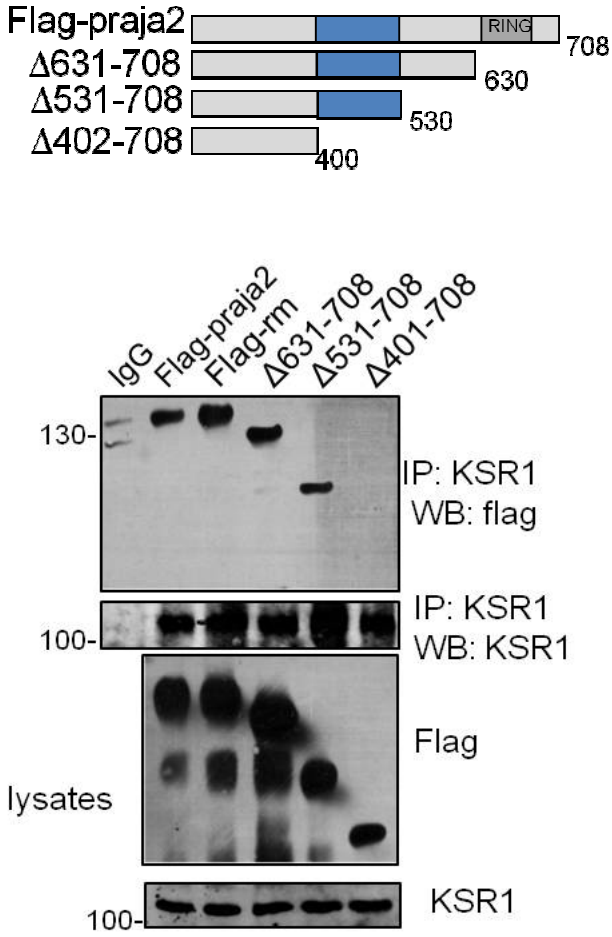

Figure 14. praja2 402-531 residues mediate the binding to KSR1. Schematic representation of human praja2 and its deletion mutants. RING domain and KSR1 binding domain are shown in grey and in blue (upper panel), respectively. HEK293 were transfected with flag-praja2, praja2 RING mutant (C634,671A; praja2rm), or with each of the three deletion mutants (Δ631-708,Δ531-708, Δ402-708). Cells were treated with MG132 (10 μM) for 6 hours before harvesting. Lysates were immunoprecipitated (IP) with anti-KSR1 and immunoblotted with anti-Flag and anti-KSR1 antibodies.

2.6 Mapping the KSR1 binding domain on praja2

Next, I analyzed which part of KSR1 interacts with praja2. To this end, overlapping 25-mer peptides derived from human KSR1 were spotted onto a membrane and overlaid with purified GST-praja2$^{431-531}$ fusion protein, as previously described (*Stefan E. et al. 2011*). I identified one binding motif at the C-terminus of KSR1 (DLQEROSFSL) as the core region required for praja2 binding (**Figure15A**). As expected, a recombinant protein carrying the core peptide of KSR1 fused at the C-terminus of the GST polypeptide was sufficient in binding flag-praja2 *in vitro* **(Figure15B)**. The peptide is located at the surface of the predicted KSR1 structure, supporting the findings of a direct interaction with praja2 (**Figure15C**).

A

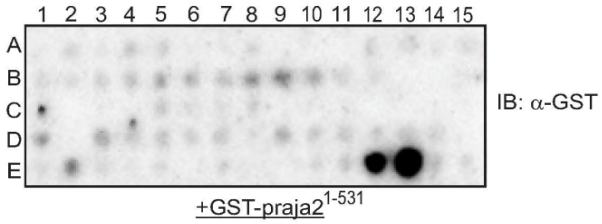

E11 GAKRVLTSVSLGKEVSEILSASWAF
E12 LGKEVSEILSASWAF**DLQERPSFSL**
E13 ASWAF**DLQERPSFSL**LADALEKLPK
E14 **PSFSL**LADALEKLPKLNRRLSHPGH
E15 DALEKLPKLNRRLSHPGHFWKSAEL

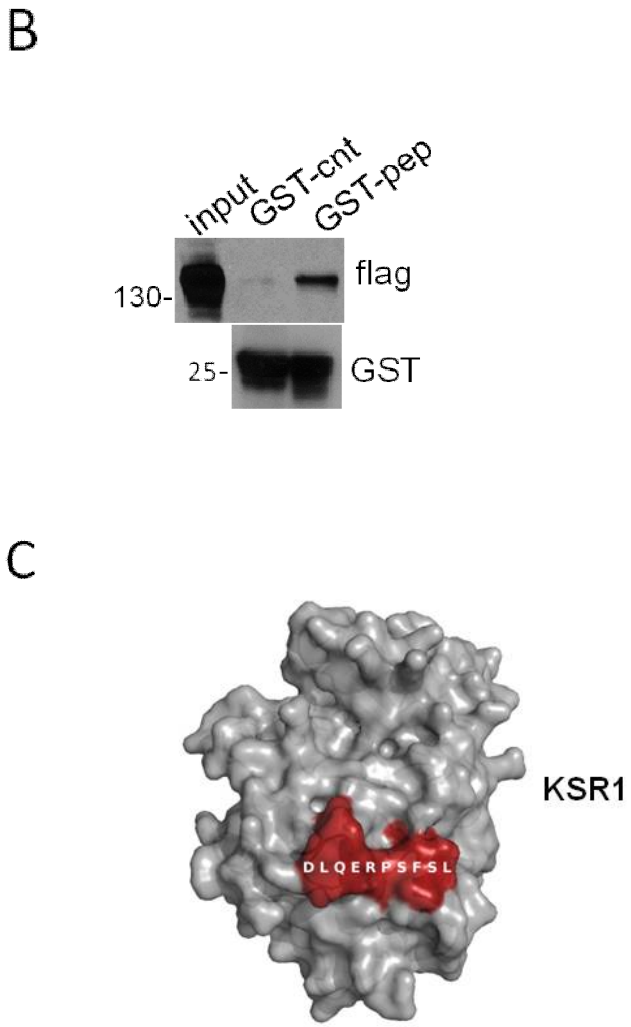

Figure 15. KSR1 necessary binding site for praja2 is on the surface of protein. (**A**) Spotted peptides (25 mer, 15 amino-acids overlap) of KSR1 were overlaid with recombinant GST-praja$_{21-531}$ followed by immunoblotting with anti-GST. The potential binding amino acids are shown in red (upper panel).(**B**)HEK293 were trasfected with flag-praja2 and the lysates were incubated over night with GST fusion protein containg a peptide sequence (GST-pep) and a scramble short sequence (GST-cnt). The proteins were immunoblotted with anti-Flag and anti-GST antibodies.(**C**)KSR1 predicted structure (down panel).The potential praja2 binding site is shown in red.

2.7 praja2 ubiquitinates KSR1

E3 ubiquitin ligase praja2 binds KSR1. Therefore, I tested if praja2 acting as E3 ligase ubiquitinates KSR1. HEK293 cells were co-transfected with praja2-flag, praja2rm-flag, and HA-ubiquitin vectors. Lysates were immunoprecipitated with anti–KSR1 antibody. The precipitates were immunoblotted with anti-HA, anti-KSR1 and anti-flag antibodies. The data indicates that expression of praja2, but not of praja2rm, induced accumulation of poly-ubiquitinated KSR1 molecules (**Figure 16A**). Next,I analysed if the activation of tyrosine kinase receptor (RTK) modulates KSR1 ubiquitination. Stimulation by epidermal growth factor (EGF) induced a strong KSR1 polyubiquitination**(Figure16B).** Expression of praja2rm dramatically impaired ubiquitination of KSR1 induced by EGF **(Figure 16C)**. An *in vitro* ubiquitination assay demonstrated that KSR1 is, indeed, a direct substrate of praja2 (**Figure 16D**).

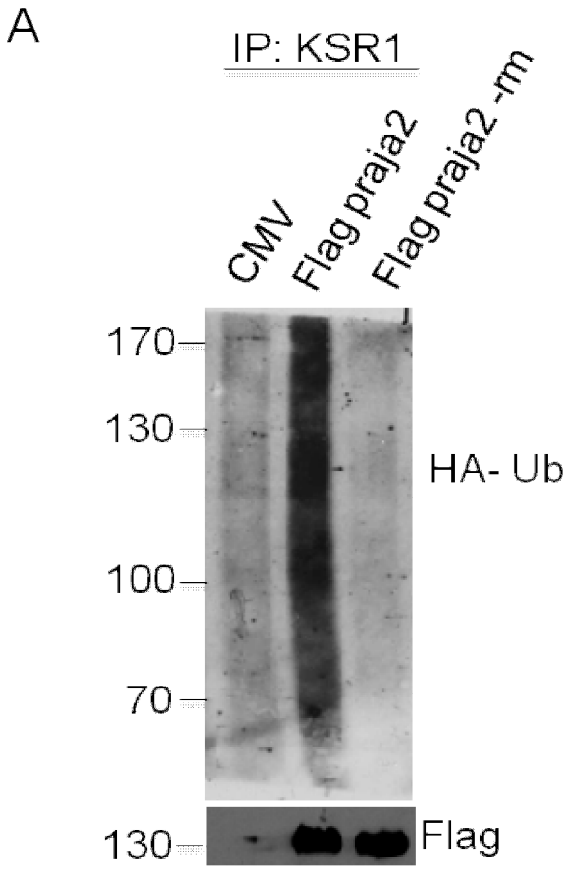
A
IP: KSR1
CMV
Flag praja2
Flag praja2 -rm
170
130
100
70
HA- Ub
130
Flag

B

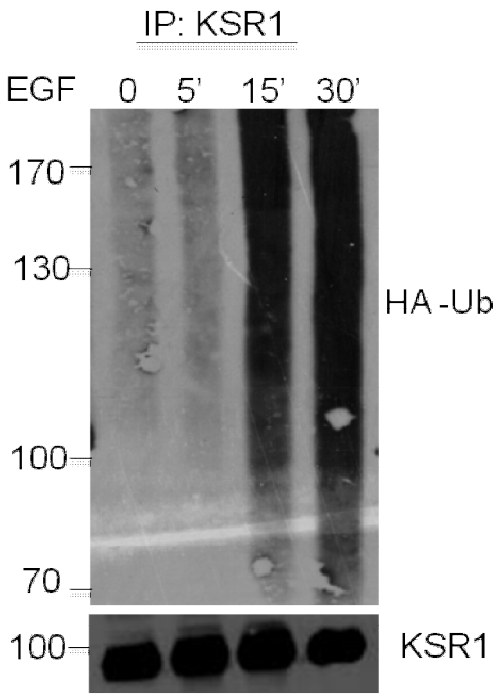
IP: KSR1
EGF 0 5' 15' 30'
170
130
100
70
HA -Ub
100
KSR1

C

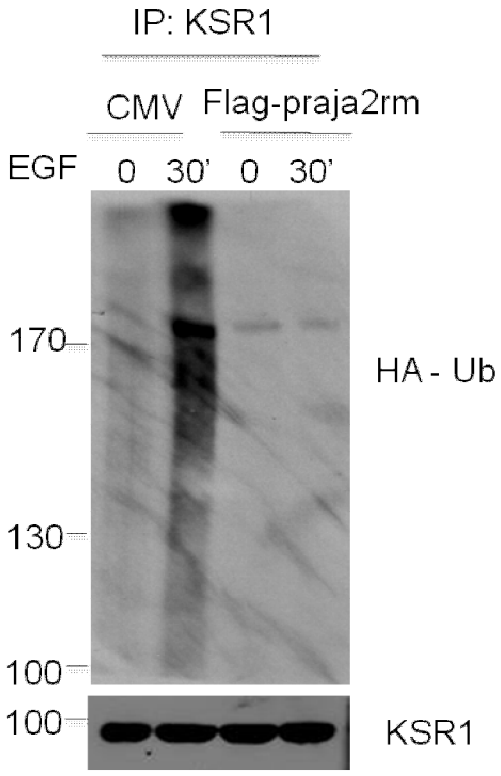
IP: KSR1
CMV Flag-praja2rm
EGF 0 30' 0 30'
170
130
100
HA - Ub
100
KSR1

D

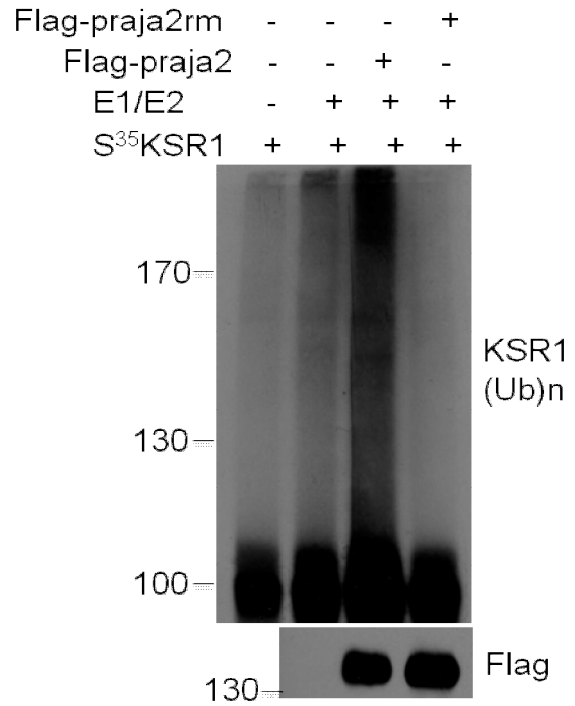

Figure 16.praja2 ubiquitinatesKSR1. (**A**) HEK293 cells were co-transfected with HA-ubiquitin, and praja2 or praja2rm. After 24 hours cells were harvested and the lysates were immunoprecipitated with anti–KSR1 and immunoblotted with anti-HA, anti-KSR1 and anti-flag antibodies. (**B**) HEK293 cells were transfected with HA-tagged ubiquitin. 24 hours after transfection, cells were either left untreated or stimulated with EGF (100ng/ml) at indicated time. Lysates were immunoprecipitated with anti-KSR1 and immunoblotted with anti-HA, anti-KSR1 antibodies. (**C**)HEK293 were co-transfected as in Figure(**A**) and stimulated at indicated time with EGF.(**D**) *In vitro* translated, ^{35}S-labeled KSR1 was incubated with his6-tagged ubiquitin, in the presence or absence of E1, UbcH5c (E2) and anti-flag precipitates from HEK293 extract transiently transfected with praja2-flag, praja2rm. The reaction mixture was denatured, size-fractionated on 7% SDS-PAGE, and analyzed by autoradiography. A fraction of the reaction mixture was immunoblotted with anti-flag antibody (lower panel).

2.8 praja2 controls ERK1/2 signaling

The findings indicate that KSR1 in response to receptor activation becomes a relevant target of the ubiquitin pathway. Given the relevant role of KSR1 in ERK1/2 signalling, we investigated if praja2 modulates RTK-dependent ERK cascade. To this end, we monitored ERK1/2 phosphorylation at its active site (Thr202/Tyr204)in cells stimulated with EGF. As shown in **Figures 17A**and **17B**, in control cells, EGF treatment induced ERK1/2 phosphorylation overtime from stimulation. Expression of praja2rmincreased both basal and EGF-induced ERK phosphorylation, by several fold over control values. Furthermore, genetic knockdown of endogenous praja2 also sustained ERK1/2 phosphorylation, compared to controls (**Figure17C**).

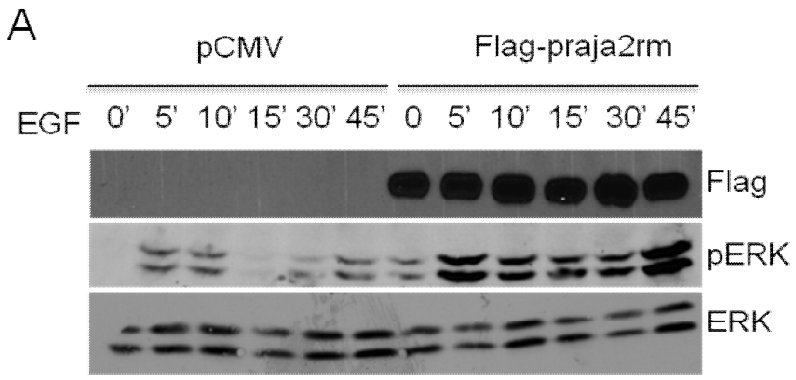
A
pCMV
Flag-praja2rm
EGF
0' 5' 10' 15' 30' 45' 0 5' 10' 15' 30' 45'
Flag
pERK
ERK

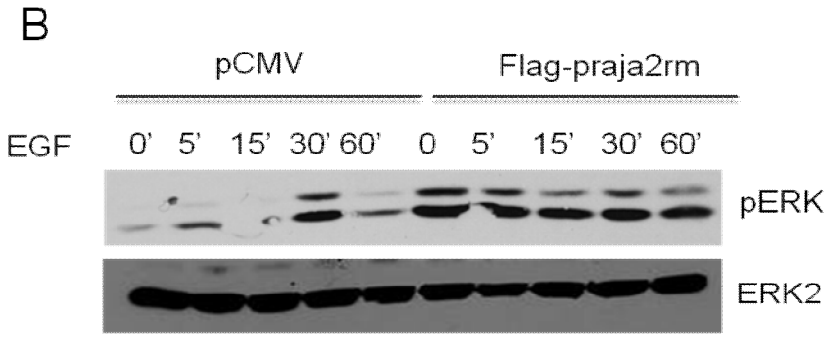
B
pCMV
Flag-praja2rm
EGF
0' 5' 15' 30' 60' 0 5' 15' 30' 60'
pERK
ERK2

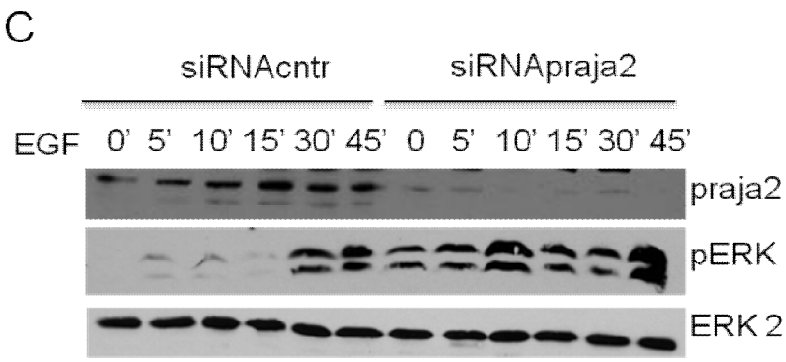

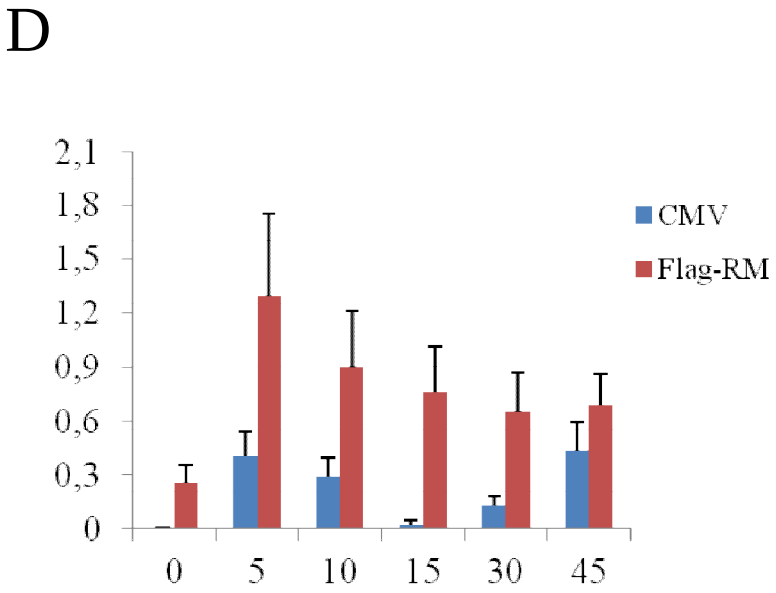

Figure 17: praja2 control ERK1\2 signaling. (**A**) HEK293 or U2OS (**B**) cells were transfected with CMV or Flag-rm. 24 hours after transfection, cells were treated EGF (100ng\ml) for indicate times . Lysates were separated on SDS-page and immunoblotted with anti p-ERK antibody. Anti-flag antibody is used as transfection control and anti-ERK2 asloading control. (**C**) HEK293 cells were transfected with control siRNA or praja2 siRNA. Than they are processed as above.(**D**).Cumulative data of the experiment shown in **A**&**B**.Data are expressed as a mean value ± S.E.M of three independent experiments.

Next, we explored the functional relevance of the praja2 binding to KSR1 in ERK signalling. Cells were pre-treated for 6h with a stearated synthetic peptide spanning the praja2 binding motif of KSR1 (KRS1pep-flag) or with a flag-tagged scrambled peptide (CNTpep-flag). As shown in **Figure 18**, both peptides efficiently accumulated within the treated cells. The cells were then stimulated with EGF. ERK phosphorylation was monitored over a time-point curve. As shown in **Figures 19**, pre-treatment with KSR1pep-flag enhanced both, basal and EGF-induced ERK phosphorylation. The effects of KSR1pep on ERK signalling were replicated in other cell lines (HEK293 and U-87 MG), suggesting a more general role of praja2 in the control of KSR1 pathway.

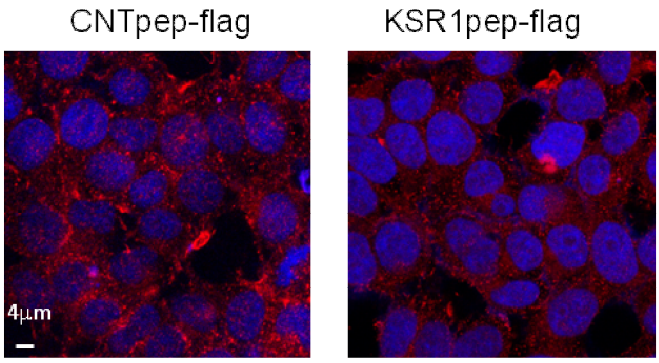

Figure 18. The synthetic peptides accumulate efficiently within the cell. HEK293 cells were treated for 8 hours with a stearated synthetic peptide containing a Flag-tag spanning the praja2 binding motif ofKSR1 (Ksr1pep-flag) or with a flag-tagged scrambled peptide (CNTpep-flag). After cells are subjected to immunostaining with monoclonal anti-flag. Images were collected and analyzed by confocal microscopy. DRAQ5 staining for nuclei detection was used (blu).

A

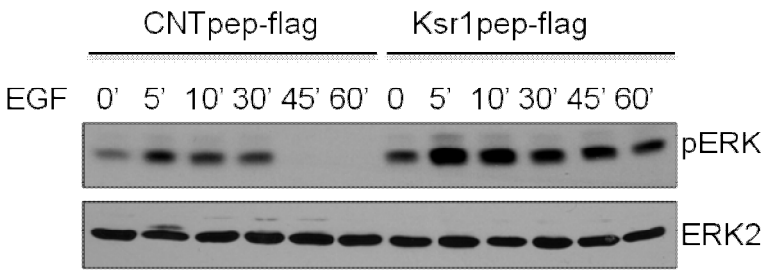

B

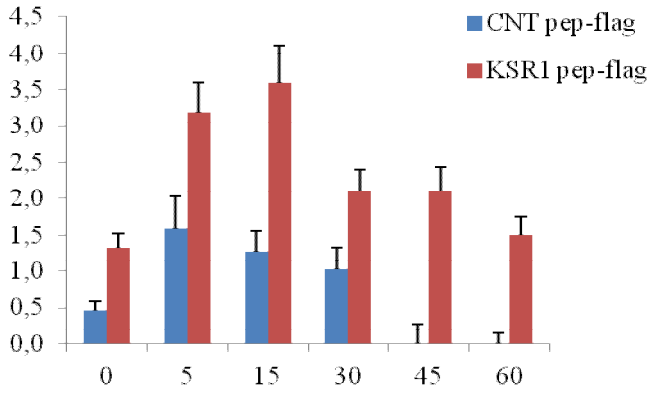

Figure 19: the binding between praja2 and KSR1 is fundamental for ERK1\2 signalling. U2OS cells were pre-trated withCNTpep-flag orKsr1pep-flag .aftercells were treated with EGF (100ng\ml) for indicate times. Lysates were separated on SDS-page and immunoblotted with anti p-ERK antibody. Anti-flag antibody is used as transfection control and anti- ERK2 asloading control.(**B**)Cumulative data of the experiment shown in (**A**).Data are expressed as a mean value ± S.E.M of four independent experiments.

DISCUSSION
AND
CONCLUSION

Here, I report for the first time a new regulatory mechanism of KSR1scaffold through ubiquitination. I found that, in course ofgrowth factors stimulation, KSR1 undergoes to rapid poly-ubiquitination, which eventually leads to attenuation of the ERK pathway. Ubiquitination of KSR1 was induced by EGF. I identified praja2 as the principal E3 ligase responsible of KSR1 ubiquitination.

Signals originated at cell membrane are efficiently transmitted to downstream effectors and rapidly attenuated, eventually leading to resensitization of the pathway. The intricate interplay between ON/OFF state of the signaling pathway gives rise to signaling waves that rapidly propagate throughout the cell, eliciting biological responses that strictly depend on the intensity and frequency of the oscillatory circuits.

In this context KSR1 plays a key role as scaffold protein involved in the propagation and regulation of the mitogenic pathway of MAP kinases.

KSR1 contribution to the regulation of the MAPK signaling is finely tuned because of anauto-regulatory series of phosphorylation/dephosphorylation events on KSR1.

Indeed, phosphorylation on KSR1 byC-TAK1, in resting condition, keeps the scaffold inactive, until a growth stimulus activates PP2A(*Muller j. et al. 2001; Roy F. et al. 2002; Ory S. et al. 2003*).Dephosphorylation of KSR1 by PP2A activates the protein that, in turn, amplifies the MAPK cascade. When the signaling has to be turned off, activated ERK1/2 phosphorylates another site on KSR1, causing the disassembly of the multikinase complex and regulating the temporal duration of the signal. (*McKay et al. 2009*).

The principal mechanism regulating KSR1 activity wasmostly based on phosphorylation. A variety of attenuation mechanisms have been identified, so far (*Alexander Y. et al. 2008 ; Sandra L Harris and Arnold J Levine 2005 ; Errede B. 1996;Dhillon AS. 2007*). In the case of ERK pathway, a negative loop between ERK and KSR1 complex ensures acycle of activation/de-activation process that limits uncontrolled mitogenic signaling. Phosphorylation of KSR1 and B-Raf by locally activated ERK dissociates theKSR1 multi-kinase complex, turning-off theERK pathway (*McKay et al. 2009*). Bi-directional regulation of KSR1 and ERK activity controls the rate, the magnitudo and the persistence of downstream mitogenic pathways.

My work added a novel twist in the ERK cascade, identifying KSR1 as a target of the ubiquitin pathway and further exploring

the regulation of MAPK signal amplitude.

Ubiquitination of KSR1 was rapidly induced by EGF pathway, indicating that there is an even more tight step of regulation between the activation of KSR1 and the inactivation and disassembly of the complex. This paralleled downregulation of ERK1/2 cascade. Interference of praja2 expression/activity or expression of a praja2 mutant carrying mutations within H2-RING domain sites, negatively impacted on KSR1 ubiquitination, enhancing ERK activation and prolonging the wave of downstream signaling. A peptide targeting the praja2 binding interface on KSR1 by preventing Praja2 binding to KSR1 and consequent ubiquitination of the scaffold increased both, basal and ligand-induced ERK phosphorylation. These findings further support the role of praja2 in the negative regulation of KSR1 signaling.

Hence, praja2 acts in response to EGF stimulation in promoting KSR1 ubiquitination and ERK attenuation, pointing to a more general role of praja2 in controlling of the strength and duration of KSR1-ERK cascade (**Figure 20**).

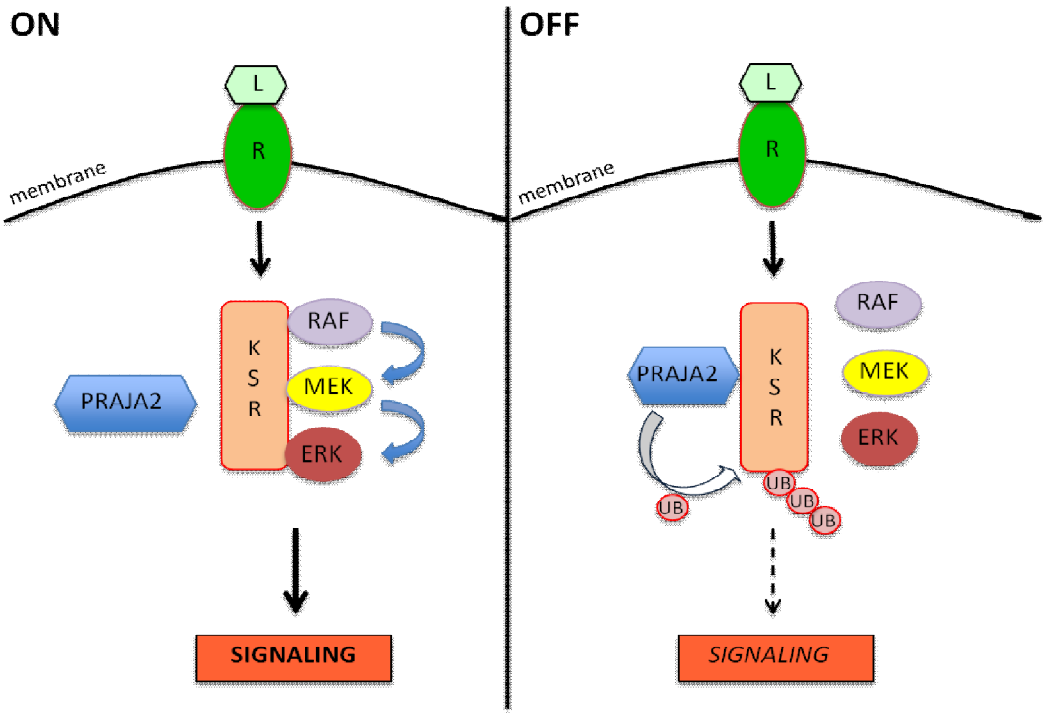

Figure 20. praja2-KSR model. Stimulation of receptors by a ligand that activates KSR1/2, which in turn induce sequential activation of mitogenic kinases (ON). Recruitment of praja2 within the multi-kinase scaffold induces poly-ubiquitination of KSR, and consequent attenuation of the ERK pathway (OFF).

In conclusion, the findings highlight the importance of the praja2-mediated ubiquitination of KSR1 in the control of mitogenic signaling. Exploring further the mechanism(s) regulating ubiquitination of KSR1 in course of growth factor stimulation, and identifying additional praja2 targets in the ERK1/2 cascade will provide essential tools to dissect and manipulate these important signaling pathways.

METHODS

Cell lines. Human embryonic kidney cell line (HEK293), glioblastoma cells (U87MG) and osteosarcoma cells (U2OS) were cultured in Dulbecco modified Eagle's medium containing 10% fetal bovine serum in an atmosphere of 5% CO2

Plasmids and transfection. Vectors encoding the flag-praja2 and GSTpraja2 were purchased from Genecopeia. praja2rm was generated by site-directed mutagenesis, while praja2 deletion mutants and GST-fusions were generated by PCR with specific oligonucleotide primers. PCR products were sub-cloned into the same vector of wild-type praja2cDNA. HA-tagged ubiquitin was provided by Dr Antonio Leonardi (University of Naples, Italy); flag-tagged KSR vectors was provided by Addgene Vector Database.GST-fusion peptides were generated by Eduard Stefan (University of Innsbruck);SMART pool siRNAs targeting coding regions were purchased from Dharmacon. The following are the siRNA sequences (Thermo Scientific) targeting human praja2: sequence 1: 5′GAAGCACCCUAAACCUUGA-3′ ;

Sequence2:5′AGACUGCUCUGGCCCAUUU-3′;

sequence 3: 5′-GCAGGAGGGUAUCAGACAA-3′;

sequence 4: 5′-GUUAGAUUCUGUACCAUUA-3′.

The siRNAs were transiently transfected using Lipofectamine 2000 (Invitrogen) at a final concentration of 100 pmol/ml of culture medium.

Antibodies and chemicals. Rabbit polyclonal antibodies directed against KSR1 (immunoblot dilution 1:1000, immunostaining dilution 1:100) and Phospho44/42 MAPK (P-ERK1/2)(immunoblot dilution 1:1000) were bought from Cell Signaling; ERK2(immunoblot dilution 1:8000) and glutathione S-transferase (GST)(immunoblot dilution 1:8000) from Santa Cruz; α−tubulin (immunoblot dilution 1:8000), flag (immunoblot dilution 1:4000, immunostaining dilution 1:400, immunoprecipitation dilution 1:200) and myc epitope (immunoblot dilution 1:1000) from Sigma; hemaglutinin epitope (immunoblot dilution 1:1000) (HA.11) from Covance; Rabbit polyclonal antibodies directed against praja2 (immunoblot dilution 1:1000,immunostainingdiluition 1:400) was purchased from Bethyl. Fluorescein- or rhodamine-tagged anti-rabbit and anti-mouse IgG secondary antibodies were purchased from Technogenetics.EGF (used 100ng/ml) were purchased from Sigma.

Western Blot Analysis. Cells were washed twice with phosphate-buffered saline and lysed in saline buffer-1% Triton-X 100 (NaCl, 150 mM; Tris-HCl, 50 mM, pH8; EDTA, 5 mM) or, for immunoprecipitation assay, in saline buffer 0.5% NP40 (50mMTris-HCl, pH 7.4, 0.15MNaCl, 100 mM EDTA,0.5% NP40) containing aprotinin (5 μg/ml), leupeptin (10 μg/ml), pepstatin (2 μg/ml), 0.5 mM PMSF, 2 mM orthovanadate, and 10 mM NaF.The lysates were cleared by centrifugation at 15,000 g for 10 min. An aliquote of whole cell lysate (WHL) (100 μg) were resolved on sodium dodecyl sulfate polyacrylamide gel (SDS-PAGE) and transferred on nitrocellulose membrane (Biorad, Milan, Italy) for 3 h. Filters were blocked for 1 h at room temperature in Tween-20 Phosphate buffer saline (TPBS) (PBS- Sigma, 0,1% Tween 20, pH 7.4) containing 5% non-fat dry milk. Blots were then incubated O/N with primary antibody. Blots were washed three times with TPBS buffer and then incubated for 1 h with secondary antibody (peroxidase-coupled anti-rabbit (GE-Healthcare) in TPBS. Reactive signals were revealed by enhanced ECL Western Blotting analysis system (Roche).

Immunoprecipitation and pull-down assay. Cells were homogenized inlysis buffer described above.Cell lysates (1.5 mg) were immunoprecipitated with the indicated antibodies. An aliquot of cell lysate (100 μg) or immunoprecipitated were resolved by SDS-PAGE gel and transferred to Protran membrane. The immunoblot analysis was performed as previously described.GST fusions were expressed and purified from BL21 (DE3) pLysS cells. 20 μl of GST or GST-praja2 beads were incubated with 2 mg of cell lysate or with in vitro translated [35S]-labeled KSR1 in 200 μllysis buffer (150 mMNaCl, 50 mMTris-HCl pH 7.5, 1 mM EDTA, 0.5% triton X-100) in rotation at 4 °C overnight. Pellets were washed four times in lysis buffer supplemented with NaCl (0.4 M final concentration) and eluted in Laemmli buffer. Eluted samples were resolved on8%-SDS PAGE gel, transferred to nitrocellulose membranes and immunoblotted with the indicated antibody. Pull down between GST-control peptide or GST-KSR1 peptide and overexpressed flag-praja2cells was performed as described above.

***In vitro* ubiquitination assay.**$^{[35S]}$-labeled KSR1was synthesized in vitro using TnT quick coupled transcription/translation system (Promega) in the presence of 45μCi of [35S]-labeled methionine. The ubiquitination assay was performed in buffer containing 50 mM Tri-HCl pH 7.5, 0.6 Mmdithiothreitol, 5mM MgCl2, supplemented with recombinant his-ubiquitin (2.5 μg/μl), 2 mM

ATP, E1 (1.5 ng/µl) (Affinity Research, Exeter, UK), purified E2 (10 ng/µl) (UbcH5b) in the presence or absence of agarose beads-bound praja2-flag or its mutants immunoprecipitated from cell lysates. The reaction mixture was incubated at 30oC for 90 min, then stopped with Laemmli buffer and resolved on 8% SDS-PAGE. Ubiquitination products were visualized by autoradiography.

Confocal microscopy and image analysis. Cells were plated on poly-L-lysine (10µg/ml) coated glass cover slips. Growing or peptides-treated cells were rinsed with PBS and fixed in 3% paraformaldehyde for 20 min. After permeabilization with 0.5% Triton X-100 in PBS for 5 min, the cells were incubated with 1× PBS, 0.1 mg/ml bovine serum albumin for 60 min at room temperature. Double immunofluorescence was carried out with the following antibodies: anti-praja2 (1:400) and anti-KSR1 (1:100) or flag-tag (1:400) antibodies. Fluorescein- or rhodamine-tagged anti-rabbit and anti-mouse IgG (Technogenetics) secondary antibodies were used.. Immunofluorescence was visualized using a Zeiss LSM 510 Meta argon/krypton laser scanning confocal microscope. Quantification of the immunofluorescent images and correlation (Pearson's) coefficient were calculated by Image-J software.

KSR1-Peptides treatment. Growing or, were described, serum-deprived cells were treated with 1 µM of scramble peptide (cnt-pep) or KSR-peptide (KSR-pep) for 9 hours before stimulation.

The following are the peptides sequences:

scramble peptide (cnt-pep) =

stearic group-FLQWADESRPSFLLMDYDKDDDKD

KSR1 peptide (KSR-pep)=

stearic group-WAFDLQERPSFSLLMDDYKDDDDK

Statistics. All data are presented as mean ± SEM and “n” indicates the number of slices. Statistical significance was evaluated by unpaired Student's t test. Statistical significance was set at $p < 0.05$.

REFERENCES

Alexander Y. Mitrophanov and Eduardo A. Groisman Positive feedback in cellular control systems Bioessays. 2008 Jun; 30(6): 542–555. doi: 10.1002/bies.20769 Review.

Amerik AY, Hochstrasser M. Mechanism and function of deubiquitinating enzymes. Biochim Biophys Acta. 2004 Nov 29;1695(1-3):189-207.

Boulton TG, Nye SH, Robbins DJ, Ip NY, Radziejewska E, Morgenbesser SD, DePinho RA, Panayotatos N, Cobb MH, Yancopoulos GD 1991 ERKs: a family of protein-serine/threonine kinasesthat are activated and tyrosine phosphorylated in responseto insulin and NGF. Cell 65:663–675

Brommage R, Desai U, Revelli JP, Donoviel DB, Fontenot GK, Dacosta CM, Smith DD, Kirkpatrick LL, Coker KJ, Donoviel MS, Eberhart DE, Holt KH, Kelly MR, Paradee WJ, Philips AV, Platt KA, Suwanichkul A, Hansen GM, Sands AT, Zambrowicz BP, Powell DR. High-throughput screening of mouse knockout lines identifies true lean and obese phenotypes.Obesity (Silver Spring). 2008 Oct.

Cacace, A.M., Michaud, N.R., Therrien, M., Mathes, K., Copeland, T., Rubin, G.M. and Morrison, D.K. 1999. Identification of constitutive and ras-inducible phosphorylation sites of KSR: implications for 14-3-3 binding, mitogen-activated protein kinase binding, and KSR overexpression. Mol. Cell. Biol

Cantara S, D'Angeli F, Toti P, Lignitto L, Castagna MG, Capuano S, Prabhakar BS, Feliciello A, Pacini F. Expression of the ring ligase PRAJA2 in thyroid cancer. J Clin Endocrinol Metab. 2012 Nov;97(11):4253-9. doi: 10.1210/jc.2012-2360. Epub 2012 Sep 4.

Choi KY1, Satterberg B, Lyons DM, Elion EA. Ste5 tethers multiple protein kinases in the MAP kinase cascade required for mating in S. cerevisiae. Cell. 1994 Aug 12;78(3):499-512.

Ciechanover A. (1998) The ubiquitin-proteasome pathway: on protein death and cell life.EMBO J. 17 (24), 7151–7160.

Copik AJ1, Baldys A2, Nguyen K3, Sahdeo S1, Ho H3, Kosaka A3, Dietrich PJ3, Fitch B3, Raymond JR2, Ford AP1, Button D1, Milla ME1. 2015 Isoproterenol Acts as a Biased Agonist of the Alpha-1A-Adrenoceptor that Selectively Activates the MAPK/ERK Pathway.

Costanzo-Garvey, D.L., Pfluger, P.T., Dougherty, M.K., Stock, J.L., Boehm, M., Chaika, O., Fernandez, M.R., Fisher, K., Kortum, R.L., Hong, E.G. et al. 2009 KSR2 is an essential regulator of AMP kinase, energy expenditure, and insulin sensitivity. Cell Metab.

Daaka Y, Luttrell LM, Lefkowitz RJ 1997 Switching of the coupling of the b2-adrenergic receptor to different G proteins by protein kinase A. Nature 390:88–91

Denouel-Galy, A., Douville, E.M., Warne, P.H., Papin, C., Laugier, D., Calothy, G., Downward, J. and Eychene, A. 1998 Murine Ksr interacts with MEK and inhibits Ras-induced transformation. Curr. Biol.

Dhanasekaran DN1, Kashef K, Lee CM, Xu H, Reddy EP.Scaffold proteins of MAP-kinase modules. Oncogene. 2007 May 14;26(22):3185-202.

Dhillon AS, von Kriegsheim A, Grindlay J, Kolch W. Phosphatase and feedback regulation of Raf-1 signaling. Cell Cycle. 2007 Jan 1;6(1):3-7. Epub 2007 Jan 9. Review.

Dougherty MK, Ritt DA, Zhou M, Specht SI, Monson DM, Veenstra TD, Morrison DK. KSR2 is a calcineurin substrate that promotes ERK cascade activation in response to calcium signals. Mol Cell. 2009 Jun 26.

Errede B, Ge QY. Feedback regulation of map kinase signal pathways. Philos Trans R Soc Lond B Biol Sci. 1996 Feb 29;351(1336):143-8; discussion 148-9. Review.

Ferrell Jr JE 1996 Tripping the switch fantastic: how a protein kinase cascade can convert graded inputs into switch-like outputs.Trends Biol Sci 21:460–466

Freemont PS (1993). The RING finger: a novel protein sequence motif related to the zinc finger. Ann NY Acad Sci 684: 174-192.

Goettel, J.A., Liang, D., Hilliard, V.C., Edelblum, K.L., Broadus, M.R., Gould, K.L., Hanks, S.K. and Polk, D.B. 2011 KSR1 is a functional protein kinase capable of serine autophosphorylation and direct phosphorylation of MEK1. Exp. Cell Res.

Grabbe, C., Husnjak, K. & Dikic, I. The spatial and temporal organization of ubiquitin networks. *Nat. Rev. Mol. Cell Biol.* 12, 295–307 (2011).

Grewal SS, Horgan AM, York RD, Withers GS, Banker GA, Stork PJ 2000 Neuronal calcium activates a Rap1 and B-Raf signaling pathway via the cyclic adenosine monophosphate-dependent protein kinase. J Biol Chem 275:3722–3728

Hafner S, Adler HS, Mischak H, Janosch P, Heidecker G, Wolfman A, Pippig S, Lohse M, Ueffing M, KolchW1994 Mechanism of inhibition of Raf-1 by protein kinase A. Mol Cell Biol 14:6696–6703

Hershko A., and Ciechanover A. (1998) The ubiquitin system. Annu Rev Biochem. 1998;67:425-79. Review.

Huang C-YF, Ferrell Jr JE 1996 Ultrasensitivity in the mitogen activated protein kinase cascade. Proc Natl Acad SciUSA93:10078–10083

Huang OW, Cochran AG. Regulation of deubiquitinase proteolytic activity. Curr Opin Struct Biol. 2013 Dec;23(6)

Joazeiro C.A., and Weissman A.M. (2000) RING finger proteins: mediators of ubiquitin ligase activity. Cell. Sep 1;102(5):549-52. Review.

Kikuchi A, Williams LT 1996 Regulation of interaction of ras p21 with RalGDS and Raf-1 by cyclic AMP-dependent protein kinase. J Biol Chem 271:588–59

Kitada T., Asakawa S., Hattori N., Matsumine H., Yamamura Y., Minoshima S., Yokochi M., Mizuno Y., Shimizu N. (1998). Mutations in the parkin gene cause autosomal recessive juvenile parkinsonism. Nature 392: 605–608.

Kolch W.Coordinating ERK/MAPK signalling through scaffolds and inhibitors. Nat Rev Mol Cell Biol. 2005 Nov;6(11):827-37.

Koveal D, Schuh-Nuhfer N, Ritt D, Page R, Morrison DK, Peti W.A CC-SAM, for coiled coil-sterile α motif, domain targets the scaffold KSR-1 to specific sites in the plasma membrane. Sci Signal. 2012 Dec 18

Levchenko A1, Bruck J, Sternberg PW.Scaffold proteins may biphasically affect the levels of mitogen-activated protein kinase signaling and reduce its threshold properties. Proc Natl Acad Sci U S A. 2000 May 23;97(11):5818-23.

Lewis TS, Shapiro PS, Ahn NG 1998 Signal transduction through MAP kinase cascades. Adv Cancer Res 74:49–139

Lignitto L, Arcella A, Sepe M, Rinaldi L, Delle Donne R, Gallo A, Stefan E, Bachmann VA, Oliva MA, Tiziana Storlazzi C, L'Abbate A, Brunetti A, Gargiulo S, Gramanzini M, Insabato L, Garbi C, Gottesman ME, Feliciello A. Proteolysis of MOB1 by the ubiquitin ligase praja2 attenuates Hippo signalling and supports glioblastoma growth. Nat Commun. 2013;4:1822. doi: 10.1038/ncomms2791.

Lignitto L, Carlucci A, Sepe M, Stefan E, Cuomo O, Nisticò R, Scorziello A, Savoia C, Garbi C, Annunziato L, Feliciello A. Control of PKA stability and signalling by the RING ligase praja2. Nat Cell Biol. 2011 Apr;13(4):412-22. doi: 10.1038/ncb2209. Epub 2011 Mar 20.

Lorick K.L., Jensen J.P., Fang S., Ong A.M., Hatakeyama S. and Weissman A.M. (1999) RING fingers mediate ubiquitin-conjugating enzyme (E2)-dependent ubiquitination. Proc Natl Acad Sci U S A. Sep 28;96(20):11364-9.

Marcus S1, Polverino A, Barr M, Wigler M. Complexes between STE5 and components of the pheromone-responsive mitogen-activated protein kinase module. Proc Natl Acad Sci U S A. 1994 Aug 2;91(16):7762-6.

Marshall CJ1. Specificity of receptor tyrosine kinase signaling: transient versus sustained extracellular signal-regulated kinase activation. Cell. 1995 Jan 27;80(2):179-85.

Matthew D. Brown and David B. Sacks. 2009 Protein Scaffolds in MAP Kinase Signalling

Mattsson K., Pokrovskaja K., Kiss C., Klein G., and Szekely L. (2001). Proteins associated with the promyelocytic leukemia gene product (PML)-containing nuclear body move to the nucleolus upon inhibition of proteasome-dependent protein degradation. Proc. Natl. Acad. Sci. USA 98: 1012–1017.

McKay MM1, Ritt DA, Morrison DK. Signaling dynamics of the KSR1 scaffold complex. Proc Natl Acad Sci U S A. 2009 Jul 7;106(27):11022-7. doi: 10.1073/pnas.0901590106. Epub 2009 Jun 18.

McKay, M.M., Ritt, D.A. and Morrison, D.K. 2009 Signaling dynamics of the KSR1 scaffold complex. Proc. Natl. Acad. Sci. U.S.A.

Michaud,N.R.,Therrien,M.,Cacace, A.,Edsall,L.C.,Spiegel,S.,Rubin, G.M.,et al 1997. KSR stimulates Raf-1 activity in a kinase- independent manner. *Proc.Natl. Acad.Sci.U.S.A.* 94, 12792–12796.

Mischak H, Seitz T, Janosch P, Eulitz M, Steen H, Schellerer M, Philipp A, Kolch W 1996 Negative regulation of Raf-1 by phosphorilation of serine 621. Mol Cell Biol 16:5409–5418

Müller,J.,Ory,S.,Copeland,T., Piwnica-Worms,H.,andMorrison, D.K. 2001. C-TAK1 regulates Ras signaling by phosphorylating the MAPK scaffold,KSR1. *Mol.Cell* 8, 983–993.

Murphy LO, Blenis J. MAPK signal specificity: the right place at the right time.Trends in Biochemical Sciences 2006;31:268–75.

Murphy LO1, Blenis J. MAPK signal specificity: the right place at the right time. Trends Biochem Sci. 2006 May;31(5):268-75. Epub 2006 Apr 17.

Nakayama M., Miyake T., Gahara Y., Ohara O., and Kitamura T. (1995). A novel RING-H2 motif protein downregulated by axotomy: its characteristic localization at the postsynaptic density of axosomatic synapse. J. Neurosci. 15: 5238–5248.

Nguyen, A., Burack, W.R., Stock, J.L., Kortum, R., Chaika, O.V., Afkarian, M., Muller, W.J., Murphy, K.M., Morrison, D.K., Lewis, R.E. et al. 2002 Kinase suppressor of Ras (KSR) is a scaffold which facilitates mitogen-activated protein kinase activation *in vivo*. Mol. Cell. Biol. 22, 3035–3045

Ohara 0., Teraoka H. (1987). Anomalous behavior of human leukocvte interferon subtypes on polyacrylamide gel electrophoresis in the presence of dodecyl sulfate. FEBS Lett 211:78-82.

Ory, S., Zhou, M., Conrads, T.P., Veenstra, T.D. and Morrison, D.K. 2003 Protein phosphatase 2A positively regulates Ras signaling by dephosphorylating KSR1 and Raf-1 on critical 14-3-3 binding sites. Curr. Biol. 13, 1356–1364

Pagès G, Guérin S, Grall D, Bonino F, Smith A, Anjuere F, et al. Defective thymocyte maturation in p44 MAP kinase (Erk 1) knockout mice. Science 1999;286:1374–7.

Pearson G, Robinson F, Beers Gibson T, Xu BE, Karandikar M, Berman K, Cobb MH. 2001 Mitogen-activated protein (MAP) kinase pathways: regulation and physiological functions. Endocr Rev;22(2):153–183.

Perlson E1, Michaelevski I, Kowalsman N, Ben-Yaakov K, Shaked M, Seger R, Eisenstein M, Fainzilber M. Vimentin binding to phosphorylated Erk sterically hinders enzymatic dephosphorylation of the kinase. J Mol Biol. 2006 Dec 15;364(5):938-44. Epub 2006 Sep 27.

Ping Yu, Yiwang Chen, Danilo A. Tagle, and Tao Cai (2002) PJA1, Encoding a RING-H2 Finger Ubiquitin Ligase, Is a Novel Human X Chromosome Gene Abundantly Expressed in Brain. Genomics. 79, 869-874.

Roskoski R Jr ERK1/2 MAP kinases: structure, function, and regulation. Pharmacol Res. 2012 Aug;66(2):105-43. doi: 10.1016/j.phrs.2012.04.005. Epub 2012 Apr 27.

Roy F, Therrien M. MAP kinase module: the Ksr connection. Curr Biol. 2002 Apr 30

Sakamaki J, Fu A, Reeks C, Baird S, Depatie C, Al Azzabi M, Bardeesy N, Gingras AC, Yee SP, Screaton RA. Role of the SIK2-p35-PJA2 complex in pancreatic β-cell functional compensation. Nat Cell Biol. 2014 Mar;16(3):234-44. doi: 10.1038/ncb2919.

Sandra L Harris and Arnold J Levine The p53 pathway: positive and negative feedback loops *Oncogene* (2005) 24, 2899–2908. doi:10.1038/sj.onc.1208615 Review.

Sepe M, Lignitto L, Porpora M, Delle Donne R, Rinaldi L, Belgianni G, Colucci G, Cuomo O, Viggiano D, Scorziello A, Garbi C, Annunziato L, Feliciello A. Proteolytic control of neurite outgrowth inhibitor NOGO-A by the cAMP/PKA pathway. Proc Natl Acad Sci U S A. 2014 Nov 4;111(44):15729-34. doi: 10.1073/pnas.1410274111. Epub 2014 Oct 20.

Stefan E, Mohan K. Malleshaiah, Billy Breton, Po Hien Ear,Verena Bachmann,Michael Beyermann,Michel Bouvier, and Stephen W. Michnick PKA regulatory subunits mediate synergy among conserved G-protein-coupled receptor cascades Published online 2011 Dec 20.

Stork O., Stork S., Pape H. C., and Obata K. (2001). Identification of genes expressed in the amygdala during the formation of fear memory. Learn. Mem. 8: 209– 19.

Vakiani E, Solit DB. KRAS and BRAF: drug targets and predictive biomarkers. Journal of Pathology 2011;223:219–29.

Vossler MR, Yao H, York RD, Pan MG, Rim CS, Stork PJ 1997 cAMP activates MAP kinase and Elk-1 through a B-Raf- and Rap1-dependent pathway. Cell 89:73–82

Wellbrock C, Karasarides M, Marais R. Nat Rev Mol Cell Biol 2004; The RAF proteins take centre stage. 5(11):875–885.

Witzel F, Maddison L, Blüthgen N. How scaffolds shape MAPK signaling: what we know and opportunities for systems approaches. Front Physiol. 2012 Dec 21;3:475. doi: 10.3389/fphys.2012.00475. eCollection 2012

Witzel F1, Maddison L, Blüthgen N How scaffolds shape MAPK signaling: what we know and opportunities for systems approaches. Front Physiol. 2012 Dec 21;3:475. doi: 10.3389/fphys.2012.00475. eCollection 2012.

Wu J, Dent P, Jelinek T, Wolfman A, Weber MJ, Sturgill TW 1993 Inhibition of the EGF-activated MAP kinase signaling pathway by adenosine 39,59-monophosphate. Science 262:1065–1068

Xing, H.R., Lozano, J. and Kolesnick, R. 2000. Epidermal growth factor treatment enhances the kinase activity of kinase suppressor of Ras. J. Biol. Chem.

Yan, F. and Polk, D.B. 2001 Kinase suppressor of ras is necessary for tumor necrosis factor αactivation of extracellular signal-

regulated kinase/mitogen-activated protein kinase in intestial epithelial cells. Cancer Res.

Yan, F., John, S.K., Wilson, G., Jones, D.S., Washington, M.K. and Polk, D.B. 2004. Kinase suppressor of Ras-1 protects intestinal epithelium from cytokine-mediated apoptosis during inflammation. J. Clin. Invest. 114, 1272–1280

Yao Y, Li W, Wu J, Germann UA, Su MS, Kuida K, et al. Extracellular signal-regulated kinase 2 is necessary for mesoderm differentiation. Proceedings of the National Academy of Sciences of the United States of America 2003;100:12759–64.

York RD1, Yao H, Dillon T, Ellig CL, Eckert SP, McCleskey EW, Stork PJ. Rap1 mediates sustained MAP kinase activation induced by nerve growth factor. Nature. 1998 Apr 9;392(6676):622-6.

Zhang H, Koo CY, Stebbing J, Giamas G. The dual function of KSR1: a pseudokinase and beyond. Biochem Soc Trans. 2013 Aug

Zhang, Y., Li, X., Carpinteiro, A., Goettel, J.A., Soddemann, M. and Gulbins, E. 2011. Kinase suppressor of Ras-1 protects against pulmonary *Pseudomonas aeruginosa* infections. Nat. Med.

nature COMMUNICATIONS

ARTICLE

Received 22 Aug 2012 | Accepted 22 Mar 2013 | Published 7 May 2013

DOI: 10.1038/ncomms2791 OPEN

Proteolysis of MOB1 by the ubiquitin ligase praja2 attenuates Hippo signalling and supports glioblastoma growth

Luca Lignitto[1,*], Antoniella Arcella[2,*], Maria Sepe[1], Laura Rinaldi[1], Rossella Delle Donne[1], Adriana Gallo[1], Eduard Stefan[3], Verena A. Bachmann[3], Maria A. Oliva[2], Clelia Tiziana Storlazzi[4], Alberto L'Abbate[4], Arturo Brunelli[5], Sara Gargiulo[5], Matteo Gramanzini[5], Luigi Insabato[5], Corrado Garbi[1], Max E. Gottesman[6] & Antonio Feliciello[1]

Human glioblastoma is the most frequent and aggressive form of brain tumour in the adult population. Proteolytic turnover of tumour suppressors by the ubiquitin–proteasome system is a mechanism that tumour cells can adopt to sustain their growth and invasiveness. However, the identity of ubiquitin–proteasome targets and regulators in glioblastoma are still unknown. Here we report that the RING ligase praja2 ubiquitylates and degrades Mob, a core component of NDR/LATS kinase and a positive regulator of the tumour-suppressor Hippo cascade. Degradation of Mob through the ubiquitin–proteasome system attenuates the Hippo cascade and sustains glioblastoma growth *in vivo*. Accordingly, accumulation of praja2 during the transition from low- to high-grade glioma is associated with significant downregulation of the Hippo pathway. These findings identify praja2 as a novel upstream regulator of the Hippo cascade, linking the ubiquitin proteasome system to deregulated glioblastoma growth.

[1] Dipartimento di Medicina Molecolare and Biotecnologie Mediche, University Federico II and IEOS-CNR, 80131 Naples, Italy. [2] I.R.C.C.S Neuromed Località Camerelle, Pozzilli, Italy. [3] Institute of Biochemistry and Center for Molecular Biosciences Innsbruck (CMBI), Innrain 80/82, A-6020 Innsbruck, Austria. [4] Dipartimento di Biologia, University of Bari, 70126 Bari, Italy. [5] Dipartimento di Scienze Biomediche Avanzate and Istituto di Biostrutture e Bioimmagini Consiglio Nazionale delle Ricerche (IBB CNR), CEINGE Biotecnologie Avanzate Scarl, University Federico II, 80131 Naples, Italy. [6] Institute of Cancer Research, Columbia University Medical Center, New York, New York 10032, USA. * These authors contributed equally to this work. Correspondence and requests for materials should be addressed to A.F. (email: feliciel@unina.it).

Gliomas are malignant brain tumours that arise from glial cells. They are the most common primary proliferative disorders of the central nervous system in the adult population. They include a heterogenous group of tumours that are characterized by a variety of differentiation and malignant phenotypes[1]. Glioblastoma multiform (GBM), which represents about 50% of total gliomas, is the most aggressive form of brain tumour, with a very poor median survival after initial diagnosis[2]. High-grade gliomas are thought to derive from low-grade variants. These variants undergo sequential genetic alterations, giving rise to cell populations with more invasive behaviour, greater activation of mitogenic pathways and loss of cell cycle control[3]. Transition from low- to high-grade glioma is also marked by activation of the hypoxia pathway, which promotes blood vessel formation, clonal evolution and consequent tumour expansion[4–10].

At the molecular level, GBMs are characterized by a wide array of genetic and epigenetic alterations. The pathogenic role of these abnormalities in glioma development has been functionally confirmed by *in vivo* studies. Thus, inactivation of tumour suppressor genes (p53), constitutive activation of membrane receptors (EGFR), induction of prosurvival pathways (PI3K/Akt), aberrant gene transcription and metabolic dysfunction have all been linked mechanistically to the development and progression of GBMs[3,11–17]. These abnormalities underlie the high recurrence rate and resistance of these tumours to current therapies. Although major advances have been made recently in identifying the relevant players that regulate GBM growth and development, so far the key mechanisms and the genes responsible of glial neoplastic transformation remain subjects of active investigation.

The ubiquitin–proteasome system (UPS) is emerging as an important control mechanism of cell metabolism, growth and survival. The UPS is the principal pathway for eliminating unneeded or damaged proteins[18]. UPS couples ubiquitylation of a target protein to its proteolytic cleavage. Ubiquitylation is a multistep process that involves the sequential action of three enzymes: activating enzymes (E1), conjugating enzymes (UBCs or E2s) and ligases (E3s). E3-ubiquitin ligases fall into two main classes characterized by a HECT domain or a RING domain[19,20]. HECT domain E3 ligases act catalytically to form a thioester intermediate during ubiquitin transfer to substrate, whereas RING E3 ligases serve as a scaffold that brings together the substrate and the E2 ligase. praja2 belongs to a growing family of mammalian RING E3-ubiquitin ligases widely expressed in cells and several tissues, including brain[21,22]. praja2 finely tunes the stability of intracellular substrates and has a significant role in critical aspects of cell signalling[23]. During cAMP stimulation, praja2 promotes ubiquitin-dependent proteolysis of the inhibitory protein kinase A (PKA) regulatory (Rs) subunits, sustaining downstream PKA signalling and significantly impacting on gene transcription and neuronal activity[24]. However, the role of praja2 in tumour cell growth and the relevant molecular targets involved are unknown.

Here, we report a mechanism of signal attenuation in human GBM based on proteolytic turnover of components of the tumour-suppressor Hippo pathway. We find that praja2 directly binds to and ubiquitylates Mps one binder 1 (MOB1), a component and core effector of the Hippo pathway. Degradation of ubiquitylated MOB1 by the proteasome inhibits this signalling cascade, favoring GBM growth. By manipulating the levels and activity of praja2, we have uncovered a pivotal role of this ligase in glial cell tumorigenesis.

Results

praja2 interacts with Hippo pathway component MOB1. To gain insight into praja2 function, we performed a yeast two-hybrid screening using a human brain cDNA library and the C-terminal domain of praja2 as bait. Two independent clones encoding the C-terminus of MOB1 co-activator protein were isolated. MOB1 is a core component of the nuclear-Dbf2-related kinase 1 (NDR1)/LATS (large tumour suppressor) kinase complex that acts as a downstream effector of the Hippo pathway. Hippo is an evolutionally conserved protein kinase cascade that has a fundamental role in the control of cell growth and organ size[25].

First, we set out to verify the direct interaction of MOB1 and praja2 detected in the two-hybrid screen. We confirmed that praja2 directly binds to MOB1 *in vitro*. A fusion protein carrying full-length praja2 fused to the C-terminus of glutathione *S*-transferase polypeptide (GST) coprecipitated *in vitro*-translated [^{35}S]-labelled MOB1 (Supplementary Fig. S1a). Reciprocal experiments using purified, recombinant GST-MOB1 confirmed interaction with praja2 expressed in HEK293 cells (Supplementary Fig. S1b). Co-immunoprecipitation assays showed that exogenous flag-praja2 and co-expressed HA-MOB1 formed a stable complex (Fig. 1a). As praja2 promotes degradation of MOB1 (see below), we treated the cells for 12 h with the proteasome inhibitor MG132 before harvesting in order to see the complex. Deletion mutagenesis and binding assays identified residues 531–630 as the praja2 segment that interacts with MOB1 (Fig. 1a). Next, we demonstrated this interaction *in vivo* by isolating endogenous praja2/MOB1 complex from cell lysates. LATS1 kinase was also present in the praja2 precipitates (Fig. 1b). *In vitro* binding assays showed that MOB1A is required for praja2–LATS1 interaction (Fig. 1c). The MOB1-binding domain relies within a region of praja2 that is also involved in PKA R interaction. Therefore, we tested if PKA binding to praja2 was affected by MOB1. The results indicate that this is, indeed, the case. Thus, PKA–praja2 interaction was significantly reduced by coexpression of exogenous MOB1A (Supplementary Fig. S2a,b). As consequence, PKA inactive holoenzyme accumulates in cells expressing MOB1A (Supplementary Fig. S2c,d).

To map the binary interaction sites, we performed a peptide spotting experiment, first to confirm interaction *in vitro* and second to determine specific amino acids required for praja2 binding to MOB1A. Overlapping 25-mer peptides derived from human MOB1 were spotted onto a membrane and overlaid with purified GST-praja2$^{531–631}$ fusion proteins as previously described[26]. We identified one potential binding site located at the C-terminus of MOB1A with the binding motif ILKRL as the core region for binding (Fig. 1d).

To test if the C-terminal region of praja2 (amino acids 531–708) interacts with MOB1A in a cellular context, we applied a protein-fragment complementation assay (PCA) based on the 'Venus' mutant of the yellow fluorescent protein (YFP)[27]. This assay is independent of a continuous stimulus; the irreversibility of this Venus-YFP PCA will trap transient protein complexes directly in the living cell[25]. Binding of the two proteins brings the unfolded fragments of the YFP-based reporter protein into proximity, allowing for folding and reconstitution of the fluorescent reporter to localize binary protein complexes *in vivo*[27] (Fig. 1e, upper panel). As shown in Fig. 1e (lower panels), we were able to detect MOB1A:praja2-CTD (praja2 C-terminal domain, residues 531–708) complexes *in vivo*. In contrast to the mainly nuclear localisation of the positive control for the protein:protein interaction of a leucine zipper dimer (Zip:Zip), the MOB1A homodimer was cytoplasmic[28]. Accordingly, we detected cytoplasmic complexes between MOB1A-VenF[2] and praja2-CTD N-terminal tagged with YFP PCA VenF[1] (Fig. 1e). *In situ* immunostaining analysis of U87MG glioblastoma cells revealed partial colocalization of endogenous praja2 and MOB1. Overlapping signals were detected at the perinuclear region and

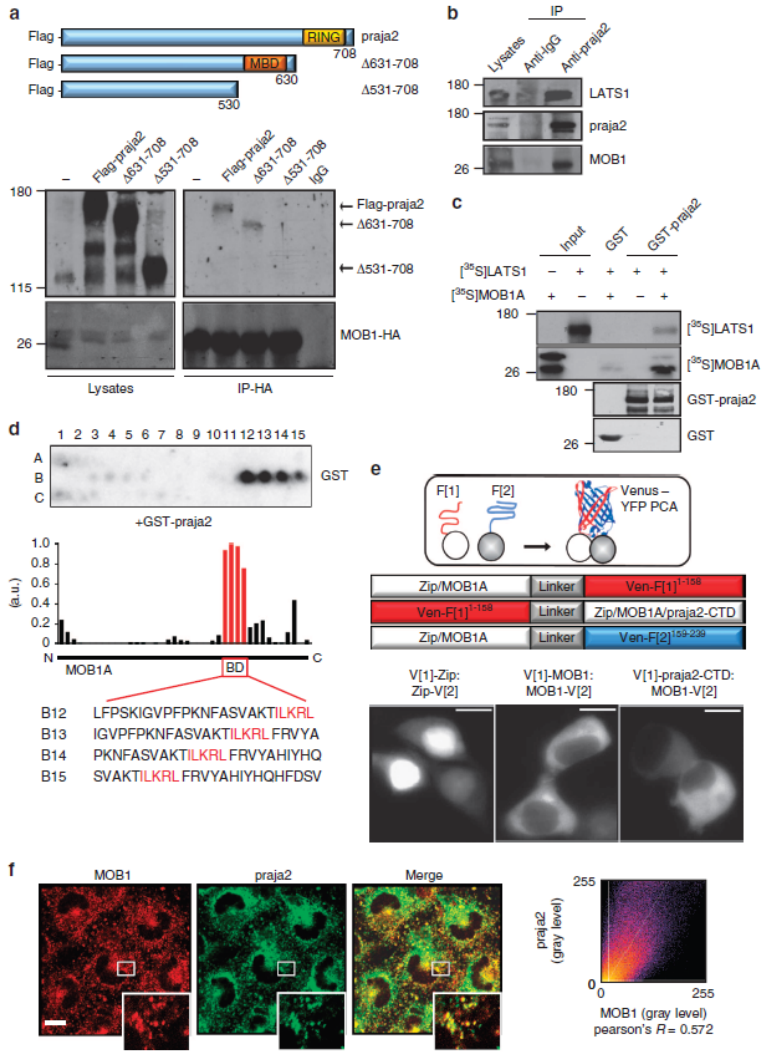

Figure 1 | praja2 forms a complex with MOB1. (**a**) Schematic representation of the praja2 constructs used (upper panel). HEK293 cells were transiently transfected with HA-MOB1A and flag-tagged praja2 (either wild-type or deletion mutants). Cells were treated for 12 h with MG132 (10 μM) before harvesting. Twenty-four following transfection, cells were harvested and lysed. Lysates were subjected to immunoprecipitation with anti-HA antibody. Precipitates were immunoblotted with anti-HA and flag antibodies (lower panels). (**b**) Endogenous praja2/MOB1/LATS1 complex was isolated from cell lysates using anti-praja2 antibody. (**c**) *In vitro*-translated [^{35}S]-labelled MOB1A and LATS1 were subjected to pulldown assays with purified GST or GST-praja2 fusion. (**d**) Spotted peptides (25 mers, 20 aa overlap) of MOB1A were overlaid with recombinant GST-praja2 followed by immunoblotting with anti-GST. The bar graph illustrates the densitometric quantification of the average of $n = 2$ dot blot experiments, coloured bars indicate the sequences (red box, referred here as binding domain (BD)) of one potential binding site in the illustrated modular structure of MOB1A. (**e**) Schematic view of the principle of the Venus-YFP PCA to capture protein complexes directly in the living cell and of the fusion proteins (indicated as circles) tested. Fluorometric imaging of transiently transfected HEK293 cells co-expressing the indicated proteins tagged with Venus-YFP PCA fragment (1) or (2) 24 h post transfection (lower panels). Scale bar, 10 μm. (**f**) U87MG cells were subjected to double immunostaining with monoclonal anti-MOB1 and polyclonal anti-praja2 antibodies. Images were collected and analysed by confocal microscopy. Magnification of selected areas is shown (insets). Scale bar, 10 μM.

in the cytoplasm (Fig. 1f), and also at centrosomal region as shown by triple labelling with anti-MOB1, anti-praja2 and anti-γ tubulin antibody (Supplementary Fig. S3a). A similar immunostaining pattern was also observed in FNP8, a primary culture of human GBM (Supplementary Fig. S3b).

praja2 ubiquitylates and degrades MOB1. We postulated that praja2 ubiquitylation promotes MOB1 degradation. We tested this hypothesis by measuring MOB1 levels in cells co-transfected with expression vectors encoding for flag-praja2 (either wild-type or RING mutant) and HA-tagged MOB1. We used two highly conserved variants of MOB1, MOB1A and MOB1B. As shown in Fig. 2a,b, expression of wild-type praja2 significantly reduced HA-MOB1A levels relative to the CMV vector control. In contrast, transfection with the inactive praja2 mutant (praja2rm) increased the concentration of HA-MOB1A. Similar results were obtained with co-transfected MOB1B (Fig. 2c,d). Endogenous MOB1 was also efficiently degraded by transfected praja2 (Fig. 2e). Treatment with MG132 reversed the reduction by praja2 of the levels of HA-MOB1A (Fig. 2f) or of endogenous MOB1 (Fig. 2g). To demonstrate that praja2 affected MOB1 stability, rather than MOB1 synthesis, the experiments were repeated in presence of cycloheximide, an inhibitor of protein synthesis. Figure 2h,i shows that MOB1 levels declined over time in control cells, with a half-life of ~5 h. Knocking down endogenous praja2 significantly increased the half-life of endogenous MOB1 (Fig. 2h,i) and of HA-MOB1A (Supplementary Fig. S4a,b). Complementary experiments demonstrated that praja2 overexpression markedly reduced HA-MOB1A stability (Fig. 2j,k), whereas endogenous MOB1 (Supplementary Fig. S4c,d) or HA-MOB1 (Fig. 2j,k) were stabilized by praja2rm overexpression.

Since praja2 is an E3-ubiquitin ligase, we asked if praja2 ubiquitylates MOB1 in living cells. Indeed, flag-praja2 promoted accumulation of poly-ubiquitylated forms of endogenous MOB1 (Fig. 2l) and of the co-transfected HA-MOB1A (Fig. 2m). Ligase activity was required for HA-MOB1A ubiquitylation; expression of praja2rm did not enhance MOB1 modification (Fig. 2l,m). An *in vitro* ubiquitylation assay confirmed that MOB1 is, in fact, a direct substrate of praja2 (Fig. 2n).

praja2 negatively regulates the Hippo pathway. YAP nuclear factor drives transcription of several genes. These include cyclin E and cyclin D, which induce quiescent cells to enter the cell cycle[29–31]. Upon reaching cell confluence and/or defined organ size, activated Hippo/MST phosphorylate the MOB1/LATS dimer, which leads to the activation of MOB1/LATS (ref. 32). Active MOB1/LATS complex phosphorylates YAP transcription factor at S127 (ref. 32). Phosphorylated YAP is trapped within the cytoplasm via interaction with 14-3-3 proteins and eventually degraded. Cytoplasmic sequestration of phosphorylated YAP suppresses the proliferating and antiapoptotic program, leading to cell cycle arrest and inhibition of organ or tumour growth[33,34].

We postulated that praja2, by reducing MOB1 levels, would downregulate LATS activity, decreasing YAP phosphorylation and negatively impacting on the downstream Hippo cascade. We tested this idea by monitoring YAP phosphorylation at S127 (pYAP) and MOB1 levels in growing and in quiescent U87MG glioblastoma cells. As control cells reached confluence, YAP phosphorylation increased ~1.7-fold over baseline levels (Fig. 3a,b). Downregulation of endogenous praja2 (*praja2* small interfering RNA (siRNA)) increased the levels of MOB1 and concomitantly enhanced YAP phosphorylation above control siRNA values (Fig. 3a,b). This was associated with marked reduction of YAP accumulation in the nuclei of *praja2* siRNA-transfected cells (Fig. 3c,d). Direct interference with endogenous praja2 activity reproduced the effects of praja2 silencing. Thus, expression of the praja2rm mutant increased the levels of MOB1 and enhanced confluence-induced YAP phosphorylation (Fig. 3e). As a read-out of YAP transcriptional activity, we measured the levels of cyclin E mRNA[35–37]. As expected, silencing of praja2 significant reduced cyclin E expression, both in U87MG cells and in primary cultures of human GBM (FNP8) (Fig. 3f).

praja2 is required for cell proliferation and tumour growth *in vivo*. The finding that praja2 downregulates the Hippo pathway provided a starting point to analyse how praja2 contributes to the phenotype of GBM cells. Hippo pathway activity is negatively correlated with growth and aggressive phenotype of GBM[38]. We predicted, therefore, that praja2 inactivation of MOB1 would enhance glial cell transformation. First, we compared praja2 expression in FNP8 and in U87MG cells. Supplementary Figure S5a shows that praja2 is expressed at comparable levels in both cell types. To link causally praja2 to glioma cell malignancy, we asked how praja2 silencing affected cell growth. siRNA duplexes targeting human praja2 efficiently knocked-down endogenous protein (Supplementary Fig. S5a). Importantly, downregulation of praja2 markedly inhibited growth of both U87MG (Fig. 3g) and FNP8 (Supplementary Fig. S5b) cells. The requirement of praja2 for cell growth was confirmed by fluorescent-activated cell sorter analysis. Thus, *praja2* siRNA-transfected U87MG cells accumulated at the G1 phase of cell cycle (Fig. 3h). A reduction at G2-M transition was also evident in the praja2-silenced cells. Taken together, these findings indicate that praja2 supports the growth of cultured GBM cells.

We further tested this notion *in vivo* using a mouse model of cancer growth. In this model, U87MG cells are injected subcutaneously into CD1 nude mice. The cells start to grow at the site of injection several days post-implantation[39]. To prove that praja2 is, in fact, required for tumour growth *in vivo*, we silenced endogenous praja2 in U87MG cells before injection by transient transfection with siRNA duplexes targeting praja2 (*praja2* siRNA) or with control non-targeting siRNAs (control siRNA). Three weeks post-injection, the mice were killed and the weight of the lesions was scored. As shown in Fig. 4a,b, downregulation of praja2 significantly inhibited tumour growth. Similar results were obtained using primary cultures of human GBM (NMDP7) (Supplementary Fig. S6). We also probed the tumour sections for Ki67, a proliferative marker and predictive parameter of glioblastoma recurrence and progression. The number of Ki67-positive cells was reduced by two-fold in tumour sections derived from *praja2* siRNA-transfected relative to cells transfected with control siRNA (Fig. 4a). The levels of the cyclin-dependent kinase inhibitor p21, a molecular marker of G1 growth arrest, were significantly higher in *praja2* siRNA-treated tumours, compared with controls (Fig. 4c,d), confirming the requirement of praja2 for cell cycle progression.

To study the role of praja2 in tumour development in a more physiological tissue context, we used an orthotopic glioblastoma model. U87MG cells transiently transfected with siRNAs (*praja2* siRNA or control siRNA) were implanted stereotaxically into the left caudate nucleus of mouse brain. The mice were killed 3 weeks later. Histological analysis of post-mortem control mouse brain revealed an homogenous tumour mass with sharp borders that was clearly delimited from the adjacent normal brain tissue. The orthotopic tumour, like the subcutaneous tumour, was composed mostly of large pleomorphic cells with abundant eosinophilic cytoplasm (Fig. 4e). Exposure of tumour cells to *praja2* siRNA, dramatically reduced tumour weight (Fig. 4e,f). A two-fold

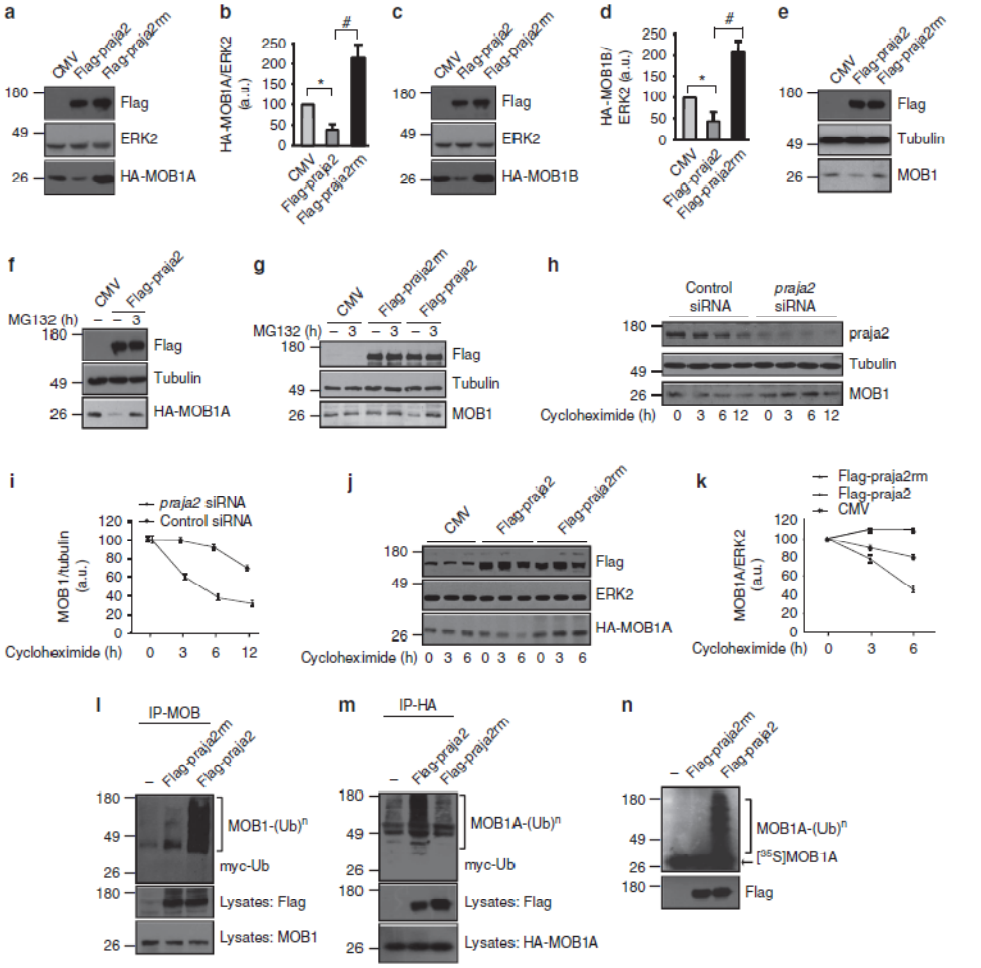

Figure 2 | praja2 ubiquitylates and degrades MOB1. (**a**–**d**) HEK293 cells were transiently co-transfected with CMV or flag-praja2 (either wild-type or RING mutant) and HA-MOB1A (**a**) or HA-MOB1B (**c**) vectors. Lysates were immunoblotted with the indicated antibodies. Quantitative analysis (mean ± s.e.m) is reported in the panels (**b**,**d**), respectively. $^{*}P<0.01$ versus CMV; $^{\#}P<0.01$ versus flag-praja2, Student's *t*-test. (**e**) Immunoblot analysis of endogenous MOB1 on lysates from cells transiently transfected with CMV, flag-praja2 or flag-praja2rm vector. Tubulin was used as loading control. (**f**) Cells were transiently co-transfected with CMV or flag-praja2 and HA-MOB1A vectors. Lysates were immunoblotted with the indicated antibodies. The cells were treated for 8 h with MG132 (20 μM) before harvesting. (**g**) Cells were transiently transfected with CMV or flag-praja2 (either wild-type or RING mutant) and treated for 8 h with MG132 (20 μM) before harvesting. Lysates were immunoblotted with the indicated antibodies. (**h**) Cells transiently transfected with control siRNA or *praja2* siRNA were treated with cycloheximide and harvested at the indicated time points after treatment. Lysates were immunoblotted with the indicated antibodies. (**i**) Cumulative analysis (mean ± s.e.m.) of the experiments shown in **h**. (**j**) Cells transiently co-transfected with HA-MOB1A and with either the expression vector for praja2 or praja2rm. CMV vector was included as control. Lysates were immunoblotted with the indicated antibodies. (**k**) Cumulative analysis of the experiments shown in **j**. The data are expressed as mean ± s.e.m. of three independent experiments. (**l**) Cells were transiently co-transfected with myc-ubiquitin and flag-praja2 or flag-praja2rm. Cells were treated for 8 h with MG132 (20 μM) before harvesting. Lysates were immunoprecipitated with anti-MOB1 antibody. The precipitates and lysates were immunoblotted with anti-MOB1, anti-myc and anti-flag antibodies. (**m**) Same as in **l**, except cells were transiently co-transfected with HA-MOB1A and lysates were immunoprecipitated with anti-HA antibody. Precipitates and lysates were immunoblotted with anti-HA, anti-myc and anti-flag antibodies. (**n**) *In vitro*-translated, [^{35}S]-labelled MOB1A was incubated with flag-praja2 or flag-praja2rm (immunopurified from transfected cells) and his6-tagged ubiquitin, in the presence of E1 and UbcH5c (E2). The reaction mixture was denatured, size-fractionated on 12% SDS-PAGE, and analysed by autoradiography. A fraction of the reaction mixture was immunoblotted with anti-flag antibody (lower panel).

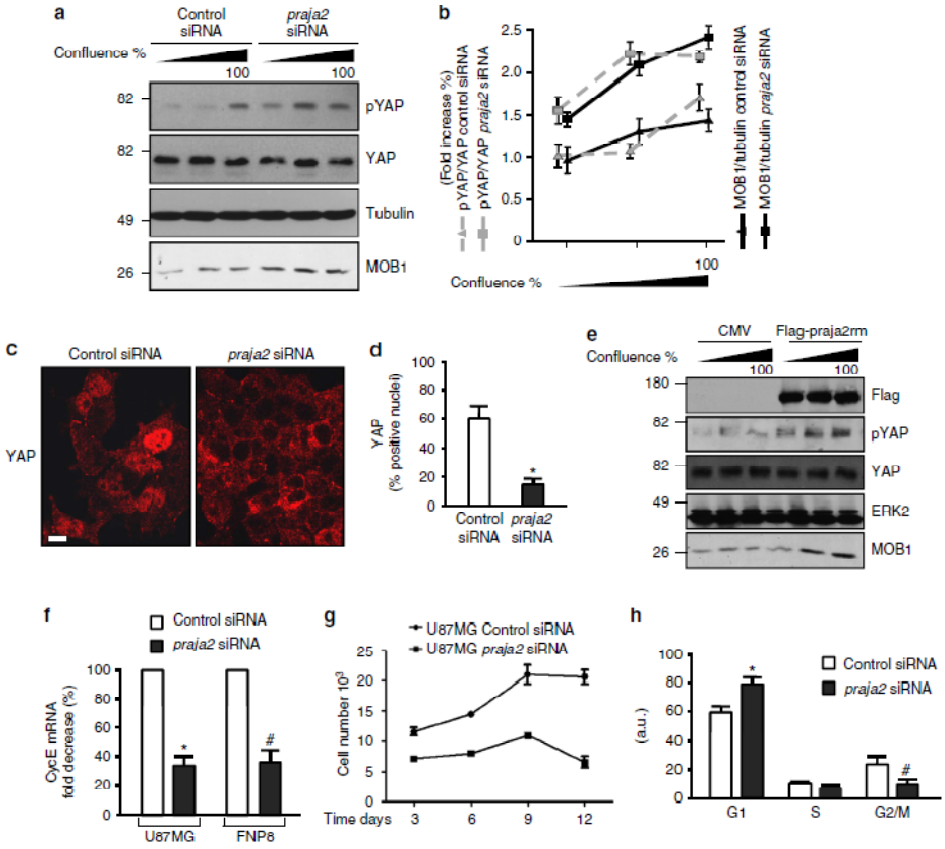

Figure 3 | praja2 inhibits the Hippo pathway and is required for GBM cell growth. (**a**) HEK293 cells were transiently transfected with the indicated siRNAs and harvested at different confluence. Lysates were immunoblotted with the indicated antibodies. (**b**) Cumulative analysis of the experiments shown in **a**. (**c**) cells were transiently transfected with siRNAs and subjected to immunostaining with monoclonal anti-YAP. Images were collected and analysed by confocal microscopy. Scale bar, 20 μm. (**d**) Quantitative analysis (mean ± s.e.m) of the experiments shown in (**c**), $^{*}P<0.01$ versus control siRNA, Student's *t*-test. (**e**) As in **a**, except the cells were transfected with flag-praja2rm or control CMV plasmid. (**f**) U87MG and FNP8 cells were transiently transfected with siRNAs and harvested at the indicated time points. Total RNA was extracted and subjected to RT-qPCR analysis for cyclin E (cycE) mRNA expression. Quantitative analysis is shown. These data are expressed as mean ± s.e.m. of three independent experiments. $^{*}P<0.01$ versus control siRNA (U87MG); $^{\#}P<0.02$ versus control siRNA (FNP8), Student's *t*-test. (**g**) Growth curve of U87MG siRNA-transfected cells. Following transfection, cells were seeded in multiwell plates, harvested at the indicated time points and counted. A mean value ± s.e.m. of three experiments is shown. (**h**) Fluorescent-activated cell sorter analysis (FACS) of U87MG cells prepared as in **c**. The analysis was performed at 48 h following transfection. $^{*}P<0.05$ versus control siRNA (G1); $^{\#}P<0.05$ versus control siRNA (G2/M).

reduction of Ki67 immunoreactive signal in these tumours further supports the role of praja2 in regulating GBM cellular proliferation (Fig. 4e). Growth of GBM lesions in living mice was monitored by positron emission tomography (PET) using the radiolabeled thymidine analogue ^{18}F-fluorothymidine (^{18}F-FLT). ^{18}F-FLT-PET analysis is routinely used *in vivo* to trace cell proliferation in a milieu of intact tumour tissue[40]. FLT-PET scanning analysis revealed a two-fold reduction of ^{18}F-FLT uptake by tumours derived from *praja2* siRNA-transfected cells compared with controls (Fig. 4g,h). These findings provide further evidence that praja2 enhances glioma growth *in vivo*.

The praja2-MOB1 axis controls glioma growth *in vivo*. The data presented above indicate that accumulation of praja2 is positively correlated with glioma growth *in vitro* and *in vivo*. As MOB1 is a praja2 substrate, we hypothesized that degradation of MOB1 by praja2 inhibits the Hippo pathway, thus enhancing GBM growth. This hypothesis is supported by several additional findings. First, knock-down of praja2 significantly upregulated MOB1 in transplanted U87MG tumours (Fig. 5a and b). Second, concomitant downregulation of MOB1 restored growth of praja2-silenced glioblastoma cells (Fig. 5c). Downregulation of praja2 activated the Hippo pathway, as shown by increased autophosphorylation of LATS1 at its activation site serine 909 (pLATS1)

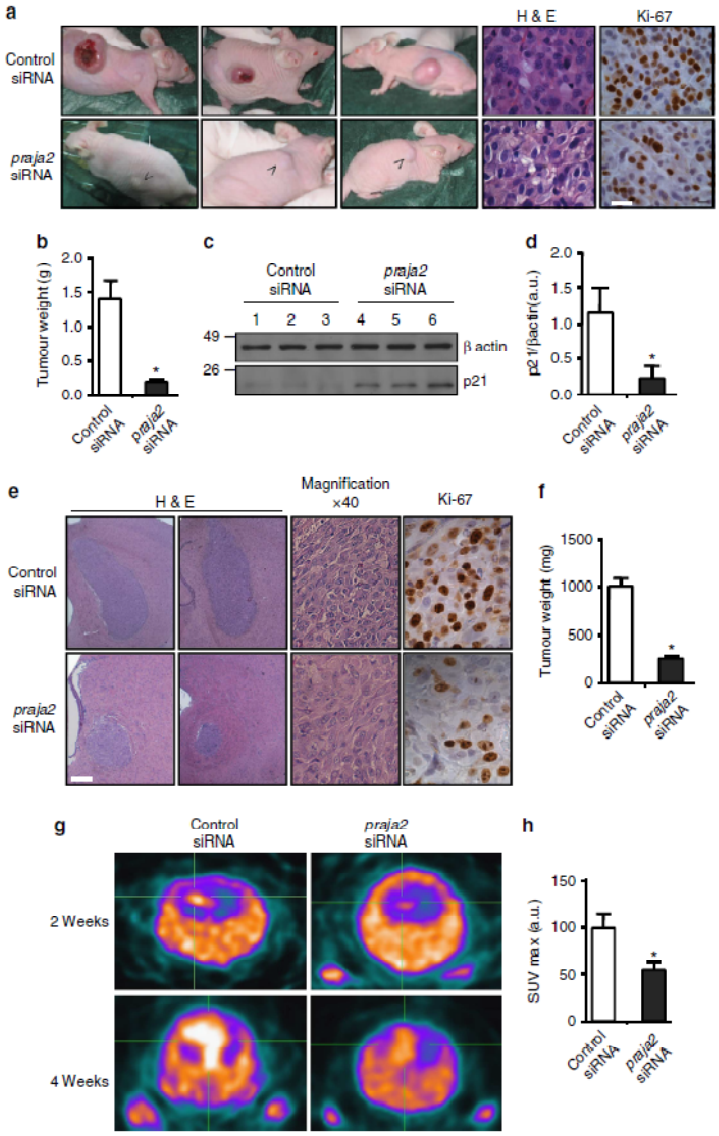

Figure 4 | praja2 is required for tumour growth *in vivo*. (**a**) U87MG cells transiently transfected with siRNAs were subcutaneously implanted into CD1 nude mice. Four weeks later, the mice were killed and the tumours excised and weighed. Tumour sections were fixed and doubly stained with hematoxylin/eosin or subjected to immunohistochemistry with anti-Ki67 antibody. Scale bar, 20 μm. (**b**) Cumulative data of tumour weight are expressed as mean ± s.e.m. Twenty mice for each experimental group were used. *$P<0.01$ versus control siRNA, Student's *t*-test. (**c**) Lysates from tumour lesions described in **a** were immunoblotted with anti-p21 (cyclin-dependent kinase (CDK) inhibitor) and anti-β actin antibodies. (**d**) Quantitative analysis of p21 levels in tumour lysates are expressed as mean ± s.e.m. of three independent experiments. *$P<0.01$ versus control siRNA, Student's *t*-test. (**e**) U87MG cells transiently transfected with control siRNA or *praja2* siRNA were stereotaxically implanted into the brain (left caudate nucleus) of nude mice. Tissue sections from tumour lesions were stained with hematoxylin/eosin or immunostained with anti-Ki67. Scale bar, 400 μm. (**f**) Quantitative analysis of the experiments shown in **e**. Data are expressed a mean value ± s.e.m. (Control siRNA: $n=15$, *praja2* siRNA: $n=10$). *$P<0.01$ versus control siRNA, Student's *t*-test. (**g**) FLT-PET analysis was performed at 2 and 4 weeks post-implantation. (**h**) Quantitative analysis of the experiment (at 2 weeks) shown in **g**. Data are expressed as mean value +/− s.e.m. *$P<0.05$ versus control siRNA, Student's *t*-test.

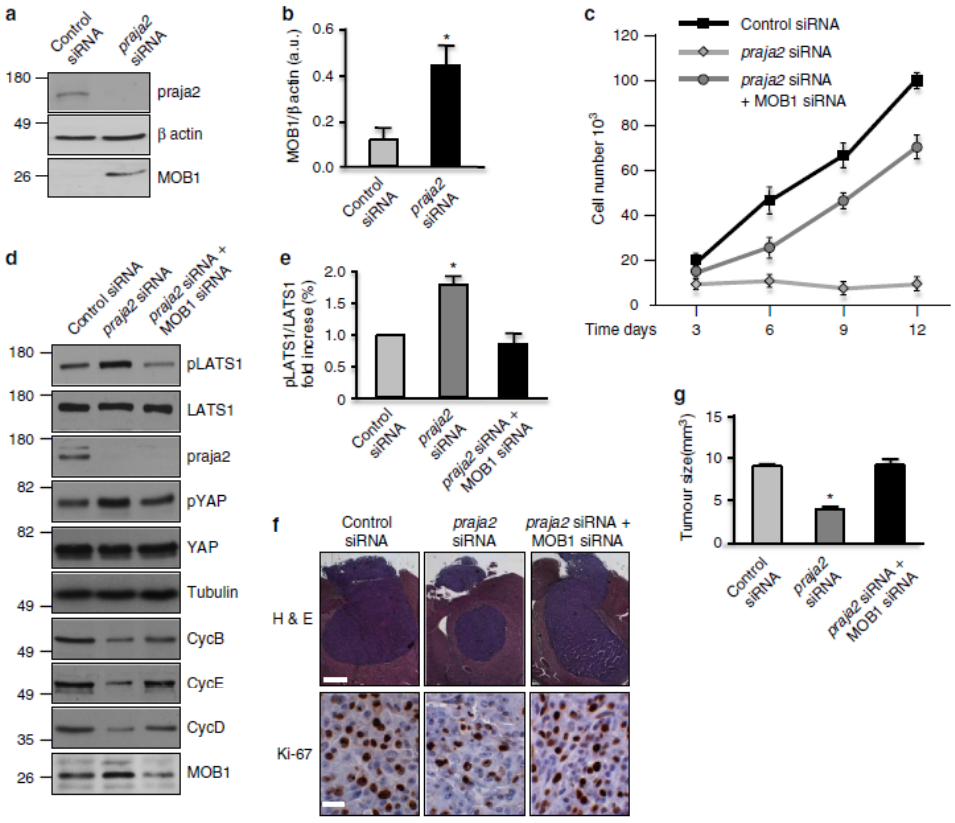

Figure 5 | The praja2-MOB1 pathway controls tumour growth. (**a**) Immunoblot analysis for MOB1 on lysates of tumour lesions excised from mice inoculated with siRNA-transfected U87MG cells. (**b**) Quantitative analysis of the experiments shown in **a**. Data are expressed as a mean value ± s.e.m. *$P<0.01$ versus control siRNA, Student's *t*-test. (**c**) Growth curve of U87MG siRNA-transfected cells. Following transfection, cells were seeded in multiwell plates, harvested at the indicated time points and counted. A mean value ± s.e.m. is shown. (**d**) U87MG cells were transfected with the indicated siRNAs. Lysates were immunoblotted with the indicated antibodies. (**e**) Quantitative analysis of autophosphorylation of LATS1 shown in **d**. *$P<0.01$ versus control siRNA, Student's *t*-test. (**f**) U87MG cells transiently transfected with control siRNA, *praja2* siRNA or *praja2* siRNA, and *MOB1* siRNA were stereotaxically implanted into the brain (left caudate nucleus) of CD1 nude mice. Tissue sections from tumour lesions were stained with hematoxylin/eosin. Scale bar, 400 μm (upper) and scale bar, 20 μm (lower). (**g**) Cumulative analysis of the experiments shown in **f**. Number of animals tested: control siRNA: $n=5$; *praja2* siRNA: $n=5$; *praja2* siRNA + *MOB1* siRNA: $n=6$. *$P<0.01$ versus control siRNA and *praja2* siRNA/*MOB1* siRNA, Student's *t*-test.

(Fig. 5d,e) and phosphorylation of YAP at S127 (Fig. 5d). This parallels a global downregulation of cyclins. The replication cyclins, cyclin E and cyclin D were downregulated 10-fold and 4.8-fold, respectively, in praja2-silenced cells. Some down-regulation of cyclin B (3.6-fold) was also observed (Fig. 5d). Consistent with our hypothesis, concomitant downregulation of MOB1 partially reversed the increase in LATS1 and YAP1 phosphorylation induced by praja2 silencing (Fig. 5d,e) Simultaneous knock-down of MOB1 partially restored cyclin expression in the praja2 knock-down cells, particularly in the case of cyclin E, whose expression increased 5.9-fold. These data along with those reported in Fig. 3 suggest that praja2 primarily regulates G1-S progression. Lastly, inhibition of the Hippo signalling by MOB1 knock-down restored tumour growth of praja2-silenced glioblastoma cells in mouse brain (Fig. 5f,g).

praja2 is overexpressed in human glioma. Given its positive role in glioma cell proliferation and xenograft tumour growth, we investigated the expression profile of praja2 in human gliomas. Tissue samples obtained from first biopsies of patients that underwent brain surgery for low-grade astrocytoma or GBM were homogenized and the protein lysates were immunoblotted with anti-praja2 antibody. Low levels of praja2 were detected in lysates from human astrocytomas, whereas praja2 concentrations were two-fold to three-fold higher in lysates from GBM samples (Fig. 6a,b). Quantitative RT–PCR analysis demonstrated that praja2 mRNA was increased in tumour biopsies of GBM, compared with astrocytoma II (Fig. 6c). This was not a consequence of amplification of the *praja2* gene in GBM lesions, as shown by fluorescence *in situ* hybridization (Supplementary Fig. S7a,b). Next, we performed immunohistochemistry on tissue sections

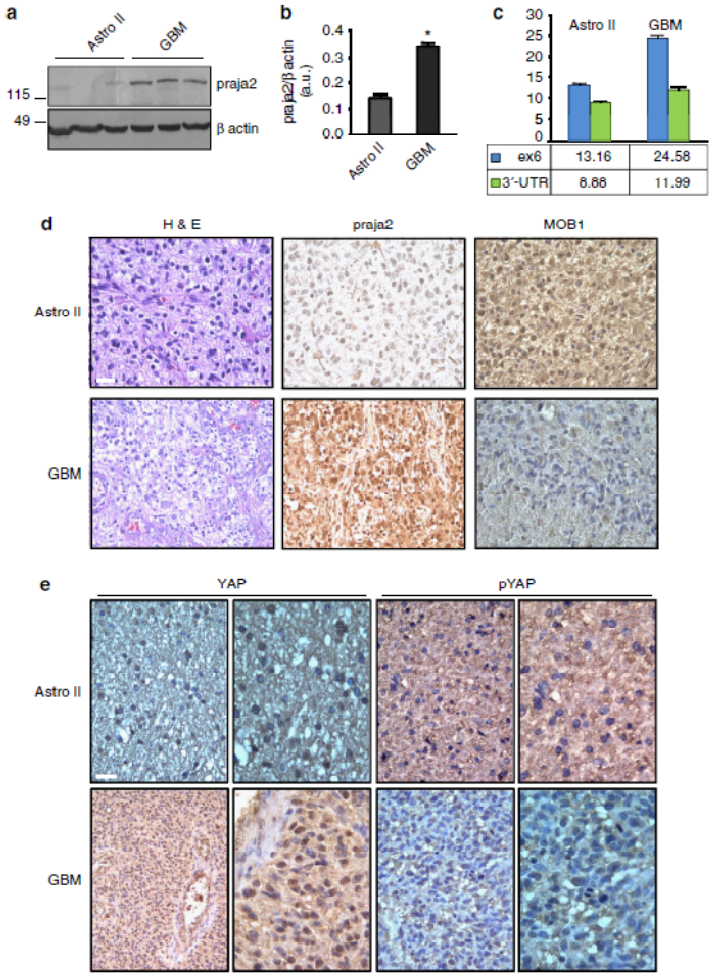

Figure 6 | praja2 is overexpressed in high-grade human glioma. (**a**) Lysates from tissue samples of astrocytoma (grade II) and GBM were immunoblotted with anti-praja2 antibody and anti-β actin antibodies. (**b**) Cumulative analysis of praja2 levels in each category of tissue lysates. *$P<0.01$ versus astrocytoma II, Student's *t*-test. (**c**) Expression analysis of praja2 mRNA by RT-qPCR. The graph shows the enhancement of praja2 transcript levels in astrocytoma II and GBM lesions. Levels of praja2 mRNA in normal human brain served as baseline. *Statistically significant values at REST 2009 analysis, Student's *t*-test. (**d**) Tissue sections from human astrocytoma II and GBM were stained with hematoxylin/eosin (H & E) or immunostained with anti-praja2 and anti-MOB1 antibody, and analysed by light microscopy. Scale bar, 25 μm. (**e**) GBM and astrocytoma tissue sections were immunostained with anti-YAP and anti-phospho YAP antibody. Enlarged sections are shown on the right of each pair of images. Scale bar, 25 μm.

derived from GBM and astrocytoma patients. The results were consistent with the immunoblotting data. Thus, more praja2 accumulated in GBM compared with astrocytoma tissues (Fig. 6d). MOB1 staining inversely correlated with glioma malignancy and praja2 levels. In particular, low-grade astrocytoma cells displayed a strong MOB1 signal that was diffusely distributed throughout the cytoplasm, whereas significantly lower concentrations of MOB1 were detected in GBM cells (Fig. 6d).

We then asked whether enhanced expression of praja2 in glioma tissues was associated with changes in the intracellular distribution of the ligase. Immunofluorescence analysis of glioma tissues is shown in Supplementary Fig. S8. In astrocytoma tissue, moderate praja2 staining was homogeneously distributed at the cell periphery (Supplementary Fig. S8a,b). As expected, strong praja2 staining was observed in GBM cells (Supplementary Fig. S8a,b). This staining was diffusely distributed throughout the cytoplasm, with some concentration at the perinuclear membrane and the nuclear compartment. Conversely, the MOB1 immunofluorescent signal was intense in astrocytoma cells, whereas only a slight signal was detected in GBM lesions

(Supplementary Fig. S8c,d). Note that GBM sections contain heterogenous cell populations marked by quite different levels of praja2 and MOB1, possibly reflecting the high rate of genomic instability that defines these tumours.

Increased levels of praja2 in GBM lesions were linked to significantly decreased YAP phosphorylation (Fig. 6e). The unmodified YAP accumulated in the nuclear compartment (Fig. 6e). In contrast, astrocytoma tissues present high levels of phosphorylated YAP, which is mostly distributed throughout the cytoplasm (Fig. 6e).

Discussion

Here, we report a mechanism of signal attenuation in human GBM based on proteolytic turnover of components of an oncosuppressive pathway. We find that praja2 directly binds to and ubiquitylates MOB1, the regulatory component of the LATS1/2 kinases of the Hippo pathway. Degradation of ubiquitylated MOB1 by the proteasome inhibits this signalling cascade, favoring GBM growth.

Proteolysis of cellular proteins by the UPS is a sophisticated mechanism controlling complex biological interactions that underlie cell survival, growth and metabolism. Accordingly, disregulation of the UPS is causally implicated in a wide variety of human diseases, including neurodegeneration and cancer. Modulating overall UPS activity is a therapeutic strategy currently being tested for treatment of several human disorders[41]. However, non-specific side effects and toxicity problems limit its use. An alternative approach, targeting the levels or activity of specific E3 ligases, is an attractive and, perhaps, more effective therapeutic strategy[42]. The E3-ubiquitin ligase MDM2 represents the prototype target of inhibitors that selectively interfere with the ubiquitylation processes in human tumours. MDM2 is a transcriptional target of p53 and tightly regulates p53 levels by marking p53 for UPS degradation[43]. This constitutes a negative feed-back loop that controls the p53-dependent stress response. Decreased levels of p53 are found in many human cancers, resulting from genetic inactivation, viral infection or amplification of the MDM2 gene[44]. Preventing MDM2–p53 interaction with small-molecule drugs restores normal p53 activity. This therapy is currently being tested in haematological and solid malignancies[45].

Changes in the expression profile of components of the ubiquitin ligase complexes have been reported in diverse tumours[20]. UbcH10, an ub-conjugating enzyme that regulates cell cycle progression, is upregulated in high-grade astrocytoma[46]. Conversely, the tumour suppressor F-box protein Fbxw7, a component of the Skp1-Cul1-F-box E3-ubiquitin ligase complex, is downregulated in high-grade glioma, and serves as prognostic biomarker for survival in glioma patients[47]. Somatic mutations of ubiquitin ligases have been identified in GBM and in other human malignancies, further supporting a pathogenic role of deregulated UPS system in brain tumours[48,49].

Our findings identify praja2 as a novel cancer-associated gene whose expression is upregulated in high-grade glioma. The expression profile of praja2 in tissue biopsies of astrocytoma and GBM lesions is consistent with a direct correlation between the levels of the ligase and the malignant phenotype of the tumour.

At the mechanistic level, we identified MOB1, the regulatory component of the LATS1/2 kinases, as a critical praja2 substrate. MOB1 family members (MOB1A and MOB1B) are products of highly conserved genes originally identified as regulators of mitotic exit and cytokinesis in yeast, and later reported as tumour suppressors and components of the Hippo-NDR/LATS pathway[25]. MOB1 interacts with and activates LATS1/2 kinases. The MOB1/LATS kinase complex phosphorylates and inactivates YAP, a transcription factor that controls entry into the cell cycle of quiescent cells. Phosphorylated YAP is recruited and ubiquitylated by the SCF (beta-TRCP) E3-ubiquitin ligase complex. Ubiquitylated YAP is degraded through the proteasome[50]. The Hippo pathway can also be attenuated by proteolytic turnover of the LATS1 Kinase. LATS1 is ubiquinitated by the HECT class E3-ubiquitin ligase ITCH, which interacts with the PPxY motifs of LATS1 through its WW domains. Proteolysis

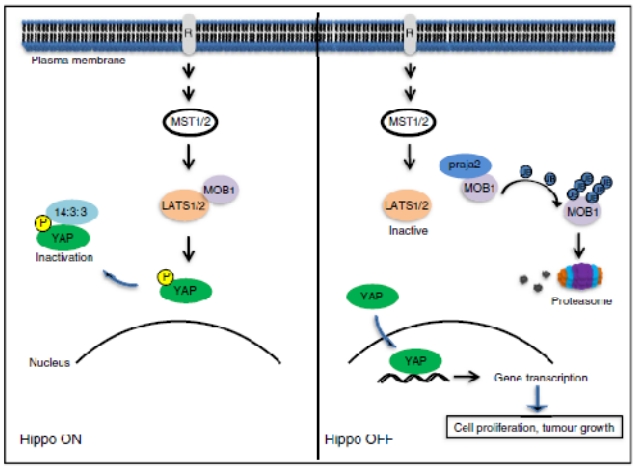

Figure 7 | Schematic diagram of the role of praja2 in the Hippo pathway. praja2-directed ubiquitylation of MOB1 and its consequent degradation by the proteasome attenuates LATS1/2 kinase activity, preventing phosphorylation and inactivation of YAP. Unphosphorylated YAP accumulates in the nucleus and drives gene transcription, promoting cell proliferation and tumour growth.

of ubiquitylated LATS1 enhances cell growth, induces epithelial-mesenchymal transition and increases tumorigenicity[51,52]. In the work described above, we report that the regulatory component of the LATS1 kinase, MOB1, is degraded by praja2 through the UPS. Proteolysis of MOB1 by praja2 attenuates the Hippo cascade and enhances proliferation of glioblastoma cells. As MOB1 interacts with NDR1/2 kinases, this suggests that praja2 may also impact on the NDR1/2-dependent signalling cascade[32]. This mechanism operates *in vivo*; downregulation of MOB1 restored the proliferative activity of praja2-silenced GBM cells and sustained tumour growth. By removing the inhibitory constraint imposed by Hippo, praja2 would favour YAP-dependent gene transcription, coupling the UPS pathway to GBM growth (Fig. 7). Notably, we found that MOB1 levels inversely correlate with praja2 abundance and glioma malignancy, supporting the role of praja2 in control of MOB1 stability *in vivo*. Moreover, upregulation of praja2 in GBM lesions is linked to significant inhibition of the Hippo pathway, confirming the mechanistic link between praja2, Hippo pathway and GBM *in vivo*.

Our results, taken together, identify the E3 ligase praja2 as a novel cancer-associated gene whose expression predicts the aggressive potential of glioma. Negative regulation of the Hippo pathway by praja2 constitutes a UPS-driven signalling circuit that sustains growth of glial cells carrying various oncogenic mutations. Unveiling the mechanism(s) regulating praja2 expression and activity in glioma cells and identifying additional relevant praja2 targets will contribute to our understanding of the role of UPS pathway in the development and progression of human GBMs. We expect this to inform the design of more effective target-oriented therapeutic strategies for aggressive human GBM.

Methods

Cells and tissues. The human embryonic kidney cell line (HEK293) was cultured in DMEM containing 10% fetal bovine serum (FBS) in an atmosphere of 5% CO_2. The glioblastoma cell line U87MG (grade-IV) was purchased from the American Type Culture Collection and maintained in modified Eagle's medium supplemented with 10% heat inactivated fetal calf serum and 2 mM L-glutamine, 100 IU ml^{-1} penicillin, 100 µg ml^{-1} streptomycin, 1x non-essential amino-acid, 1 mM sodium pyruvate, at 37 °C, 5% CO_2 and 95% of humidity. Primary glioblastoma cell lines (FNP8 and NMDP7) were prepared from enzymatic digestion of bioptic samples surgically removed from Neuromed patients. All patients gave their informed consents and were shown to carry glioblastoma multiforme (according to WHO classsification). All tumours were positive for vimentin, GFAP (glial fibrillary acidic protein) and EGFR.

Transfection of plasmids and siRNAs. Vectors encoding for wild-type or mutant praja2, ubiquitin, MOB1A and MOB1B were described previously[53,54]. Transfection efficiency was monitored by including a GFP vector in the trasfection mixture. SMARTpool siRNAs targeting distinct segments of coding regions of praja2 and MOB1 were purchased from Dharmacon. The following are the siRNA sequences (Thermo Scientific) targeting human praja2: sequence 1: 5′-GAAGC ACCCUAAACCUUGA-3′; sequence 2: 5′-AGACUGCUCUGGCCCAUUU-3′; sequence 3: 5′-GCAGGAGGGUAUCAGACAA-3′; sequence 4: 5′-GUUAGAUU CUGUACCAUUA-3′. The following are the siRNA sequences (Thermo Scientific) targeting human MOB1: sequence 1: 5′-AUGAAUGGGUUGCAGUUAA-3′; sequence 2: 5′-GCAGAUGGAACGAACAUAA-3′; sequence 3: 5′-GCACCAA AGUAUAUUGAUU-3′; sequence 4: 5′-GGUUAAAUGUUGAUACGAA-3′. siRNAs were transiently transfected using Lipofectamine 2000 (Invitrogen) at a final concentration of 100 pmol ml^{-1} of culture medium. For siRNA experiments, similar data were obtained using a mixture or four or two independent siRNAs.

Antibodies and chemicals. Goat and rabbit polyclonal antibodies directed against MOB1 were purchased from SantaCruz and Cell Signalling, and used at working dilutions of 1:300 (for immunostaining) and 1:1000 (for immunoblot); extracellular signal-regulated kinase 2 (ERK2) (dilution 1:3000), GST (dilution 1:5000),YAP (dilution 1:1000 for immunoblot and 1:300 for immunostaining), cydin D1 (dilution 1:1000), cyclin B1 (dilution 1:1000) and cydin E (dilution 1:1000) were purchased from SantaCruz; haemagglutinin epitope (HA.11, dilution 1:1000) was purchased from Covance; α-tubulin, γ-tubulin, flag and myc epitope (dilutions 1:3000) were purchased from Sigma; phospho(Ser127)YAP (dilution 1:1000), phospho(Ser909)LATS1 (dilution 1:1.000) and LATS1 (dilution 1:1000) were purchased from Cell Signalling; praja2 (dilution 1:5.000 for immunoblot and 1:300 for immunostaining) was purchased from Bethyl laboratories; polyclonal antibody directed against human praja2 (immunoblotting dilution 1:500; immunostaining dilution 1:300) was generated in rabbit using the following epitope: residues 60–250.

Immunoprecipitation and pulldown assay. Cells were homogenized and subjected to immunoprecipitation and immunoblot analyses as described previously[24]. GST fusions were expressed and purified from BL21 (DE3) pLysS cells. GST or GST–praja2, beads (20 µl) were incubated with 2 mg of cell lysate or with *in vitro*-translated [^{35}S]-labelled MOB1A in 200 µl lysis buffer (150 mM NaCl, 50 mM Tris-HCl at pH 7.5, 1 mM EDTA and 0.5% Triton X-100) in rotation at 4 °C overnight. Pellets were washed four times in lysis buffer supplemented with NaCl (0.4 M final concentration) and eluted in Laemmli buffer. Eluted samples were immunoblotted with the indicated antibody. In the case of GST/GST-MOB1A pulldowns, we precipitated praja2-flag expressed in HEK293 cells for 3 h (lysis buffer: 10 mM sodium phosphate pH 7.2, 150 mM NaCl, 0.5% Triton X-100 supplemented with standard protease inhibitors). Resin-associated complexes were washed at least four times with the lysis buffer and eluted with Laemmli sample buffer.

***In vitro* ubiquitylation assay**. [^{35}S]-labelled MOB1A was synthesized *in vitro* using a TnT Quick coupled transcription/translation system (Promega) in the presence of 45 µCi of [^{35}S]-labelled methionine using as template a pcDNA3 vector carrying Myc/His-MOB1A transgene. The ubiquitylation assay was carried out as described previously[53].

Animals and tumour cell implantation. Male CD1 nude mice (20–22 g body weight; Charles River, Calco, CO, Italy) were kept under controlled conditions (temperature, 22 °C; humidity, 40%) on a 12-h light/dark cycle with food and water *ad libitum*. Experiments were performed following the guidelines for animal care and use proposed by the National Institutes of Health (Bethesda, MD). Mice were subcutaneously implanted with 1×10^6 U87MG cells per 0.5 ml, under anaesthesia. The weight of subcutaneous tumours was assessed after 1 month. In another set of experiments, U87MG cells were stereotaxically implanted into the left caudate nucleus (by using the following coordinates: 0.6 mm anterior to the bregma; 1.7 mm lateral to the midline; and 4.5 mm ventral from the surface of skull of mice under ketamine (100 mg kg^{-1}, i.p.)/xylazine (10 mg kg^{-1}, i.p.) anaesthesia. Cells (0.3×10^6 cells per 5 µl) were implanted at an infusion rate of 1 µl min^{-1}.

Immunohistochemistry. Formalin-fixed, paraffin-embedded tissues from the tumours were selected. Representative slides of each tumour were stained with hematoxylin and eosin. Immunohistochemistry for praja2 and Ki67 (Ventana, Tucson, Ariz.) was performed automatically with a Nexes instrument (Ventana). Antibody detection was performed using a multilink streptavidin–biotin complex method, and antibodies were visualized by a diaminobenzidine chromagen method. Negative control samples were incubated with primary antibodies only. The number of Ki67-positive cells was determined in four random fields (1 cm^2 each) by using the ImageJ 1.31v software (National Institutes of Health). Stereological techniques for electron microscopic morphometry were applied to normal brain and brain tumour slides. Our aim was to obtain objective baseline data for the study of expression of praja2 in these tissues. The results, expressed mainly in numerical densities of positive cells in the control and pathological tissue revealed increasing gradients throughout grading of the tumour tissues. Each section was subjected to count stereology of cells positive for praja2. The counting was performed using a microscope (Axio Imager M1 microscope) equipped with software Image Pro Plus 6.2. This automatically calculates the density of praja2 positive cells per area (mm^2). To evaluate the expression of MOB1, YAP and phospho YAP in tumour cells, 4-m serial sections from representative blocks were cut, mounted on poly-L-lysine coated glass slides and used for the immunohistochemical staining. Representative sections were incubated with the anti-MOB1, anti-YAP and anti-phospho YAP antibodies. Subsequently, the slides were incubated with biotinylated secondary antibodies, peroxidase-labelled streptavidin (DAKO LSAB kit HRP, Carpinteria, CA) and chromogenic substrate diaminobenzidine (DAB, Vector Laboratories, Burlingame, USA) for the development of the peroxidase activity. Slides were counterstained with hematoxylin, dehydrated and cover-slipped with a synthetic mounting medium (Entellan, Merck, Germany). Only cells with a definite cytoplasmic staining were judged as positive for the MOB1 antibody, whereas for YAP and phospho-YAP nuclear and cytoplasmic positivity were evaluated, respectively.

Small animal PET Imaging and data analysis. Before PET studies, mice were injected in the tail vein with 9.5 MBq of ^{18}F-FLT, and were kept awake in a ventilated cage (26 °C) during a tracer uptake period of 60 min. Anaesthesia was performed with intraperitoneal administration of ketamine (100 mg kg^{-1}) and xylazine (10 mg kg^{-1}) (injection volume, 100 µl per 10 g) during the entire scanning period. Imaging was performed with the dedicated small animal PET scanner eXplore Vista GE Healthcare. The static PET data were acquired for 30 min. Image data sets were corrected for random coincidences, scatter and physical decay to the time of injection. No attenuation correction was applied. The measured

reconstructed spatial resolution of the Explore Vista scanner is ~1.6 mm full-width at half maximum (FWHM) at the center of the field of view. The counting rates in the reconstructed images were converted to activity concentrations (SUV units) by use of a system calibration factor (1.035 Bq ml^{-1} per cps per voxel) derived from the imaging of a mouse-size water-equivalent phantom containing ^{18}F. Maximum (SUVmax) and mean (SUVmean) standardized uptake values (SUVs) (SUV = tissue activity (MBq per cc)/(injected dose (MBq)/body weight (g))), and the 'metabolic volume' of the lesions were calculated from the PET studies. Quantitative data were obtained using GE eXplore Vista software, on the base of a 'region growing' procedure, by adding all spatially connected voxels with SUV >50%. FLT uptake between control and siRNA-treated mice were compared.

Immunofluorescence and confocal analysis. Sections from human glioblastoma biopsies were subjected to double staining with DAPI and primary antibodies. Fluorescent signals were visualized using a Zeiss LSM 510 Meta argon/krypton laser scanning confocal microscope. Four images from each optical section were averaged to improve the signal-to-noise ratio. Images from a minimum of four sections per tumour and four different samples of each category of tumours were collected and analysed. Immunofluorescence on cultured cells was performed as described previously[24].

Fluorescence-activated cell sorting. For cell cycle analysis, samples were labelled with propidium iodide. Cells were fixed with 70% ethanol in phosphate-buffered saline (PBS) and routinely kept at +4 C° overnight. Cells were washed twice with PBS, resuspended in PBS containing 40 µg ml^{-1} propidium iodide (Sigma), 7 units µl^{-1} RNase DNase-free (Eppendorf) and incubated at room temperature for 20 min. Cells were analysed using a CyAn ADP flow cytometer (Dako Cytomation, Ely, UK) using Summit software. Results are presented as mean ± s.e.m. of three separate experiments.

***In vitro* protein binding assays.** GST hybrid proteins were expressed in *Escherichia coli* (strain BL21). Induction, cell lysis and affinity purification of hybrid proteins were performed as recommended by the supplier of the pGEX vectors (GE Healthcare). GST hybrid proteins (GST, GST-MOB1A) immobilized on glutathione beads were incubated for 3 h with cell lysates from HEK293 cells transiently expressing flag-praja2. Resin-associated complexes were washed at least four times with the standard lysis buffer (10 mM sodium phosphate pH 7.2, 150 mM NaCl, 0.5% Triton X-100) and eluted with Laemmli sample buffer (2% SDS, 50 mM Tris-HCl pH 6.8, 0.2 mg ml^{-1} bromphenol blue, 0.1 M DTT, 10% (v/v) glycerol).

References

1. Newton, H. B. Glioblastoma multiforme. *Curr. Treat Options Neurol.* **10,** 285–294 (2008).
2. Preusser, M. *et al.* Current concepts and management of glioblastoma. *Ann. Neurol.* **70,** 9–21 (2011).
3. Louis, D. N. Molecular pathology of malignant gliomas. *Annu. Rev. Pathol.* **1,** 97–117 (2006).
4. Li, Z. *et al.* Hypoxia-inducible factors regulate tumorigenic capacity of glioma stem cells. *Cancer cell* **15,** 501–513 (2009).
5. Bar, E. E. Glioblastoma, cancer stem cells and hypoxia. *Brain Pathol.* **21,** 119–129 (2011).
6. Amberger-Murphy, V. Hypoxia helps glioma to fight therapy. *Curr Cancer Drug Targets* **9,** 381–390 (2009).
7. Bayley, J. P. & Devilee, P. Warburg tumours and the mechanisms of mitochondrial tumour suppressor genes. *Barking up the right tree? Curr. Opin. Genet. Dev.* **20,** 324–329 (2010).
8. Bao, S. *et al.* Glioma stem cells promote radioresistance by preferential activation of the DNA damage response. *Nature* **444,** 756–760 (2006).
9. Clevers, H. The cancer stem cell: premises, promises and challenges. *Nat. Med.* **17,** 313–319 (2011).
10. Dimov, I., Tasic-Dimov, D., Conic, I. & Stefanovic, V. Glioblastoma multiforme stem cells. *Sci. World J.* **11,** 930–958 (2011).
11. Jansen, M., Yip, S. & Louis, D. N. Molecular pathology in adult gliomas: diagnostic, prognostic, and predictive markers. *Lancet Neurol.* **9,** 717–726 (2010).
12. Charles, N. A., Holland, E. C., Gilbertson, R., Glass, R. & Kettenmann, H. The brain tumour microenvironment. *Glia* **59,** 1169–1180 (2011).
13. Lino, M. & Merlo, A. Translating biology into clinic: the case of glioblastoma. *Curr. Opin. Cell Biol.* **21,** 311–316 (2009).
14. Brennan, C. Genomic profiles of glioma. *Curr. Neurol. Neurosci. Rep.* **11,** 291–297 (2011).
15. Riddick, G. & Fine, H. A. Integration and analysis of genome-scale data from gliomas. Nature reviews. *Neurology* **7,** 439–450 (2011).
16. Yan, H. *et al.* IDH1 and IDH2 mutations in gliomas. *N. Engl. J. Med.* **360,** 765–773 (2009).
17. Argyriou, A. A., Giannopoulou, E. & Kalofonos, H. P. Angiogenesis and anti-angiogenic molecularly targeted therapies in malignant gliomas. *Oncology* **77,** 1–11 (2009).
18. Ciechanover, A. Proteolysis: from the lysosome to ubiquitin and the proteasome. Nature reviews. *Mol. Cell Biol.* **6,** 79–87 (2005).
19. Ravid, T. & Hochstrasser, M. Diversity of degradation signals in the ubiquitin-proteasome system. Nature reviews. *Mol. Cell Biol.* **9,** 679–690 (2008).
20. Lipkowitz, S. & Weissman, A. M. RINGs of good and evil: RING finger ubiquitin ligases at the crossroads of tumour suppression and oncogenesis. *Nat. Rev. Cancer* **11,** 629–643 (2011).
21. Nakayama, M., Miyake, T., Gahara, Y., Ohara, O. & Kitamura, T. A novel RING-H2 motif protein downregulated by axotomy: its characteristic localization at the postsynaptic density of axosomatic synapse. *J. Neurosci.* **15,** 5238–5248 (1995).
22. Yu, P., Chen, Y., Tagle, D. A. & Cai, T. PJA1, encoding a RING-H2 finger ubiquitin ligase, is a novel human X chromosome gene abundantly expressed in brain. *Genomics* **79,** 869–874 (2002).
23. Lignitto, L., Sepe, M., Carlucci, A. & Feliciello, A. An intimate connection between ubiquitination and compartmentalized cAMP signaling. *Cell cycle* **10,** 2051–2052 (2011).
24. Lignitto, L. *et al.* Control of PKA stability and signalling by the RING ligase praja2. *Nat. Cell Biol.* **13,** 412–422 (2011).
25. Hergovich, A. MOB control: reviewing a conserved family of kinase regulators. *Cell Signal.* **23,** 1433–1440 (2011).
26. Stefan, E. *et al.* PKA regulatory subunits mediate synergy among conserved G-protein-coupled receptor cascades. *Nat. Commun.* **2,** 598 (2011).
27. Michnick, S. W., Ear, P. H., Manderson, E. N., Remy, I. & Stefan, E. Universal strategies in research and drug discovery based on protein-fragment complementation assays. *Nat. Rev. Drug Discov.* **6,** 569–582 (2007).
28. Mrkobrada, S., Boucher, L., Ceccarelli, D. F., Tyers, M. & Sicheri, F. Structural and functional analysis of Saccharomyces cerevisiae Mob1. *J. Mol. Biol.* **362,** 430–440 (2006).
29. Wu, S., Huang, J., Dong, J. & Pan, D. Hippo encodes a Ste-20 family protein kinase that restricts cell proliferation and promotes apoptosis in conjunction with salvador and warts. *Cell* **114,** 445–456 (2003).
30. Zhao, B., Tumaneng, K. & Guan, K. L. The Hippo pathway in organ size control, tissue regeneration and stem cell self-renewal. *Nat. Cell Biol.* **13,** 877–883 (2011).
31. Yu, F. X. *et al.* Regulation of the Hippo-YAP pathway by G-protein-coupled receptor signaling. *Cell* **150,** 780–791 (2012).
32. Hergovich, A. & Hemmings, B. A. Mammalian NDR/LATS protein kinases in Hippo tumour suppressor signaling. *Biofactors* **35,** 338–345 (2009).
33. Sudol, M. & Harvey, K. F. Modularity in the Hippo signaling pathway. *Trends Biochem. Sci.* **35,** 627–633 (2010).
34. Zeng, Q. & Hong, W. The emerging role of the Hippo pathway in cell contact inhibition, organ size control, and cancer development in mammals. *Cancer cell* **13,** 188–192 (2008).
35. Xiao, G. H. *et al.* The NF2 tumour suppressor gene product, merlin, inhibits cell proliferation and cell cycle progression by repressing cyclin D1 expression. *Mol. Cell Biol.* **25,** 2384–2394 (2005).
36. Striedinger, K. *et al.* The neurofibromatosis 2 tumour suppressor gene product, merlin, regulates human meningioma cell growth by signaling through YAP. *Neoplasia* **10,** 1204–1212 (2008).
37. Huang, J., Wu, S., Barrera, J., Matthews, K. & Pan, D. The Hippo signaling pathway coordinately regulates cell proliferation and apoptosis by inactivating Yorkie, the Drosophila Homolog of YAP. *Cell* **122,** 421–434 (2005).
38. Xu, Y., Stamenkovic, I. & Yu, Q. CD44 attenuates activation of the Hippo signaling pathway and is a prime therapeutic target for glioblastoma. *Cancer Res.* **70,** 2455–2464 (2010).
39. Kiaris, H., Schally, A. V. & Varga, J. L. Antagonists of growth hormone-releasing hormone inhibit the growth of U-87MG human glioblastoma in nude mice. *Neoplasia* **2,** 242–250 (2000).
40. Bading, J. R. & Shields, A. F. Imaging of cell proliferation: status and prospects. *J Nuclear Med.* **49**(Suppl 2): 64S–80S (2008).
41. Paul, S. Dysfunction of the ubiquitin-proteasome system in multiple disease conditions: therapeutic approaches. *BioEssays* **30,** 1172–1184 (2008).
42. Goldenberg, S. J., Marblestone, J. G., Mattern, M. R. & Nicholson, B. Strategies for the identification of ubiquitin ligase inhibitors. *Biochem. Soc. Trans.* **38,** 132–136 (2010).
43. Haupt, Y., Maya, R., Kazaz, A. & Oren, M. Mdm2 promotes the rapid degradation of p53. *Nature* **387,** 296–299 (1997).
44. Marine, J. C. & Lozano, G. Mdm2-mediated ubiquitylation: p53 and beyond. *Cell Death Differ.* **17,** 93–102 (2010).
45. Cheok, C. F., Verma, C. S., Baselga, J. & Lane, D. P. Translating p53 into the clinic. Nature reviews. *Clin. Oncol.* **8,** 568 (2011).
46. Jiang, L. *et al.* Expression of ubiquitin-conjugating enzyme E2C/UbcH10 in astrocytic tumours. *Brain Res.* **1201,** 161–166 (2008).
47. Hagedorn, M. *et al.* FBXW7/hCDC4 controls glioma cell proliferation in vitro and is a prognostic marker for survival in glioblastoma patients. *Cell Div.* **2,** 9 (2007).

48. Veeriah, S. *et al.* Somatic mutations of the Parkinson's disease-associated gene PARK2 in glioblastoma and other human malignancies. *Nat. Genet.* **42,** 77–82 (2010).
49. Kanno, H. *et al.* Somatic mutations of the von Hippel-Lindau tumour suppressor gene and loss of heterozygosity on chromosome 3p in human glial tumors. *Cancer Res.* **57,** 1035–1038 (1997).
50. Zhao, B., Li, L., Tumaneng, K., Wang, C. Y. & Guan, K. L. A coordinated phosphorylation by Lats and CK1 regulates YAP stability through SCF(beta-TRCP). *Genes Dev.* **24,** 72–85 (2010).
51. Ho, K. C. *et al.* Itch E3-ubiquitin ligase regulates large tumour suppressor 1 stability [corrected]. *Proc. Natl Acad. Sci. USA* **108,** 4870–4875 (2011).
52. Salah, Z. Melino, G. & Aqeilan, R. I. Negative regulation of the Hippo pathway by E3 ubiquitin ligase ITCH is sufficient to promote tumorigenicity. *Cancer Res.* **71,** 2010–2020 (2011).
53. Carlucci, A. *et al.* Proteolysis of AKAP121 regulates mitochondrial activity during cellular hypoxia and brain ischaemia. *EMBO J.* **27,** 1073–1084 (2008).
54. Praskova, M., Xia, F. & Avruch, J. MOBKL1A/MOBKL1B phosphorylation by MST1 and MST2 inhibits cell proliferation. *Current Biol.* **18,** 311–321 (2008).

Acknowledgements

This work was supported by a grant from 'Associazione Italiana per la Ricerca sul Cancro' (IG 11788), by UICC 'Yamagiwa-Yoshida Memorial International Cancer Study Grant' and 'Schaefer Research Scholar Award, Columbia University NY' (to A.F.). E.S. was supported by the Austrian Science Fund (FWF: P22608). We Thank Drs Joseph Avruch for kindly providing MOB1A and MOB1B vectors, Michael Byermann for dot blot membranes, Felice Giangaspero for helpful discusson, Loredana Stasio and Silvana Capuozzo for help in immunohistochemistry. We thank Michael Beyermann for dot blot membranes and Michi Ausserlechner for access to the imaging platform.

Author contributions

L.L., E.S. and A.F. designed the experiments. L.L. carried out most of the experiments except the following: R.D.D. Fig. 1b, L.R Fig. 1c, Fig. 2g. E.S. and V.A.B. Fig. 1d, Fig. 1e, Supplementary Figs S1b,S2a–d; C.G. Fig. 1f, Fig. 3c, Fig. 3d, Supplementary Fig. S3a, Fig. 3b, Supplementary Fig. S8a–d; M.S. Fig. 2a–d, Fig. 2h, Fig. 2i, Supplementary Fig. S4c,d; A.G.: Fig. 2j, Fig. 2k Supplementary Fig. S4A. Supplementary Fig. S4B; A.A. and M.A.O. Fig. 3g, Fig. 4a–f, Fig. 5a, Fig. 5b, Fig. 5f, Fig. 5g, Fig. 6a, Fig. 6b, Supplementary Fig. S5a, Supplementary Fig. S5b, Supplementary Fig. S6; A.B., S.G. and M.G. Fig. 4g, Fig. 4h; T.S. and A.L.A. Fig. 6c, Supplementary Fig S7a, Supplementary Fig. S7b; L.L. Fig. 6d, Fig. 6e; L.L. and A.F. wrote the manuscript, with contributions from M.E.G. and E.S.

Additional information

Supplementary Information accompanies this paper at http://www.nature.com/naturecommunications

Competing financial interests: The authors claim no competing financial interests associated with this paper.

Reprints and permission information is available online at http://npg.nature.com/reprintsandpermissions/

How to cite this article: Lignitto, L. *et al.* Proteolysis of MOB1 by the ubiquitin ligase praja2 attenuates Hippo signalling and supports glioblastoma growth. *Nat. Commun.* 4:1822 doi:10.1038/ncomms2791 (2013).

Proteolytic control of neurite outgrowth inhibitor NOGO-A by the cAMP/PKA pathway

Maria Sepe[a], Luca Lignitto[a], Monia Porpora[a], Rossella Delle Donne[a], Laura Rinaldi[a], Giuseppe Belgianni[a], Gianna Colucci[a], Ornella Cuomo[b], Davide Viggiano[b,1], Antonella Scorziello[b], Corrado Garbi[a], Lucio Annunziato[b], and Antonio Feliciello[a,2]

[a]Dipartimento di Medicina Molecolare e Biotecnologie Mediche and [b]Dipartimento di Neuroscienze, Scienze Riproduttive ed Odontostomatologiche, University Federico II, 80131 Naples, Italy

Edited* by Susan S. Taylor, Howard Hughes Medical Institute, University of California at San Diego, La Jolla, CA, and approved September 26, 2014 (received for review June 4, 2014)

Protein kinase A (PKA) controls major aspects of neurite outgrowth and morphogenesis and plays an essential role in synaptic plasticity and memory. However, the molecular mechanism(s) of PKA action on neurite sprouting and activity are still unknown. Here, we report that in response to neurotrophin or cAMP stimulation the RING ligase praja2 ubiquitinates and degrades NOGO-A, a major inhibitor of neurite outgrowth in mammalian brain. Genetic silencing of praja2 severely inhibited neurite extension of differentiating neuroblastoma cells and mesencephalic neurons and axon outgrowth and sprouting of striatal terminals in developing rat brain. This phenotype was rescued when both praja2 and NOGO-A were depleted, suggesting that NOGO-A is, indeed, a biologically relevant target of praja2 in neuronal cells. Our findings unveil a novel mechanism that functionally couples cAMP signaling with the proteolytic turnover of NOGO-A, positively impacting on neurite outgrowth in mammalian brain.

cAMP | PKA | proteasome | ubiquitin | NOGO-A

Neurite outgrowth plays an essential role in embryonic development, neuronal differentiation, and central nervous system (CNS) plasticity. Outgrowth can be also altered in several neurological disorders, as well as by neuronal injury and degeneration (1, 2). Extracellular signals, such as neurotrophins (NTFs) and neurotransmitters, regulate neurite outgrowth, dendritic arborization, and synaptic activity, establishing a dynamic neuronal network in developing and adult CNS. NTFs and neurotransmitters act at the cell membrane by generating intracellular second messengers that, in turn, reversibly modulate the activity of signaling proteins and effector enzymes (3, 4).

cAMP is an ancient second messenger that controls a variety of biological cues. In neurons, essential functions such as neurite outgrowth and morphogenesis, synaptic transmission, and plasticity require tightly regulated responses to cAMP/protein kinase A (PKA) stimulation (5). PKA holoenzyme localizes in subcellular microdomains through interactions with A-Kinase-Anchor-Proteins (AKAPs). AKAP forms a local transduction unit, which includes signaling/metabolic enzymes, receptors, ion channels, adaptor molecules, and mRNAs (6, 7). Space-restricted activation of PKA provides a control mechanism to direct, integrate, and locally attenuate the cAMP cascade (8). praja2 belongs to a growing family of mammalian RING ligases abundantly expressed in the brain that finely tune the stability of intracellular substrates and play an essential role in critical aspects of cell signaling. In response to cAMP stimulation, praja2 couples ubiquitination and proteolysis of the inhibitory PKA regulatory (R) subunits by the proteasome to a sustained cAMP/PKA signaling, significantly impacting on synaptic plasticity and long-term memory (9). In addition to enhancing cAMP signaling, the role of praja2 in neuronal differentiation and dendritic network in the CNS and the molecular targets involved are unknown.

NOGO-A is a member of the reticulon (RTN) family of integral membrane proteins with a conserved C terminus reticulon homology domain (RHD) and abundantly expressed in oligodendrocytes and in distinct neuronal subpopulations (10, 11). NOGO-A was originally identified as a potent inhibitor of neurite outgrowth (1, 10). In the adult CNS and in injured neurons, NOGO-A restricts the capacity of an axon to grow and regenerate. Genetic ablation of NOGO-A promotes neuritogenesis and fasciculation of oligodendrocytes and culture of dorsal root ganglion neurons, functionally improving neuronal plasticity and recovery of post-ischemic adult rat brain (12).

Although the role of NOGO-A in neurite outgrowth is well established, regulation of NOGO-A levels in differentiating neurons and the mechanism(s) involved have been, to date, unknown. Here, we report a novel mechanism of neuritogenesis based on proteolytic turnover of NOGO-A (13). In response to cAMP or neurothrophin stimulation, RING ligase praja2 ubiquitinates and degrades NOGO-A. Proteolysis of NOGO-A by praja2 is functionally linked to neurite outgrowth in both differentiating neurons and developing rat brain.

Results

praja2 Interacts with NOGO-A. We isolated novel praja2 interactors/substrates by screening a human brain cDNA library. Two positive clones encoding for the conserved C terminus of RTNs were further characterized. Among different RTNs with still unclear functions, RTN4 variants, also known as NOGO-A, NOGO-B, and NOGO-C, play a role in inhibiting axonal growth, neuronal regeneration, and synaptic activity.

First, we demonstrated that praja2 interacts with NOGO-A in cell extracts. Recipient cells were transiently transfected

Significance

Damage of the central nervous system (CNS) and neurodegenerative disorders represent the principal cause of morbidity and mortality among adults. An injured CNS is unable to regenerate dendritic or neurite connections because they spontaneously occur in the peripheral nervous system. Inhibitory influences of the glial cells and of myelin-associated inhibitors oppose the spontaneous regeneration of CNS neurons. Here, we identify a positive mechanism of neuronal differentiation, which acts in response to activation of intracellular pathway(s) to remove an inhibitory constraint of neurite outgrowth. Unveiling the molecular events regulating the regenerative capacity of neurons will impact on therapeutic initiatives to stem the course of brain damage or neurodegeneration.

Author contributions: M.S. and A.F. designed research; M.S., L.L., M.P., R.D.D., L.R., G.B., G.C., O.C., D.V., and A.S. performed research; M.S., L.L., A.S., C.G., L.A., and A.F. analyzed data; and A.F. wrote the paper with contributions from M.S., D.V., and L.A.

The authors declare no conflict of interest.

*This Direct Submission article had a prearranged editor.

[1]Present address: Dipartimento di Medicina e Scienze della Salute, University of Molise, 86010 Campobasso, Italy.

[2]To whom correspondence should be addressed. Email: felidel@unina.it.

This article contains supporting information online at www.pnas.org/lookup/suppl/doi:10.1073/pnas.1410274111/-/DCSupplemental.

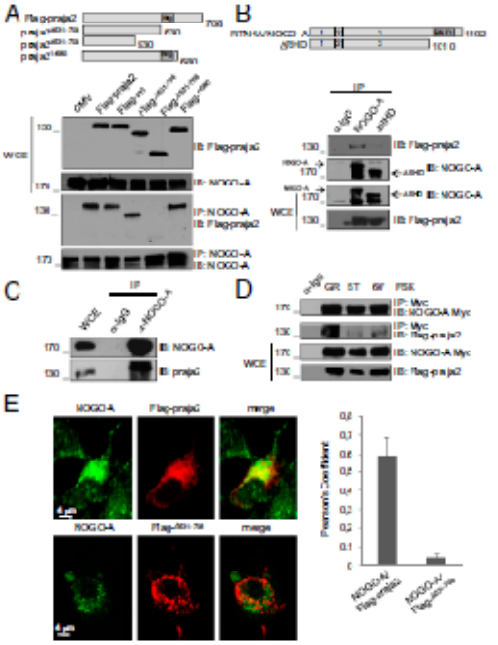

Fig. 1. praja2 interacts with NOGO-A. (*A*) Schematic representation of human praja2 constructs (*Upper*). Flag-praja2, the RING mutant (praja2rm), or the deletion mutants (Δ531–708, Δ531–708, and 1–680) were transiently transfected in HEK293 cells. Cells were treated with MG132 (10 μM) for 6 h before harvesting. Lysates were subjected to coimmunoprecipitation with anti-NOGO-A and anti-Flag antibodies (*Lower*). WCE, whole-cell extracts. (*B*) Schematic representation of NOGO-A constructs. Coimmunoprecipitation of flag-praja2 and NOGO-A or NOGO-ΔRHD (*Lower*). (*C*) Isolation of endogenous NOGO-A and praja2 complex from lysates (2 mg) of SH-SY5Y cells. (*D*) Transfected cells were left untreated (GR, growing) or serum-starved (ST) overnight and then stimulated with FSK. Lysates were subjected to coimmunoprecipitation assay with the indicated antibodies. All of the coimmunoprecipitation experiments were repeated at least three times. (*E*) Immunofluorescence analysis of SH-SY5Y cells transiently transfected with Flag-praja2 and Flag-Δ531–708 vectors. The bar graph represents the Pearson's coefficient of four independent experiments. At least 25 cells for each experimental group were analyzed. The data are expressed as mean ± SEM.

with Flag-tagged praja2 and Myc-NOGO-A (the longest NOGO variant). Coimmunoprecipitation assays demonstrated that flag-praja2 and the coexpressed NOGO-Myc formed a stable complex (Fig. 1*A*). praja2 ligase activity was not required for NOGO-A binding, as a praja2 inactive mutant carrying an alanine substitution of two critical residues within the RING domain (cys634 and cys671) (Flag-praja2rm) was able to bind NOGO-A as well as the wild-type protein (Fig. 1*A*). Deletion mutagenesis and binding analysis identified residues 531–708 of praja2 as the segment required for binding to NOGO-A (Fig. 1*A*). The RHD of NOGO-A mediates interaction with praja2 because a NOGO-A mutant lacking the C-terminal segment did not bind praja2 (Fig. 1*B*). A complex containing endogenous praja2 and NOGO-A was isolated from cell lysates (Fig. 1*C*). praja2 is phosphorylated by PKA (9). Moreover, Fig. 1*D* shows that serum deprivation significantly reduced the amount of praja2/NOGO-A complex recovered in the immunoprecipitates. The binding was only partially restored by forskolin treatment after 60 min of stimulation.

Because the RHD motif is highly conserved among RTNs, we tested if other family members form a complex with praja2. Fig. S1 shows that RTN2C and RTN3C bind praja2, suggesting that binding to praja2 is a general feature of the RTN protein family.

In situ immunostaining analysis of human neuroblastoma cells demonstrated that flag-praja2, but not its deletion mutant flag-Δ531–708, partially colocalized with NOGO-A. Overlapping signals were detectable in the perinuclear region, cytoplasm, and cell membrane, supporting the existence of a complex in intact cells (Fig. 1*E*).

Proteolysis of NOGO-A by praja2. By acting as E3-ubiquitin ligase, praja2 should destabilize RTNs. Indeed, wild-type praja2 severely reduced the levels of coexpressed NOGO-A (Fig. 2 *A* and *B*). In contrast, in cells expressing the praja2 ring mutant (Flag-praja2rm), NOGO-A accumulated to the same extent as in control cells that were not transfected with praja2 (Fig. 2 *A* and *B*). A similar effect was observed also on the other RTN variants (Fig. S2). Proteasome inhibition by MG132 treatment prevented

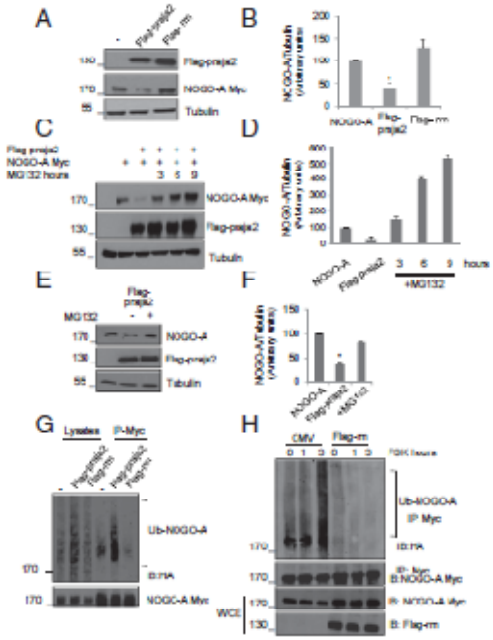

Fig. 2. praja2 ubiquitinates and degrades NOGO-A. (*A*) Immunoblot of lysates from cells transiently transfected with vectors encoding Flag-praja2 (either wild type or RING mutant) and Myc-tagged NOGO-A. (*B*) Quantitative analysis (mean ± SEM) of three independent experiments shown in *A*. **P* < 0.01 versus control (NOGO-A). (*C*) Immunoblot analysis of lysates from cells transfected with NOGO-A alone or with Flag-praja2. MG132 (10 μM) was added 6 h before harvesting. (*D*) Quantitative analysis of (mean ± SEM) three independent experiments shown in *C*. (*E* and *F*) HEK293 cells were transfected with flag-praja2 and treated for 3 h with MG132 (20 μM) before harvesting. Lysates were immunoblotted with the indicated antibodies. (*F*) Quantitative analysis of three independent experiments shown in *E*. **P* < 0.01 versus NOGO-A and flag-praja2+MG132. (*G*) Lysates from transfected cells were immunoprecipitated with anti-Myc antibody. The precipitates were immunoblotted with anti-HA and anti-Myc. (*H*) Same as in G, with the exception that transfected cells were serum-deprived overnight and then stimulated with FSK.

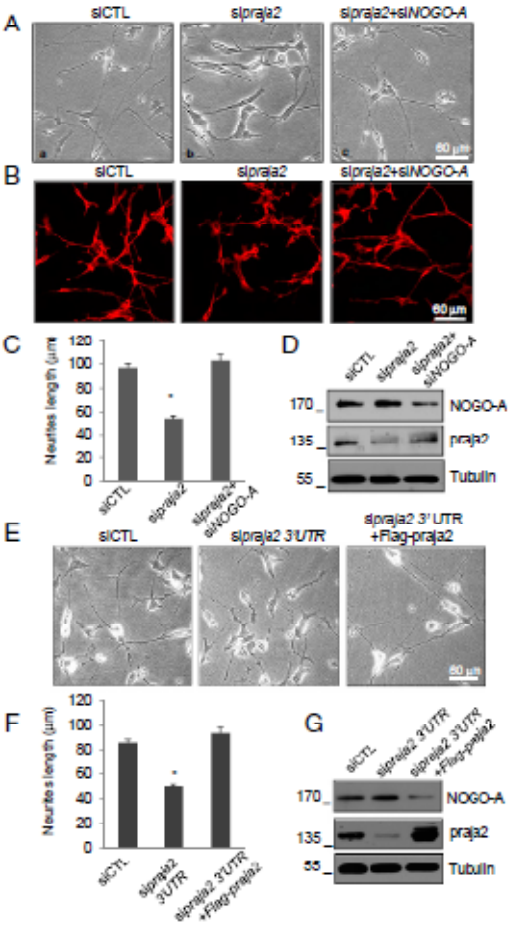

Fig. 3. Praja2 controls axonal outgrowth. (*A*) Differentiating SH-SY5Y cells were transiently transfected with the indicated siRNAs. Images were collected and analyzed by phase-contrast microscope. (*B*) Same as in *A*, with the exception that cells were immunostained with anti–α-tubulin antibody and analyzed by confocal microscopy. (*C*) Cumulative data are expressed as a mean value ± SEM of four independent experiments. **P* < 0.05 versus siCTL. Number of cells analyzed: control siRNA (50), *praja2 siRNA* (50), *praja2 siRNA +NOGO-A siRNA* (59). (*D*) Immunoblot analysis of SH-SY5Y–transfected cells. (*E*) Differentiating SH-SY5Y cells were transiently transfected with the indicated siRNAs and with Flag-praja2 vector. (*F*) Cumulative data of three independent experiments shown in *E*. **P* < 0.01 versus siCTL and *siPraja2 3′ UTR*+Flag-praja2. (*G*) Immunoblot for NOGO-A, praja2, and tubulin using lysates from SH-SY5Y–transfected cells.

praja2-mediated NOGO-A degradation and induced a time-dependent rise of exogenous (Fig. 2 *C* and *D*) and endogenous (Fig. 2 *E* and *F* and Fig. S3) NOGO-A levels. Next, we investigated if praja2 promotes ubiquitination of NOGO-A. As expected, overexpression of praja2, but not praja2rm, leads to accumulation of poly-ubiquitinated NOGO-A (Fig. 2*G*). praja2 activity is induced by PKA (9). Therefore, we tested if PKA activation regulates ubiquitination of NOGO-A. Cells were serum starved overnight and subsequently treated with forskolin (FSK), an adenylate cyclase activator. As shown in Fig. 2*H*, raising intracellular cAMP levels positively impacted on NOGO-A ubiquitination, even at 3 h from forskolin treatment. Expression of Flag-praja2rm downregulated both basal and FSK-stimulated NOGO-A ubiquitination, confirming the role of praja2 in the control of NOGO-A stability.

praja2 Is Required for NOGO-A Degradation and Neurite Outgrowth in Differentiating Neurons. In light of the inhibitory role of NOGO-A in neurite outgrowth of developing or injured neurons, we asked whether, by affecting NOGO-A stability, praja2 regulates neurite elongation in differentiating neuronal cells. To this end, we used SH-SY5Y neuroblastoma cells as a model system. SH-SY5Y cells differentiate in vitro in the presence of retinoic acid (RA) and brain-derived neurotrophic factor (BDNF) (14). RA-treated cells exhibit a neuron-like morphology and express neuron-specific proteins. Addition of BDNF into the medium of RA-treated cells induces additional major morphological changes and promotes neurite formation. We reproduced this neural-like phenotype by sequentially treating SH-SY5Y cells with RA and BDNF (Fig. 3 *A*, a). Genetic knockdown of praja2 using a mixture of four siRNAs targeting praja2 reversed the neural-like phenotype of treated cells (Fig. 3 *A*, b and *C*). Similar effects were obtained using two independent siRNAs targeting distinct coding regions (Fig. S4) or the 3′ UTR of praja2 mRNA. Moreover, the neurite extension in siRNA-transfected cells could be rescued by re-expression of exogenous praja2 (Fig. 3 *E* and *F*). The relative abundance of NOGO-A and praja2 in transfected cells is shown (Fig. 3*G*).

The effects of praja2 downregulation on neurite extension might result from either impairment of cAMP signaling or the accumulation of NOGO-A. To discriminate between these possibilities, we performed a double knockdown for praja2 and NOGO-A. Downregulation of NOGO-A restored, at least in part, neurite extension in praja2-silenced neuroblastoma cells (Fig. 3 *A*, c and *C*). The data were confirmed by immunostaining differentiating SH-SY5Y cells with anti–α-tubulin antibody (Fig. 3*B*). Fig. 3*D* shows the levels of praja2 and

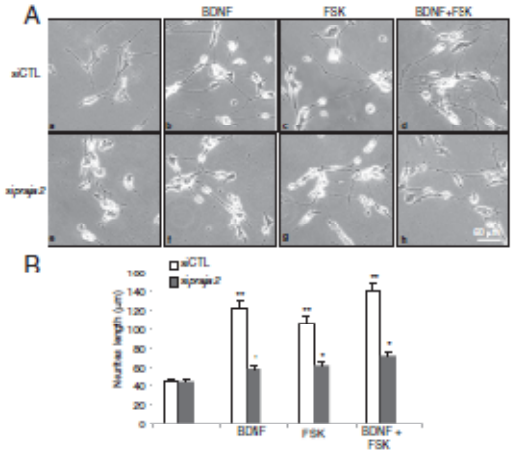

Fig. 4. praja2 is required for cAMP-induced neurite outgrowth. (*A*) Differentiating neuroblastoma cells transfected with control siRNA or *praja2* siRNA were left untreated (a, e) or treated with BDNF (50 ng/mL) (b, f), FSK (40 μM) (c, g), or with both agonists (FSK and BDNF) (d, h) for 3 d. Images were collected by phase-contrast microscope. (*B*) A mean of three independent experiments that gave similar results is shown. **P* < 0.01 versus BDNF, FSK, and BDNF/FSK-stimulated siCTL; ***P* < 0.05 versus unstimulated cells.

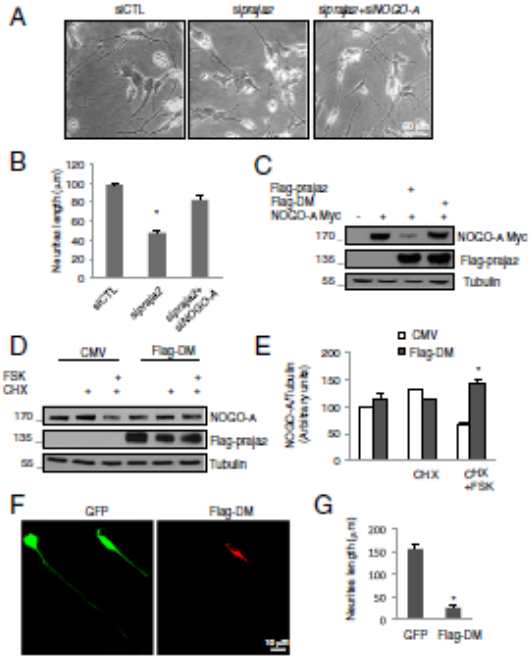

Fig. 5. praja2 mediates cAMP effects on neurite outgrowth. (*A*) Differentiating SH-SY5Y cells were transfected with the indicated siRNAs and treated with FSK (10 μM), and neurite lengths were scored 3 d later. (*B*) Cumulative data of three independent experiments as a mean value ± SEM are shown. **P* < 0.05 versus siCTL. (*C*) Expression levels of Flag-praja2, Flag-DM, and NOGO-A. (*D*) Immunoblot analysis of lysates from SH-SY5Y cells transiently transfected with CMV and praja2-DM treated with cycloheximide (100 μg/mL) and forskolin (40 μM). (*E*) Cumulative data of five independent exeperiments are expressed as a mean value ± SEM. **P* < 0.05 versus controls [CMV ± cycloheximide (CHX)] and flag-DM (CHX ± FSK). (*F*) Differentiating SH-SY5Y cells cotransfected with praja2-DM and GFP vector were immunostained with anti-Flag antibody and analyzed by confocal microscopy. (*G*) Cumulative data of three experiments as a mean value ± SEM are shown. **P* < 0.01 versus GFP.

NOGO-A in siRNA-transfected cells. Although praja2 regulates RTN stability, no major morphological changes of the endoplasmic reticulum were observed following praja2 knockdown (Fig. S5). Moreover, in situ immunostaining analysis showed overlapping signals between NOGO-A and calreticulin, whereas only a partial colocalization could be assigned to praja2 and calreticulin (Fig. S6).

praja2 Mediates cAMP Effects on NOGO-A Stability and Neurite Outgrowth. Activation of the cAMP/PKA pathway positively regulates neurite outgrowth in a wide variety of species, profoundly impacting brain development and synaptic plasticity (15–17). Accordingly, treating neuroblastoma cells with forskolin or BDNF promoted neurite outgrowth and extension (Fig. 4 *A*, b and c, and *B*). These effects were similar when cells were cotreated with both agonists (FSK and BDNF) (Fig. 4 *A*, d and *B*). Silencing of praja2 prevented neurite extension induced by FSK and BDNF (Fig. 4 *A* and *B*, f and g), this phenotype was rescued when both praja2 and NOGO-A were depleted (Fig. 5 *A* and *B*), suggesting that praja2 is, indeed, a relevant downstream effector of cAMP signaling on neuronal differentiation. The neurite extention induced by FSK was PKA-dependent, as treatment with the PKA inhibitor H89 reduced neurite elongation in both control and praja2-depleted cells (Fig. S7). PKA phosphorylation of praja2 at Ser342/Thr389 is required for ligase activity (9). Therefore, we monitored NOGO-A levels in cells expressing a praja2 mutant carrying substitution of Ser342/Thr389 to Ala (double mutant, praja2DM). As suspected, praja2DM failed to degrade coexpressed NOGO-A, compared with wild-type praja2 (Fig. 5*C*). When expressed in differentiating neuroblastoma cells, praja2DM prevented FSK-induced proteolysis of NOGO-A (Fig. 5 *D* and *E*) and severely reduced neurite extension (Fig. 5 *F* and *G*).

Next, we investigated the role of praja2 in mesencephalic neurons both in culture and in developing rat brain. As expected, praja2 silencing significantly reduced neurite extension of cultured mesencephalic neurons. The total length of neurites in *praja2* siRNA-treated neurons was significantly lower compared with controls, as observed at three different time periods after transfection (Fig. 6 *A* and *B*). Notably, after 6 d of silencing, the length of tyrosine hydroxylase (TH)-positive axons, clearly recognizable from the typical axonal varicosities, was reduced by 55.5% in *praja2* siRNA-treated neurons (neurite lengths were

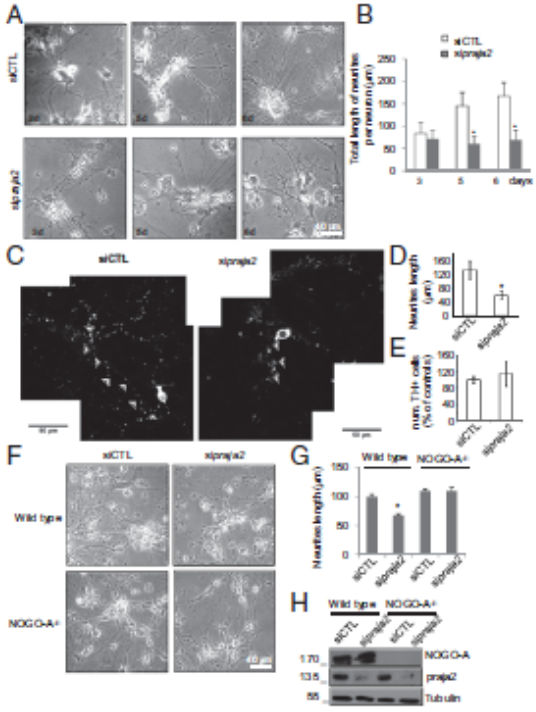

Fig. 6. praja2 controls neurite outgrowth in mesencephalic neurons. (*A*) Midbrain neurons were transiently transfected with *praja2* siRNA or control siRNA, and neurite extension was calculated at the indicated days from transfection. (*B*) Neurite lengths are expressed as mean ± SEM; **P* < 0.05 versus siCTL of three independent experiments. (*C*) Neurite branching of TH-positive neurons in vitro (midbrain primary cultures) under basal conditions and after downregulation of praja2 with siRNA. (*D* and *E*) Quantification of principal neurite lengths and number of TH-positive neurons in culture. Neurite lengths of TH+ mesencephalic neurons from control (34) and siRNA praja2-transfected (24) cells. (*F*) Neurite extension ofcontrol and NOGO-A KO neurons (NOGO-A$^{-/-}$) transiently transfected with *praja2* siRNA or control siRNA. (*G*) Quantification of neurite lengths from *F* of three independent experiments. **P* < 0.05 versus siCTL and sipraja2 in NOGO-A$^{-/-}$. (*H*) NOGO-A and praja2 levels in mesencephalic neurons from *F* and *G*.

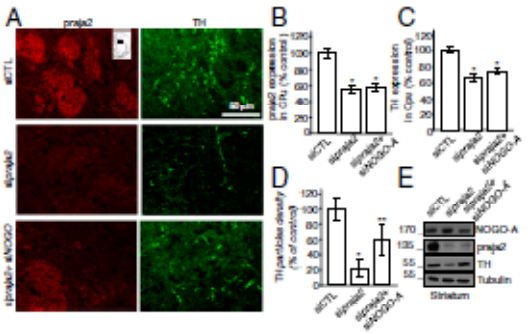

Fig. 7. praja2 controls neurite outgrowth in developing mammalian brain. (*A*) Immunofluorescence images of TH and praja2 in the CPu from rat brain perfused in the lateral ventricle with either control siRNA, *praja2* siRNA, *NOGO-A* siRNA, and *praja2 siRNA+NOGO-A* siRNA. (*Inset*) The position of the region analyzed. Quantification of total fluorescence intensity of praja2 (*B*) and TH (*C*) in CPu is reported. (*D*) The density of TH-positive varicosities in the dorsal striatum was assessed on average of six sections. To automatically delineate the fibers, the images were first thresholded and subsequently quantified with the Analyze particles tool of Image J. One-tailed statistical test was used. In particular, $*P < 0.05$ versus siCTL and $**P < 0.05$ versus *sipraja2*. (*E*) Immunoblot analysis of whole lysates from striatum of neonatal mice perfused with the indicated siRNAs.

123.5 ± 26.5 μm in control siRNA condition and 59.8 ± 12.8 μm in *praja2* siRNA neurons) (Fig. 6 *C* and *D*). Reduction of axonal length with *praja2* siRNA was not accompanied by a significant loss of TH-positive cell bodies (Fig. 6*E*). Furthermore, genetic knockdown of praja2 in mesencephalic neurons isolated from NOGO-A KO mice had no effects on neurite elongation, compared with wild-type neurons. These results indicate that praja2 controls neurite elongation by targeting NOGO-A (Fig. 6 *F*–*H*).

praja2 Regulates NOGO-A Levels and Axon Outgrowth in Developing Rat Brain. High levels of praja2 are found in the nigro-striatal pathway, a system involved in several neurological disorders, such as Parkinson's disease and attention deficit hyperactivity disorder. Therefore, we tested the influence of praja2 on axonal sprouting in the caudate-putamen (CPu) of postnatal rat brain. Interestingly, genetic knockdown of praja2 in this area decreased the overall intensity of TH signal, a marker of mesencephalic neurons, and significantly reduced the number of TH-positive dopaminergic varicosities in the dorsal striatum (Fig. 7 *A*–*D*). The data suggest that the effects of siRNA are the consequence of downregulation of the protein at presynaptic levels. It is also possible that the injected siRNA may work on postsynaptic neurons that in turn regulate dopaminergic endings via NOGO-A. To understand whether the effects of praja2 were mediated by NOGO-A, a third group of animals received both siRNAs for praja2 and NOGO-A. Results show that concomitant downregulation of NOGO-A partly reversed the effects of praja2 silencing on the number of axonal varicosities (Fig. 7 *A*–*D*).

Immunoblot analysis of lysates from the CPu area confirmed that silencing of praja2 reduced TH expression (Fig. 7*E*). To address whether the reduction of TH-positive terminals in the CPu was due to neuronal loss, we measured the number of dopamine (TH-positive) neurons in the substantia nigra pars compacta (SNpc), the region of origin of CPu dopamine fibers. Fluorescence intensity, neuronal density, and neuronal diameter were not significantly changed in the SNpc of siRNA-treated animals (Fig. S8).

Discussion

Here, we demonstrate that cAMP promotes degradation of NOGO-A through the ubiquitin proteasome system. We identify praja2 as the E3 ubiquitin ligase that mediates cAMP destabilization of NOGO-A. Degradation of NOGO-A by praja2 is a mechanism that underlies cAMP-induced neurite outgrowth of differentiating neuronal cells. Genetic downregulation of praja2 prevents NOGO-A degradation and inhibits axon outgrowth and branching in cultured neurons and in the nigro-striatal dopaminergic pathway of rat brain.

BDNF is essential for neuronal development, survival, and differentiation. Acting through a dedicated receptor at the cell membrane, BDNF stimulates a number of second messenger pathways that, in turn, activate distinct classes of adaptors, scaffolds, and signaling enzymes (18). cAMP and its effector enzyme PKA have been implicated in mediating some of the effects of BDNF stimulation on neuronal differentiation and activity. BDNF stimulation of PLCγ induces transient release of calcium from intracellular stores, activating calcium-sensitive adenylate cyclases and consequent elevation of cAMP levels (19, 20). Activation of PKA by cAMP increases the number and extension of neurites and varicosities, accelerating neuritogenesis and neurite outgrowth rate in a variety of mammalian neurons (21, 22). Conversely, genetic or pharmacological inhibition of PKA severely downregulated neurite outgrowth and extension, supporting the role of the cAMP/PKA pathway in critical aspects of neuronal differentiation (16). PKA phosphorylation of CREB and CREB-directed gene transcription represents the principal mechanism of cAMP action in promoting and sustaining neuronal differentiation (23). Additionally, a variety of intracellular substrates and downstream effectors of cAMP signaling have been identified and mechanistically linked to neuronal differentiation (24, 25).

Our results disclose a previously unrecognized mechanism of cAMP action on neuronal differentiation based on the regulated proteolysis of NOGO-A, a major inhibitor of neurite outgrowth in mammalian brain (26). cAMP induces proteolysis of NOGO-A through the ubiquitin proteasome system (UPS). Decrease of NOGO-A levels removes the inhibitory constraint on neurite outgrowth, preventing growth cone collapse and sustaining neurite extension and morphogenesis (Fig. 8). We identified praja2 as the ubiquitin ligase responsible for ubiquitination and proteolysis of NOGO-A. praja2 is phosphorylated by the associated PKA, which stimulates its ubiquitin ligase activity (9). Genetic knockdown

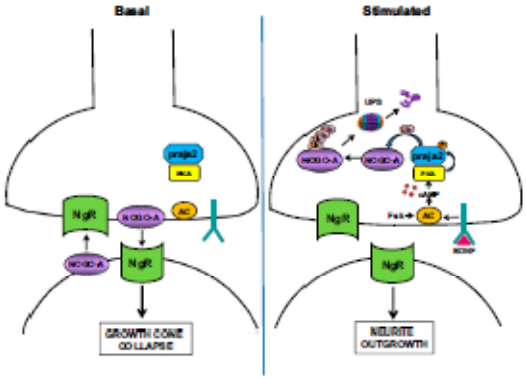

Fig. 8. Model of praja2–NOGO-A pathway. Under basal conditions, NOGO-A inhibits neurite outgrowth. Activation of adenylate cyclase (AC) by BDNF or by Forskolin (Fsk) increases cAMP levels and dissociates PKA holoenzyme. Active PKA catalytic subunit phosphorylates praja2, which in turn ubiquitinates and degrades NOGO-A through the UPS. The drop in NOGO-A levels promotes neurite outgrowth.

of praja2 or expression of a phosphorylation-defective praja2 mutant prevented cAMP-induced NOGO-A degradation and severely inhibited neurite extension in differentiating neurons. Notably, downregulation of NOGO-A levels in praja2-silenced cells restored neurite outgrowth to control values. Moreover, praja2 silencing was ineffective in downregulating neurite extension in NOGO-A KO neurons. Altogether, these findings are consistent with the notion that inhibition of neurite outgrowth by praja2 silencing depends on increased NOGO-A levels, rather than on global downregulation of cAMP signaling.

In conclusion, negative regulation of the NOGO-A pathway by cAMP and praja2 constitutes a novel UPS-driven signaling circuit that promotes and sustains biological processes underlying neuronal differentiation and synaptic activity. Unveiling the mechanism(s) regulating praja2 expression and activity in neurons and identifying relevant praja2 substrates operating in vivo will contribute to our understanding of the role of cAMP and UPS in the regulation of brain development and plasticity and may well impact on therapeutic initiatives for neurodegenerative disorders.

Materials and Methods

Cell Lines. HEK293 and a neuroblastoma cell line (SHSY-5Y) were maintained in DMEM supplemented with 10% heat-inactivated FBS at 37 °C, 5% (vol/vol) CO_2, and 95% humidity. To induce differentiation, neuroblastoma cells were treated for 5 d with 10 μM of all-trans RA (Sigma) and then with BDNF (14, 27). Midbrain primary cultures were obtained from brains of 16-d-old Wistar rat embryos (28) (29). Primary dopaminergic neuron cultures were isolated from NOGO-A KO mouse brain (30).

siRNA Administration into the Rat Brain. Postnatal Wistar rats were studied in a period of partial immaturity of the mesostriatal dopamine system (31). Experiments were performed according to the international guidelines for animal research. The experimental protocol was approved by the Animal Care Committee of the University of Naples Federico II. Three-day-old Wistar rats were intracerebroventricularly injected with targeting naked siRNAs (2 μL, 0.5 μmol/L in cerbrospinal fluid with 0.05% trypan blue) or control naked siRNAs, according to previously published protocol for neonatal mice (32). siRNA injection was repeated at postnatal day 6 (P6), and animals were killed at P9. $n = 7$ for each experimental group.

Plasmids and Transfection. Flag-praja2rm was generated by site-directed mutagenesis, whereas praja2-deletion mutant was generated by PCR. NOGO-A ΔRHD was generated by PCR from GenScript. All of the RTN vectors, including NOGO-A, were previously described (11, 33).

ACKNOWLEDGMENTS. We thank Drs. S. M. Strittmatter, J. Iwahashi, and W. Araki for providing RTN vectors; M. E. Schwab for providing NOGO-A knockout mice; and M. E. Gottesman for critical reading of the manuscript. This work was supported by a grant from Associazione Italiana Ricerca sul Cancro (IG 11788). M.S. was supported by a fellowship from Progetto Operativo Regionale Campania FSE 2007-2013, Project CREME.

1. Karnezis T, et al. (2004) The neurite outgrowth inhibitor Nogo A is involved in autoimmune-mediated demyelination. *Nat Neurosci* 7(7):736–744.
2. Horner PJ, Gage FH (2000) Regenerating the damaged central nervous system. *Nature* 407(6807):963–970.
3. Huang EJ, Reichardt LF (2001) Neurotrophins: Roles in neuronal development and function. *Annu Rev Neurosci* 24:677–736.
4. Poo MM (2001) Neurotrophins as synaptic modulators. *Nat Rev Neurosci* 2(1):24–32.
5. Taskén K, Aandahl EM (2004) Localized effects of cAMP mediated by distinct routes of protein kinase A. *Physiol Rev* 84(1):137–167.
6. Feliciello A, Gottesman ME, Avvedimento EV (2001) The biological functions of A-kinase anchor proteins. *J Mol Biol* 308(2):99–114.
7. Beene DL, Scott JD (2007) A-kinase anchoring proteins take shape. *Curr Opin Cell Biol* 19(2):192–198.
8. Taylor SS, et al. (2005) Dynamics of signaling by PKA. *Biochim Biophys Acta* 1754(1-2):25–37.
9. Lignitto L, et al. (2011) Control of PKA stability and signaling by the RING ligase praja2. *Nat Cell Biol* 13(4):412–422.
10. Grandpré T, Nakamura F, Vartanian T, Strittmatter SM (2000) Identification of the Nogo inhibitor of axon regeneration as a Reticulon protein. *Nature* 403(6768):439–444.
11. Iwahashi J, Hamada N, Watanabe H (2007) Two hydrophobic segments of the RTN1 family determine the ER localization and retention. *Biochem Biophys Res Commun* 355(2):508–512.
12. Bonglorno D, Petratos S (2010) Molecular regulation of Nogo-A in neural cells: Novel insights into structure and function. *Int J Biochem Cell Biol* 42(7):1072–1075.
13. Ahmed Z, et al. (2006) Schwann cell-derived factor-induced modulation of the NgR/p75NTR/EGFR axis disinhibits axon growth through CNS myelin in vivo and in vitro. *Brain* 129(Pt 6):1517–1533.
14. Encinas M, et al. (2000) Sequential treatment of SH-SY5Y cells with retinoic acid and brain-derived neurotrophic factor gives rise to fully differentiated, neurotrophic factor-dependent, human neuron-like cells. *J Neurochem* 75(3):991–1003.
15. Beyer C, Karolczak M (2000) Estrogenic stimulation of neurite growth in midbrain dopaminergic neurons depends on cAMP/protein kinase A signalling. *J Neurosci Res* 59(1):107–116.
16. Sánchez S, et al. (2004) A cAMP-activated pathway, including PKA and PBK, regulates neuronal differentiation. *Neurochem Int* 44(4):231–242.
17. Agiah C, Gordon T, Posse de Chaves EI (2008) cAMP promotes neurite outgrowth and extension through protein kinase A but independently of Erk activation in cultured rat motoneurons. *Neuropharmacology* 55(1):8–17.
18. Cunha C, Brambilla R, Thomas KL (2010) A simple role for BDNF in learning and memory? *Front Mol Neurosci* 3:1.
19. Cheng PL, et al. (2011) Self-amplifying autocrine actions of BDNF in axon development. *Proc Natl Acad Sci USA* 108(45):18430–18435.
20. Yoshii A, Constantine-Paton M (2010) Postsynaptic BDNF-TrkB signaling in synapse maturation, plasticity, and disease. *Dev Neurobiol* 70(5):304–322.
21. Wang Q, Zheng JQ (1998) cAMP-mediated regulation of neurotrophin-induced collapse of nerve growth cones. *J Neurosci* 18(13):4973–4984.
22. Gao Y, Nikulina E, Mellado W, Filbin MT (2003) Neurotrophins elevate cAMP to reach a threshold required to overcome inhibition by MAG through extracellular signal-regulated kinase-dependent inhibition of phosphodiesterase. *J Neurosci* 23(37):11770–11777.
23. Spencer TK, Mellado W, Filbin MT (2008) BDNF activates CaMKIV and PKA in parallel to block MAG-mediated inhibition of neurite outgrowth. *Mol Cell Neurosci* 38(1):110–116.
24. Shabb JB (2001) Physiological substrates of cAMP-dependent protein kinase. *Chem Rev* 101(8):2381–2411.
25. Tojima T, Kobayashi S, Ito E (2003) Dual role of cyclic AMP-dependent protein kinase in neuritogenesis and synaptogenesis during neuronal differentiation. *J Neurosci Res* 74(6):829–837.
26. Wang KC, et al. (2002) Oligodendrocyte-myelin glycoprotein is a Nogo receptor ligand that inhibits neurite outgrowth. *Nature* 417(6892):941–944.
27. Edsjö A, Holmquist L, Påhlman S (2007) Neuroblastoma as an experimental model for neuronal differentiation and hypoxia-induced tumor cell dedifferentiation. *Semin Cancer Biol* 17(3):248–256.
28. Scorziello A, et al. (2001) Differential vulnerability of cortical and cerebellar neurons in primary culture to oxygen glucose deprivation followed by reoxygenation. *J Neurosci Res* 63(1):20–26.
29. Fath T, Ke YD, Gunning P, Götz J, Ittner LM (2009) Primary support cultures of hippocampal and substantia nigra neurons. *Nat Protoc* 4(1):78–85.
30. Simonen M, et al. (2003) Systemic deletion of the myelin-associated outgrowth inhibitor Nogo-A improves regenerative and plastic responses after spinal cord injury. *Neuron* 38(2):201–211.
31. Tarazi FI, Tomasini EC, Baldessarini RJ (1998) Postnatal development of dopamine and serotonin transporters in rat caudate-putamen and nucleus accumbens septi. *Neurosci Lett* 254(1):21–24.
32. Lee JP, McKercher S, Muller FJ, Snyder EY (2008) Neural stem cell transplantation in mouse brain. *Curr Protoc Neurosci* Chapter 3:Unit 3.10.
33. Kume H, Konishi Y, Murayama KS, Kametani F, Araki W (2009) Expression of reticulon 3 in Alzheimer's disease brain. *Neuropathol Appl Neurobiol* 35(2):178–188.